

CFD Simulation of a Riser VIV

by

**Hann-Ching Chen and Kevin Huang, Ocean Engineering Program, Department of Civil
Engineering, Texas A&M University**

Chia-Rong Chen, Department of Mathematics, Texas A&M University

Richard S. Mercier, Offshore Technology Research Center

Final Project Report

**Prepared for the Minerals Management Service
Under the MMS/OTRC Cooperative Research Agreement**

1435-01-04-CA-35515

Task Orders 35983 and 39774

MMS Project Number 481

December 2007

OTRC Library Number: 12/2007A186

“The views and conclusions contained in this document are those of the authors and should not be interpreted as representing the opinions or policies of the U.S. Government. Mention of trade names or commercial products does not constitute their endorsement by the U. S. Government”.



For more information contact:

Offshore Technology Research Center
Texas A&M University
1200 Mariner Drive
College Station, Texas 77845-3400
(979) 845-6000

or

Offshore Technology Research Center
The University of Texas at Austin
1 University Station C3700
Austin, Texas 78712-0318
(512) 471-6989

A National Science Foundation Graduated Engineering Research Center

Table of Contents

1	PROJECT DESCRIPTION	1
1.1	Background	1
1.2	Present Work	3
2	DEVELOPMENT OF ADVANCED CFD CAPABILITIES	4
2.1	Riser Motion Modal Solver	4
2.2	Riser Motion Direct Solver	5
3	2D SIMULATIONS OF FLOW PAST A FIXED/VIBRATING RISER.....	7
3.1	General Description.....	7
3.2	Data Grid	8
3.3	Riser Interference Analysis Procedures	9
3.4	CFD Simulation Results.....	10
3.5	Discussion	18
4	3D VIV SIMULATIONS OF A HORIZONTAL RISER IN UNIFORM CURRENT ..	20
4.1	General Description.....	20
4.2	Analysis Approach	22
4.3	Simulation Results.....	24
4.4	Discussion	36
5	3D VIV SIMULATIONS OF A HORIZONTAL RISER IN SHEARED CURRENT ..	37
5.1	General Description.....	37
5.2	Simulation Procedures.....	37
5.3	Simulation Results.....	38
5.4	Discussion	51
6	3D VIV SIMULATIONS OF A 3000 FT VERTICAL RISER	52
6.1	General Description.....	52
6.2	Description of CFD Approach	52
6.3	Simulation Results.....	54
6.4	Discussion	63

7	3D VIV SIMULATIONS USING DIRECT INTEGRATION RISER MOTION SOLVER	64
7.1	General Description.....	64
7.2	CFD Approach	64
7.3	Simulation Results – Cases 1 and 2.....	65
7.4	Simulation Results – Case 3	69
7.5	Simulation Results – Case 4.....	70
7.6	Discussion	72
8	SUMMARY AND CONCLUSIONS.....	74
	References.....	76
	Publications under Project.....	79

List of Tables and Figures

Table

Table 1.	10 ¾” Riser Top Tensions	10
----------	--------------------------------	----

Figures

Figure 1.	Von Neumann Stability of the Riser Motion Direct Solver.....	6
Figure 2.	Overset Grid for Wake Field Computation.....	8
Figure 3.	Overset Grid for Wake Field Computation – Vicinity of Riser Surface.....	9
Figure 4.	Flow Chart for Riser Interference Analysis	9
Figure 5.	Vorticity Contours for a Fixed Riser	11
Figure 6.	Fixed Riser Wake Field In-line Velocity 3D View – Top: Huse’s Formula, Bottom: CFD Result	12
Figure 7.	Fixed Riser Wake Field In-line Velocity Contours – Top: Huse’s Formula, Bottom: CFD Result	13
Figure 8.	Effective Drag Coefficient for a Fixed Riser.....	14
Figure 9.	Vorticity Contours for a Vibrating Riser	15
Figure 10.	Wake Field In-line Velocity Distribution behind a Vibrating Riser.....	16
Figure 11.	Effective Drag Coefficient for a Vibrating Riser.....	17
Figure 12.	Riser Displacement along Riser – Huse’s Formula	18
Figure 13.	Riser Displacement along Riser – FANS.....	18
Figure 14.	Plan View of Riser VIV Test Setup.....	20
Figure 15.	Data Grids in 3D, Left: Undeformed Riser, Right: Deformed Riser	23
Figure 16.	Data Grid near Riser Surface	23
Figure 17.	Horizontal Riser VIV Evolution in Uniform Current, Left: U = 0.4 m/s, Right: U = 0.8 m/s.....	25
Figure 18.	Horizontal Riser VIV Snap Shot – Uniform Current U = 0.4 m/s.....	26
Figure 19.	Horizontal Riser VIV Snap Shot – Uniform Current U = 0.8 m/s.....	26
Figure 20.	Horizontal Riser In-Line Modal Response – Uniform Current U = 0.4 m/s	27
Figure 21.	Horizontal Riser In-Line Modal Response – Uniform Current U = 0.8 m/s	27
Figure 22.	Mean Drag Coefficients for Horizontal Riser VIV in Uniform Current	28
Figure 23.	RMS of Lift Coefficients for Horizontal Riser VIV in Uniform Current.....	28

Figure 24.	Horizontal Riser Motion Trajectory in Uniform Current, Left: $U = 0.4$ m/s, Right: $U = 0.8$ m/s.....	29
Figure 25.	Horizontal Riser Motion Trajectory at $x/L = 0.25$ in Uniform Current $U = 0.4$ m/s.....	30
Figure 26.	Horizontal Riser Motion Trajectory at $x/L = 0.35$ in Uniform Current $U = 0.4$ m/s.....	30
Figure 27.	Horizontal Riser Motion Trajectory at $x/L = 0.55$ in Uniform Current $U = 0.4$ m/s.....	31
Figure 28.	Horizontal Riser Cross Flow Response Envelope in Uniform Current $U = 0.4$ m/s, $t = 193\sim 200$	32
Figure 29.	Horizontal Riser Cross Flow Response Envelope in Uniform Current $U = 0.8$ m/s, $t = 193\sim 200$	33
Figure 30.	Horizontal Riser In-line VIV RMS a/D in Uniform Current $U = 0.4$ m/s	33
Figure 31.	Horizontal Riser Cross Flow VIV RMS a/D in Uniform Current $U = 0.4$ m/s	34
Figure 32.	Horizontal Riser In-line VIV RMS a/D in Uniform Current $U = 0.8$ m/s	34
Figure 33.	Horizontal Riser Cross Flow VIV RMS a/D in Uniform Current $U = 0.8$ m/s	35
Figure 34.	Horizontal Riser Cross Flow VIV Max RMS a/D in Uniform Current.....	35
Figure 35.	Horizontal Riser VIV Motions at $x/L=0.25$ and 0.75	36
Figure 36.	Riser VIV Simulation Procedure	38
Figure 37.	Linearly Sheared Current Profiles	39
Figure 38.	Vortex Shedding Patterns and Horizontal Riser Responses, $U_{max} = 0.4$ m/s, Left: Sheared Current, Right: Uniform Current.....	40
Figure 39.	Snap Shots of Horizontal Riser VIV in Sheared Current, Top: $U_{max} = 0.4$ m/s, Bottom: $U_{max} = 0.8$ m/s.....	41
Figure 40.	Vorticity Contours in Sheared Current, Top: $U_{max} = 0.4$ m/s, Bottom: $U_{max} = 0.8$ m/s.....	42
Figure 41.	Drag Coefficient Distributions for Horizontal Riser, $U_{max} = 0.4$ m/s.....	43
Figure 42.	Lift Coefficient Distribution for Horizontal Riser, $U_{max} = 0.4$ m/s	43
Figure 43.	Drag Coefficient Distribution for Horizontal Riser, $U_{max} = 0.8$ m/s	44
Figure 44.	Lift Coefficient Distribution for Horizontal Riser, $U_{max} = 0.8$ m/s	44
Figure 45.	Horizontal Riser Cross Flow VIV RMS a/D , $U_{max} = 0.4$ m/s	45
Figure 46.	Horizontal Riser Cross Flow VIV RMS a/D , $U_{max} = 0.8$ m/s	46
Figure 47.	Horizontal Riser Cross Flow VIV Max RMS a/D	46
Figure 48.	Horizontal Riser Motion Trajectory Comparison, $U_{max} = 0.4$ m/s, Left: Sheared Current, Right: Uniform Current	47

Figure 49.	Horizontal Riser Motion Trajectory Comparison, $U_{max} = 0.8$ m/s, Left: Sheared Current, Right: Uniform Current	48
Figure 50.	Horizontal Riser In-line VIV Modal Response Amplitude	49
Figure 51.	Horizontal Riser Cross Flow VIV Modal Response Amplitude.....	50
Figure 52.	Horizontal Riser In-line VIV Modal Response Energy	50
Figure 53.	Horizontal Riser Cross Flow VIV Modal Response Energy	51
Figure 54.	Vertical Riser Modal Shapes	53
Figure 55.	Vertical Riser VIV Comparison, Left: Uniform Current 0.4 m/s, Right: Sheared Current 0.4 m/s.....	55
Figure 56.	Vertical Riser VIV Snapshot, Sheared Current	59
Figure 57.	Vertical Riser VIV Snapshot, Uniform Current	59
Figure 58.	Vertical Riser Cross Flow VIV Modal Response	60
Figure 59.	Vertical Riser Cross Flow VIV RMS a/D - Uniform Current	61
Figure 60.	Vertical Riser Cross Flow VIV RMS a/D - Sheared Current	61
Figure 61.	Vertical Riser Cross Flow VIV Induced Stress – Uniform Current	62
Figure 62.	Vertical Riser Cross Flow VIV Induced Stress – Sheared Current	63
Figure 63.	Riser VIV Snapshots from Simulations with Direct Solver – Case 1, Elevation View.....	66
Figure 64.	Riser VIV Snapshots from Simulations with Direct Solver – Case 1, Top View ...	67
Figure 65.	Comparison of Riser Cross Flow VIV RMS a/D – Case 1	68
Figure 66.	Comparison of Riser Cross Flow VIV RMS a/D – Case 2.....	68
Figure 67.	Riser VIV Snapshots from Simulations with Direct Solver– Case 3, Top: Elevation View, Bottom: Top View	69
Figure 68.	Comparison of Riser Cross Flow VIV RMS a/D – Case 3.....	70
Figure 69.	Riser VIV Snapshots from Simulations with Direct Solver – Case 4, Top: Elevation View, Bottom: Top View	71
Figure 70.	Comparison of Riser Cross Flow VIV RMS a/D – Case 4.....	72

1 Project Description

1.1 Background

Vortex-induced vibration (VIV) is an important issue in the design of deepwater riser systems, including drilling, production and export risers. The VIV can produce a high level of fatigue damage in a relatively short period of time for risers exposed to severe current environments. The wake interference between various risers in the same riser array may also lead to collisions between adjacent risers. As some of the recently discovered reservoirs are located in a water depth near 10,000 ft (3,000 m), it is desirable to develop advanced computational fluid dynamics (CFD) tools that can provide reliable prediction of riser VIV in ultra deep water environments.

Partially driven by the need for offshore oil and gas production in deepwater fields, numerical simulation of riser VIV has been an active research area in recent years. Experiments are sometimes preferable to provide design data and verification. However, deepwater risers have aspect ratios that are so large that model testing is constrained by many factors, such as experimental facility availability and capacity limits, model scale limit, difficulty of current profile generation, and cost and schedule concerns. Under such conditions, CFD simulation provides an attractive alternative to model tests. The advantages of CFD simulation are obvious:

1. It is less sensitive to the riser length, therefore the water depth is not a technical barrier for the CFD approach.
2. Every aspect of the riser VIV phenomenon can be analyzed, including riser global motion behavior, vortex shedding details, drag and lift force components, etc.
3. Complex flow fields (due to the existence of nearby risers or hull structures, for example) and current profiles (such as submerged or bottom currents) can be readily handled.

Note that the deepwater current profiles tend to be more complex than in shallow water. For example, the typical loop current eddies in the Gulf of Mexico are usually submerged several hundred meters underneath the surface, while in some fields in offshore West Africa and offshore Brazil, the current may reverse direction along the water column. Obviously not all of these current profiles can be easily simulated in a wave basin. The CFD approach provides a cost effective alternative to evaluate the riser VIV and related issues under these complex current conditions. With a validated CFD code the complexity of the current profiles can be readily accommodated, usually through changing the far field fluid velocities and boundary conditions. Nevertheless, the disadvantage of the CFD approach is also obvious – it is very time consuming, even with the help of the fastest computers and parallel computational technology.

Many software tools have been developed in the oil and gas industry to perform riser VIV analysis. However, the majority of them are based on empirical formulas, heavily relying on model test data. This approach could provide satisfactory VIV predictions for shallow water risers, where their length over diameter ratio (L/D) is fairly small, and model tests could be easily carried out to provide input data and/or verification. Deepwater risers are likely to have

high order mode vibration in strong currents. Under such conditions, model testing in a wave tank is difficult due to tank size or model scale limitations, while field experiments are feasible but costly. Furthermore, there are some important characteristics associated with deepwater riser VIV yet to be studied and understood, such as:

1. deepwater risers tend to experience multi-mode vibration, therefore it would be overly conservative to assume single-mode lock-in, and
2. the excited modes in deepwater riser VIV could be very high, while higher modes are more sensitive to damping, hence showing strong nonlinear behavior.

In a word, time domain CFD simulations are very promising and appropriate for deepwater riser VIV analysis.

There are numerous experimental and numerical investigations on the subject of a circular cylinder undergoing vortex-induced vibrations (VIV). Blevins (1990) summarized some of the early research work on flow induced vibrations. Govardhan and Williamson (2000) reviewed some experimental assessment of vortex formation modes. Some of the VIV studies on low mass ratio cylinders have been reviewed by Willden and Graham (2004). Various VIV numerical investigations have been reviewed by Dong and Karniadakis (2005). Lucor et al. (2006) reviewed some research work on complex modes. Some existing CFD codes for riser VIV analysis have also been reviewed and compared in Chaplin et al. (2005). Trim et al. (2005) presented experimental details for a long riser under various current conditions. Holmes et al. (2006) used a fully 3D simulation approach to analyze riser VIV and the effect of strakes. Several other existing CFD codes for practical riser VIV analysis were reviewed by Chaplin et al. (2005).

Over the past several years, we have developed a Finite-Analytic Navier-Stokes (FANS) computer code for riser VIV simulations (Chen et al. 2006) at Texas A&M University. Some of the previous applications of this code include:

- 2-D simulations of flow past a fixed riser at high Reynolds numbers,
- surface roughness effects,
- 2-D simulations of elastically mounted risers undergoing VIV at high Reynolds numbers: single isolated riser and arrangements of multiple risers,
- 3-D large eddy simulation of flow past a fixed riser,
- 3-D large eddy simulation of an elastically mounted riser undergoing VIV,
- simulations of an elastically mounted riser outfitted with a fairing, and
- simulations of an elastically mounted riser with helical strakes.

The above simulation results clearly demonstrated the capability of the FANS code for time-domain simulation of VIV responses of 2D and short 3D ($L/D \sim 10$) risers at high Reynolds number with or without VIV suppression devices. In this report, the FANS code has been further extended for 3D simulations of long and flexible marine risers with L/D up to 3,000.

1.2 Present Work

It is well known that the riser VIV responses are affected by many parameters including the Reynolds number, surface roughness, strakes, fairings, 3D sheared currents and ambient turbulence. In order to provide accurate analyses of the VIV phenomena, the Finite-Analytic Navier-Stokes (FANS) numerical method has been employed in conjunction with a chimera domain decomposition approach to investigate the complex deepwater riser VIV induced by various current profiles. As noted earlier, the FANS method has been successfully used for VIV analysis of smooth and roughened risers in uniform currents. In this research, the method has been further extended for the prediction of VIV responses of deepwater risers under both the uniform and sheared current profiles. The simulation results were compared with available experimental data to assess the accuracy of the CFD predictions.

In order to extend the predictive capability of the FANS code from relatively short 3D risers with $L/D \sim 10$ to long 3D risers with $L/D \sim 1,000$, the following numerical investigations have been performed and summarized in this report:

- development of modal solver for riser finite element motion equation,
- development of direct solver for riser finite element motion equation,
- 2-D simulations of flow past a fixed riser at high Reynolds numbers,
- 2-D simulations of flow past a forced motion riser at high Reynolds numbers,
- 3-D simulations of flow past a horizontally positioned riser in uniform current,
- 3-D simulations of flow past a horizontally positioned riser in shear current,
- 3-D simulations of flow past a vertically positioned riser in uniform current,
- 3-D simulations of flow past a vertically positioned riser in shear current,
- validation of FANS simulation results with experimental data, and
- comparison of FANS results with numerical results obtained by commercial codes.

The simulation results clearly demonstrate the capability of the FANS code for accurate prediction of VIV responses of deepwater risers under uniform and sheared currents.

2 Development of Advanced CFD Capabilities

In our previous CFD studies of 3D riser VIV (Chen et al., 2006), the risers were treated as rigid cylinders with relatively short span of the order of $L/D \sim 10$. Although the VIV-induced flow and forces are fully three-dimensional, the risers are allowed to undergo only two-dimensional (y and z) horizontal motions with the same displacements in the spanwise direction. This can be achieved by solving the horizontal displacements in the y and z directions using spanwise-averaged drag and lift forces. For long 3D risers with $L/D \sim O(10^3)$, however, it is necessary to represent the flexible riser as a tensioned beam with different displacements along the spanwise direction. In the present study of VIV responses of flexible deepwater risers, the three-dimensional riser displacements are solved directly using the finite element motion equation with either the modal or direct solvers, as described in the following sections.

2.1 Riser Motion Modal Solver

For a tensioned beam, the motion equation is expressed as equation (1):

$$T \frac{d^2 y}{dx^2} + \frac{dy}{dx} \frac{dT}{dx} - \frac{d^2}{dx^2} \left(EI \frac{d^2 y}{dx^2} \right) + f_y = m \ddot{y} \quad (1)$$

where T is the effective tension, EI is the bending stiffness, f_y is the external force, m is the unit mass of the riser, x is the riser axial direction, and y is perpendicular to the riser. When the riser is positioned horizontally, we have $\frac{dT}{dz} \approx 0$. Because the riser is relatively long ($L/D \sim 1,000$), the effect of EI is negligible. Therefore, equation (1) is simplified as equation (2):

$$T \frac{d^2 y}{dx^2} + f_y = m \ddot{y} \quad (2)$$

The lateral displacement $y(x,t)$ at any time t and position x along the length of the riser may be expressed as the superposition of the modal shapes, or

$$y(x,t) = \sum_i \alpha_i(t) \xi_i(x) \quad (3)$$

where α_i is the modal coefficient, and ξ_i is the modal shape given by equation (4) for a pinned boundary condition at both the riser top and bottom.

$$\xi_i(x) = \sin \frac{i\pi \cdot x}{L} = \sin \lambda_i x \quad (4)$$

Substituting equation (3) into (2), taking the inner product with respect to ξ_j , and noting that $\langle \xi_i * \xi_j \rangle = 0$ for $i \neq j$, and $\xi_i'' = -\lambda_i^2 \xi_i$, we obtain equation (5):

$$m\alpha_j'' + T\lambda_j^2\alpha_j = \frac{\langle f_y * \xi_j \rangle}{\|\xi_j\|^2} \quad (5)$$

where m is the modal mass, $T\lambda_j^2$ is the modal stiffness, and the RHS is the modal excitation force. The modal natural frequency of the tension beam is

$$\omega_j = \sqrt{\frac{T\lambda_j^2}{m}} = j\pi\sqrt{\frac{T}{mL^2}} \quad (6)$$

which is the same as the standard solution of a taut string.

Once we have f_y at each time step, the modal coefficient α_j is solved using equation (5). The lateral displacement $y(x,t)$ is then calculated through modal superposition. Note that the RHS of equation (5) will be integrated in the y and z directions separately to give the modal excitation forces in the in-line and cross flow directions. Hence equation (5) is solved in both y and z directions individually for the modal responses in the in-line and cross flow directions. No artificial or structural damping is included, although they can be included by adding a damping term to Equation (1) and following the same procedures to derive the equivalent form of Equation (5). We used the 4th order Runge-Kutta method to integrate equation (5). This scheme is explicit and stable for small time step integrations, such as the cases considered here.

The VIV induced stress at the pipe outer diameter can be calculated as $\sigma(x,t) = \frac{ED_o}{2} y''(x,t)$, where E is the Young's modulus. Therefore, the following equation can be derived:

$$\sigma(x,t) = \frac{ED_o}{2} \sum_i \alpha_i \lambda_i^2 \xi_i \quad (7)$$

Once the stress time histories are known, the VIV-induced fatigue may be estimated through either the simplified rms-Tz formula or the Rain Flow Counting technique.

2.2 Riser Motion Direct Solver

The riser deflections can also be calculated directly by integrating the structural accelerations in equation (1) at each elevation and time step without introducing the modal decomposition. In this approach, the riser equation of motion (1) is discretized in time and space, resulting in equation (8) using the finite difference method:

$$\frac{EI}{h^4} x_{j-2}^n - \left(\frac{T_j}{h^2} - \frac{w_j}{2h} + \frac{4EI}{h^4} \right) x_{j-1}^n + \left(\frac{2T_j}{h^2} + \frac{6EI}{h^4} + \frac{m}{\tau^2} \right) x_j^n - \left(\frac{T_j}{h^2} + \frac{w_j}{2h} + \frac{4EI}{h^4} \right) x_{j+1}^n + \frac{EI}{h^4} x_{j+2}^n = RHS_j^n \quad (8)$$

with

$$RHS_j^n = f_{x_j}^n + \frac{2m}{\tau^2} x_j^{n-1} - \frac{m}{\tau^2} x_j^{n-2}$$

where h is the riser segment length, τ is the time step, and n is the segment node number. It is an implicit scheme, and its Von Neumann stabilities are verified for two different EI values, as shown in Figure 1. The plot shows the amplification factor $|G|$ is always less than or equal to 1.0. Therefore, the scheme is unconditionally stable.

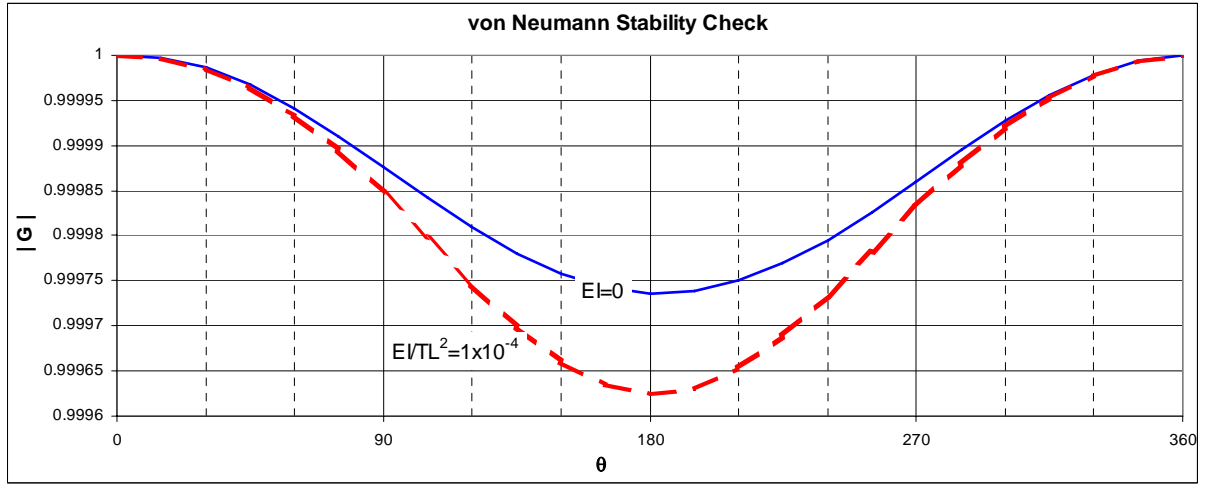


Figure 1. Von Neumann Stability of the Riser Motion Direct Solver

Equation (8) is a linear equation system with dimension of N , where N is the number of segments along the riser axial direction. The matrix on the LHS of the equation is $N \times N$ and with a bandwidth of 5. It is then inverted by a simple LU decomposition method for a banded matrix.

In the present study, the risers are assumed to have pinned connections at the two ends. Other boundary conditions could also be applied by modifying the equations of motion at the boundary nodes. No structural damping was included.

3 2D Simulations of Flow Past a Fixed/Vibrating Riser

3.1 General Description

Interference is an important design consideration for deepwater applications. In many design practices no collisions are allowed between objects such as risers, flowlines, umbilicals, tendons/mooring lines, and hull structures. Among them interference between top tensioned risers is of particular interest. The reason is that a top tensioned riser array has strict limitations on surface wellhead layout and subsea wellhead layout. When the water depth is on the order of 10,000 ft or greater, the riser string experiences much larger lateral displacement due to the current force. To avoid riser clashing, a very large subsea wellhead pattern might be required. This would impose challenges to riser system design, especially when a large number of top tensioned risers is planned.

In the conventional design approach, riser interference analysis is usually carried out quasi-statically. The wake field behind the upstream riser is calculated by Huse's formula [Huse 1993, 1996]. The VIV induced drag coefficient amplification of the upstream riser is approximated by multiplying the base drag coefficient by an amplification factor. Furthermore, an effective drag diameter is used to calculate the wake field behind the upstream riser undergoing VIV. This approach is simple and straightforward. However, it might also introduce conservatism and uncertainty into the design. Consequently, it is desirable to evaluate the VIV effect on the upstream riser effective drag coefficient and wake field using the advanced CFD tools.

The analysis results presented in this section serve the following purposes:

1. compare the wake flow field to the experimental data (Huse's formula) and validate the data grids and CFD approach,
2. examine localized features of the detailed flow fields that are not included in Huse's formula, and
3. provide a riser interference example case and illustrate the significance of the findings.

In this simulation, the effective drag coefficients and wake fields are obtained for both fixed and vibrating risers. The Reynolds number was chosen as 3×10^5 . A study case is selected with typical Gulf of Mexico 10-year loop current and a typical single casing production riser. The riser system data, including air weight, submerged weight, and top tensions, are then presented. In the example case, the riser interference analysis is performed based on the obtained effective drag coefficients, and the results are compared to those obtained by Huse's formula.

3.2 Data Grid

The overset grid (Chimera) technique provides an effective way to handle riser movement. Figures 2 and 3 show the data grids used in this study. The body grid has a dimension of 182 (azimuthal) \times 41 (radial) \times 12 (elevations), while the background grid has a dimension of 201 (parallel to current) \times 101 (transverse to current) \times 12 (elevations). The data grids have been delicately generated with very fine grid sizes inside the riser boundary layer and vortex shedding zones. Previous validation of the data grids can be found in Pontaza and Chen (2004). The body grid and background grid are overlapped to an extent such that these two grid sets can “communicate” with each other efficiently and accurately. The overlapping region depends on the instantaneous riser position, and is dynamically determined at each time step.

The data grids are normalized by the characteristic length, which is chosen as the riser outer diameter (OD). Therefore, these data grids are generic and applicable to problems with different riser sizes and far field velocity. The background grid covers a region of 20 times the OD in the flow direction, and 14 times the OD in the transverse direction. The simulation starts with an initial uniform flow on the background data grid, and reaches a relatively periodic state after a period of transitional flow.

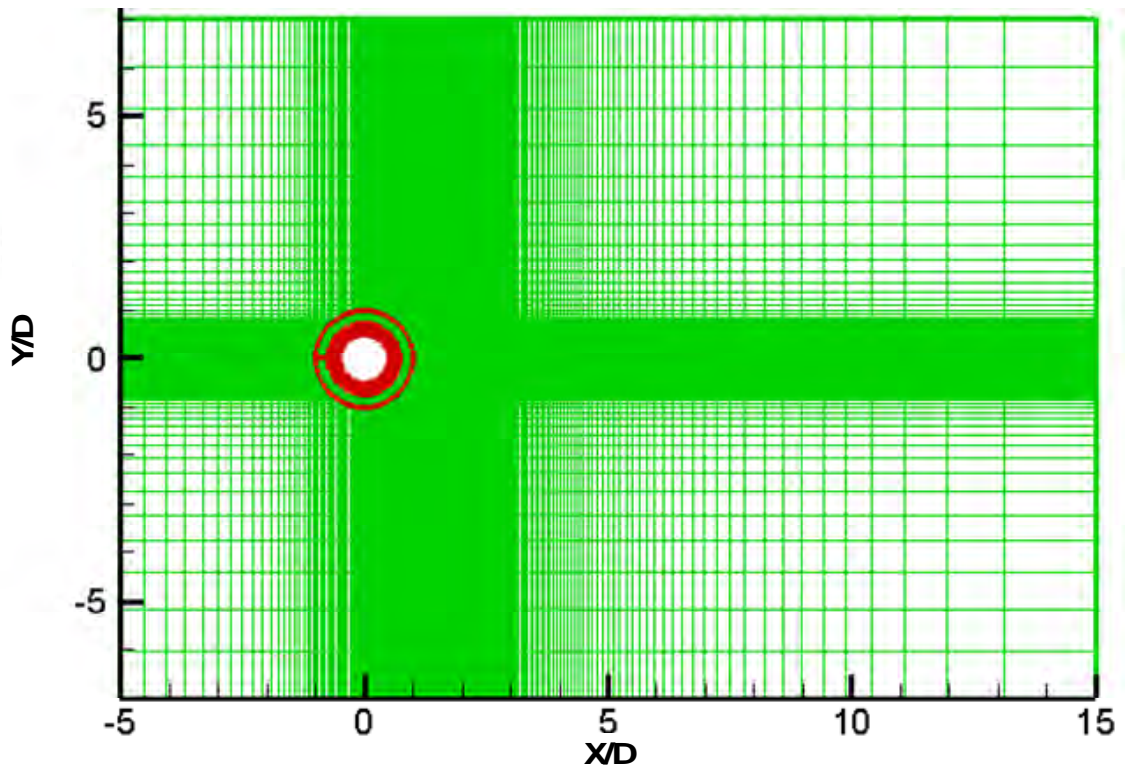


Figure 2. Overset Grid for Wake Field Computation

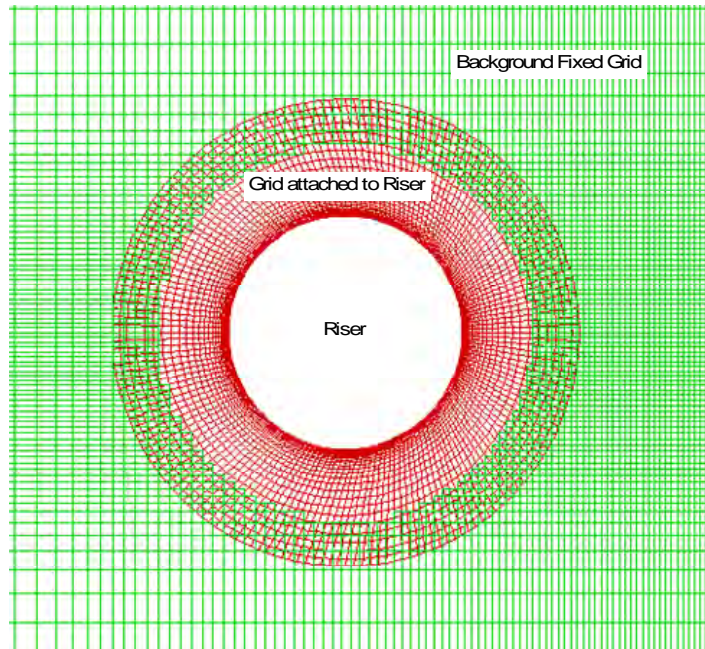


Figure 3. Overset Grid for Wake Field Computation – Vicinity of Riser Surface

3.3 Riser Interference Analysis Procedures

The riser interference is checked by using a quasi-static approach under a typical 10-year loop current profile in the Gulf of Mexico. The effective drag coefficients of the downstream risers are calculated based on the obtained wake field. Details of the analysis procedures are shown in Figure 4. Since at the outset both the downstream riser deflection and the effective drag coefficients are unknown, initial assumptions are needed to start the iterations. The riser string is divided into small segments. Each segment has its own effective drag coefficient, which is calculated based on Huse's formula or the CFD approach. Both of them are used in this section, and the results are compared as well. In the CFD approach, it is more accurate to position two risers in the same computational domain and compute the effective drag coefficients on both risers directly, as illustrated in Pontaza et al. (2005a). However, this would require a CFD simulation for each different riser position pair, requiring significantly more computational effort. Hence, this latter approach is not adopted here.

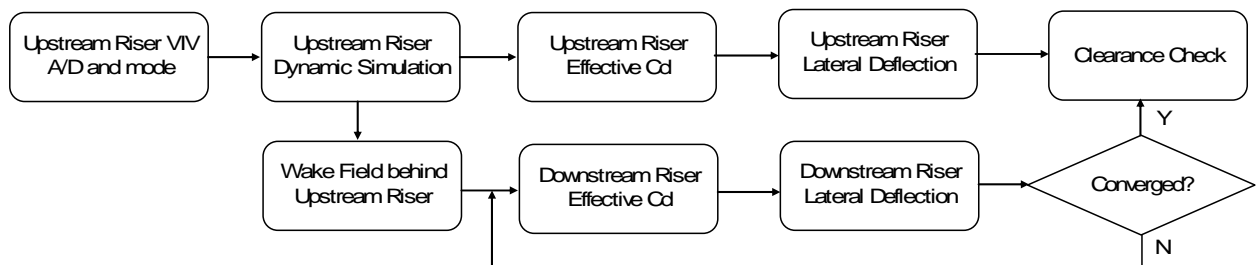


Figure 4. Flow Chart for Riser Interference Analysis

3.4 CFD Simulation Results

A typical 10 3/4" single casing production riser has been sized for 10,000 ft water depth as shown in Table 1. Conventional hydro-pneumatic tensioners are assumed. More details of this ultra deepwater riser system can be found in Huang (2005).

Table 1. 10 3/4" Riser Top Tensions

Riser Type	Riser Mode	Nominal T _o (kips)	Wet Wt (kips)	TF
10 3/4" Single Casing Riser	Normal Operating	1026	769	1.34
	Well Killed	1350	1036	1.31

The riser clearance is checked in a 10-yr loop current condition in the Gulf of Mexico. The current profile has a maximum speed of about 3 knots at 1,500 ft below the mean sea surface. In this section the upstream riser VIV amplitude-to-diameter ratio (A/D) and frequency are calculated by using a separate VIV analysis tool as:

- Single mode excited: 86th,
- A/D = 0.28,
- Frequency = 1.6 Hz.

The upstream riser is assumed to be in heavy mode (well killed) and undergoing VIV. The downstream riser is assumed in normal operating condition and without VIV. A typical riser spacing at the topsides wellbay is used. The riser spacing on the sea floor is usually a design parameter. Here, we chose this parameter based on previous TLP project experience with water depth extrapolation.

Simulations have shown a rapidly varying effective drag coefficient within each vortex shedding and riser vibration cycle. Considering the varying frequency is high, the riser vibration amplitude in the current plane (in-line vibration) is expected to be small. Therefore, time averaged mean drag coefficients are used to calculate the riser deflections. This quasi-static approach is valid if the clearance satisfies a certain minimum value.

Wake Field behind a Fixed Cylinder

Figure 5 shows the flow field vorticity contours for a fixed riser. Figures 6 and 7 show the comparisons of the wake field velocity distributions obtained by Huse's formula and the CFD approach. The comparisons show very good agreement. It also confirms the validity of the CFD approach. Figure 8 provides the time history of the effective drag coefficient. It has a mean value of 1.0, which is consistent with the published Cd vs Re curve and design codes such as API RP 2RD.

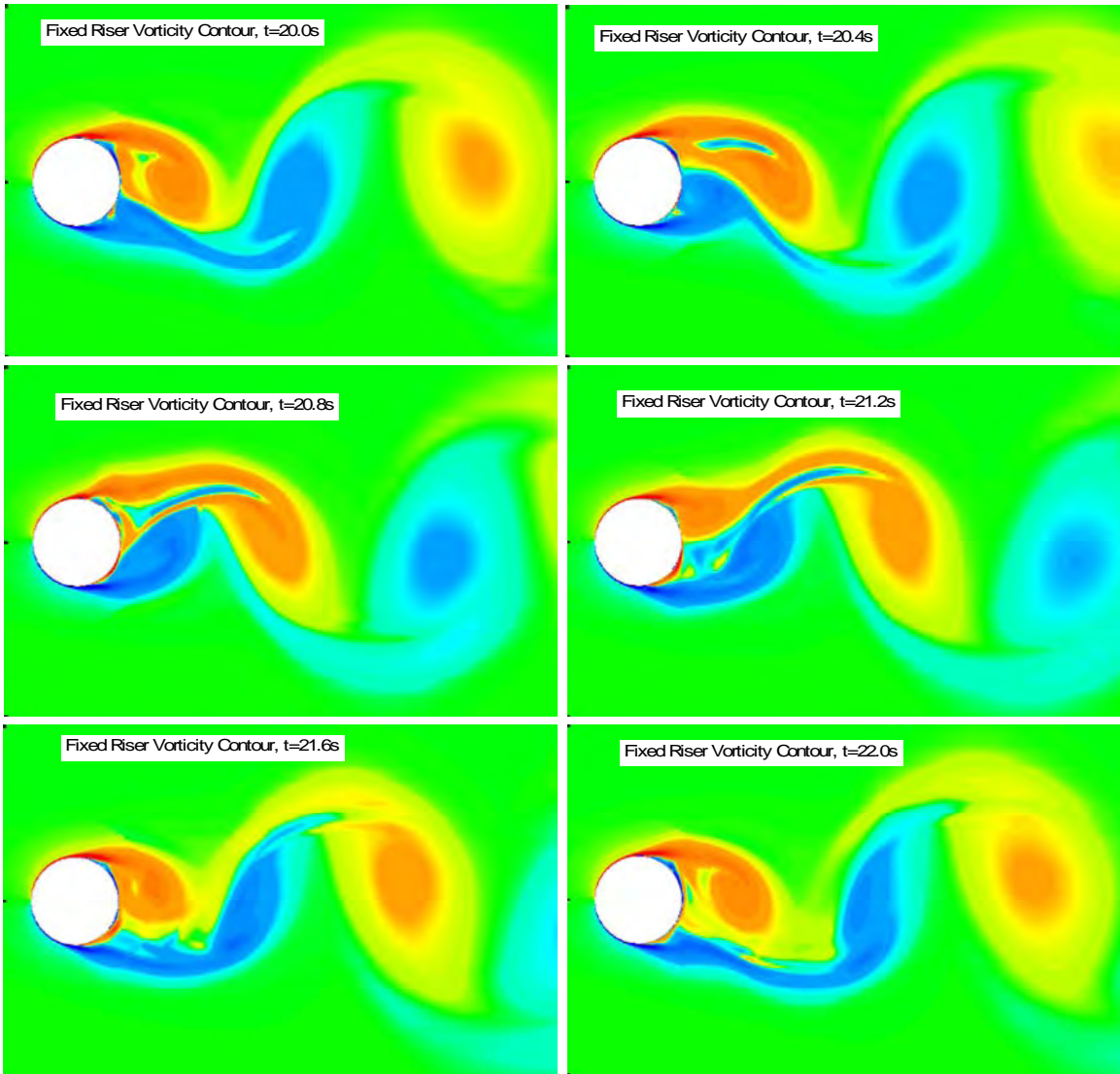


Figure 5. Vorticity Contours for a Fixed Riser

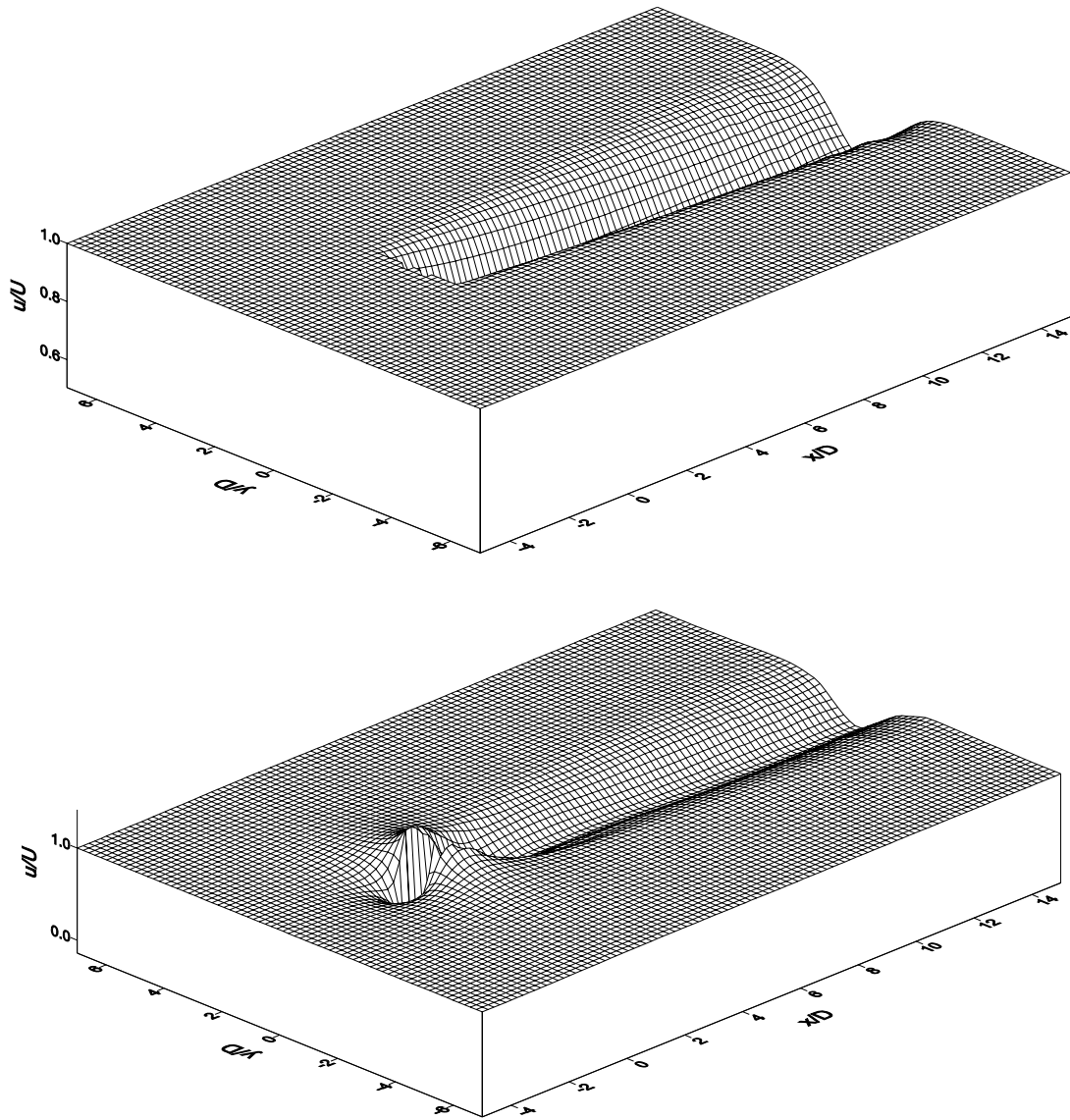


Figure 6. Fixed Riser Wake Field In-line Velocity 3D View – Top: Huse's Formula, Bottom: CFD Result

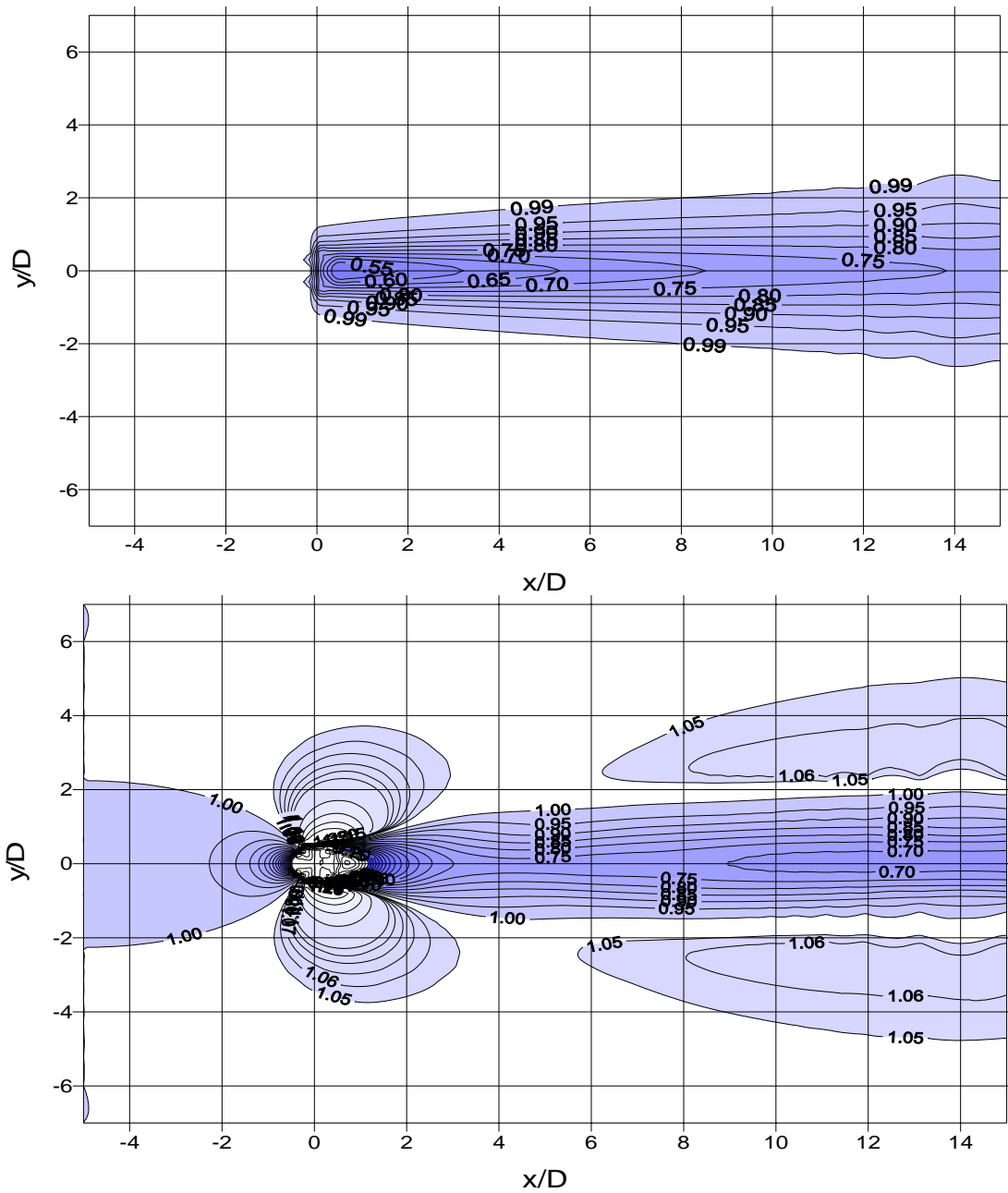


Figure 7. Fixed Riser Wake Field In-line Velocity Contours – Top: Huse's Formula, Bottom: CFD Result

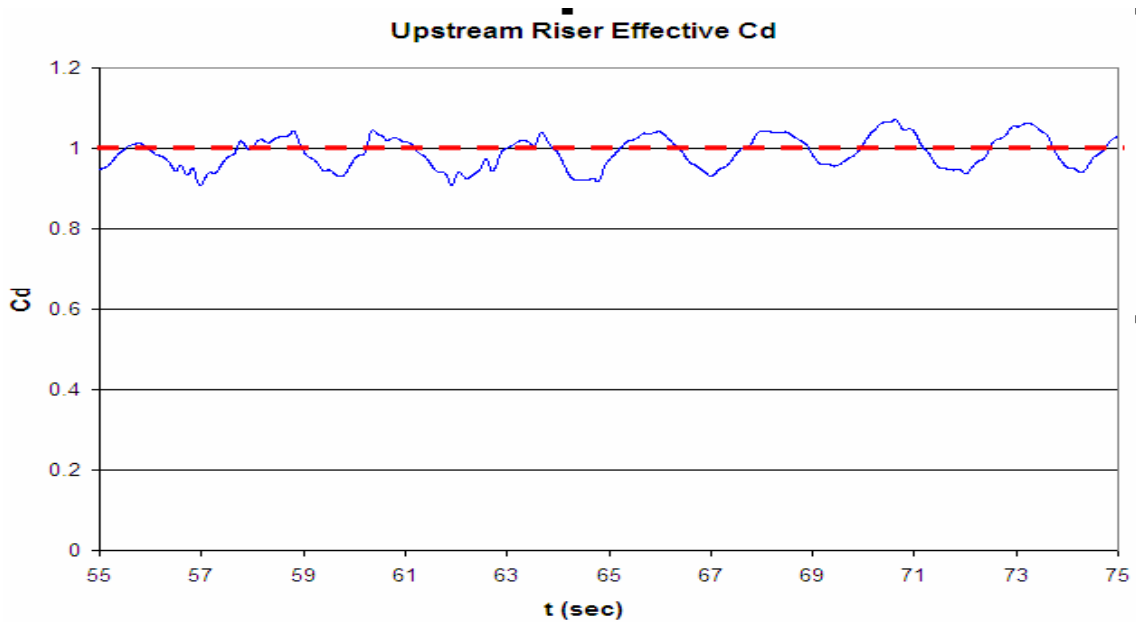


Figure 8. Effective Drag Coefficient for a Fixed Riser

Wake Field behind a Cylinder Undergoing VIV

Figure 9 shows the flow field vorticity contours for the vibrating riser. Figure 10 shows the wake field velocity distributions. The observations are as follows:

1. The wake half-width is not sensitive to the riser VIV, at least when A/D does not exceed the order of 1.
2. The fluid velocity directly behind the riser is slightly lower than for the fixed riser case. In other words, the wake velocity at the center line $y = 0$ increases slightly when the riser vibrates.
3. The fluid velocity is higher than the far field inlet current speed in the regions $y < -2D$ and $y > 2D$. As a result, the downstream riser would be subject to a higher drag force at these regions, which alleviates the riser interference problem.

Figure 11 presents the effective drag coefficient time history. The drag coefficient varies at the riser vibration frequency, with values ranging from 0.5 to 2.8. The drag force variation is mainly due to the pressure zone shifting on the riser surface. The averaged mean value of 1.37 is then used for the upstream riser with VIV.

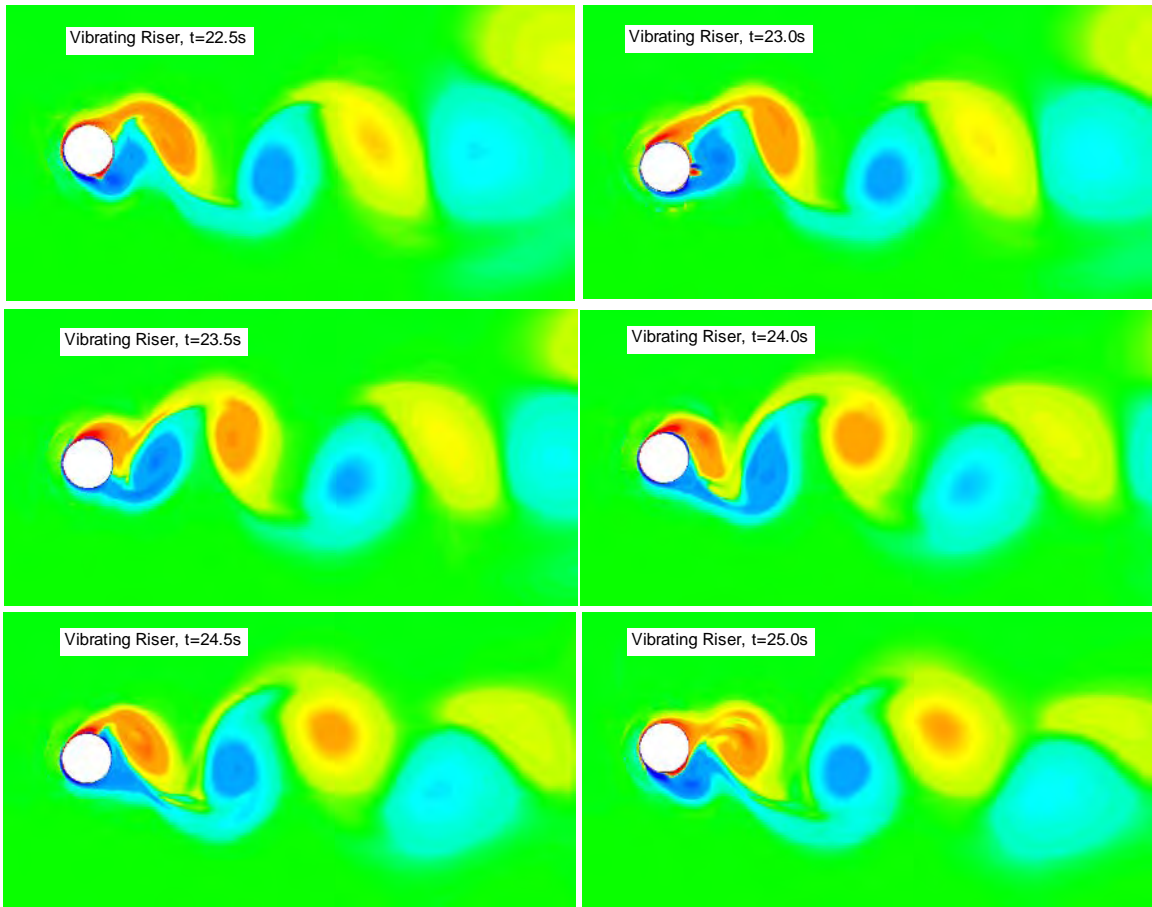


Figure 9. Vorticity Contours for a Vibrating Riser

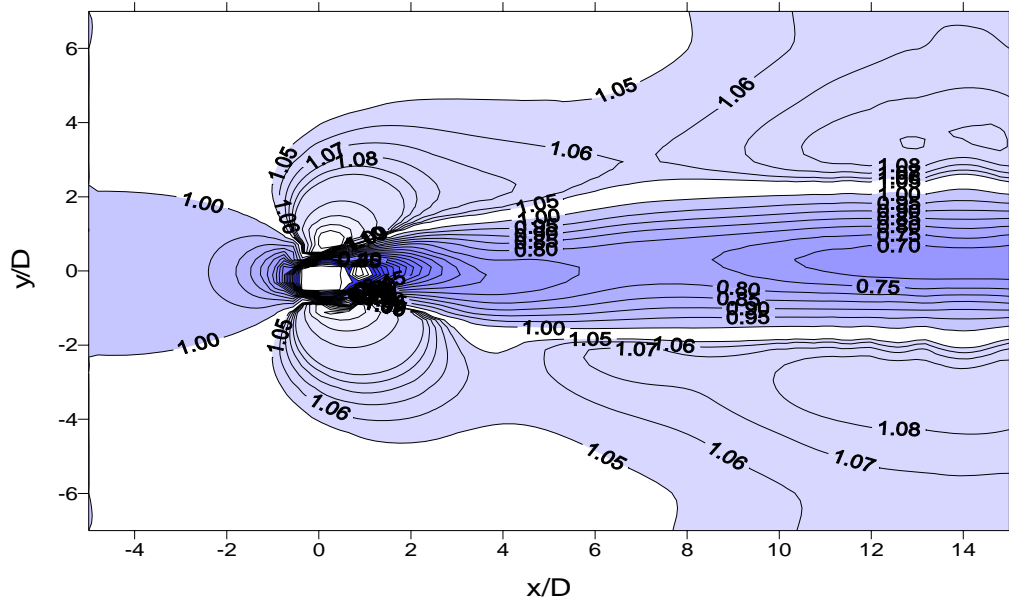
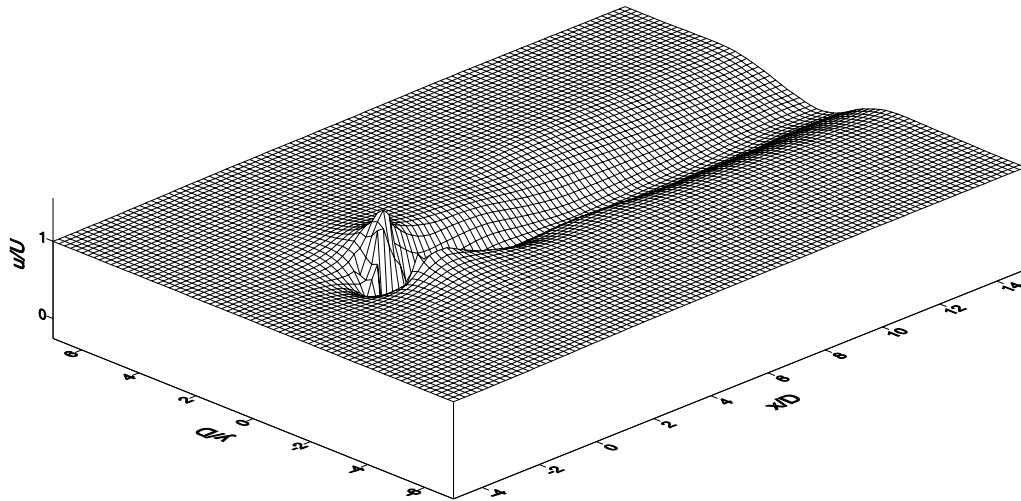


Figure 10. Wake Field In-line Velocity Distribution behind a Vibrating Riser

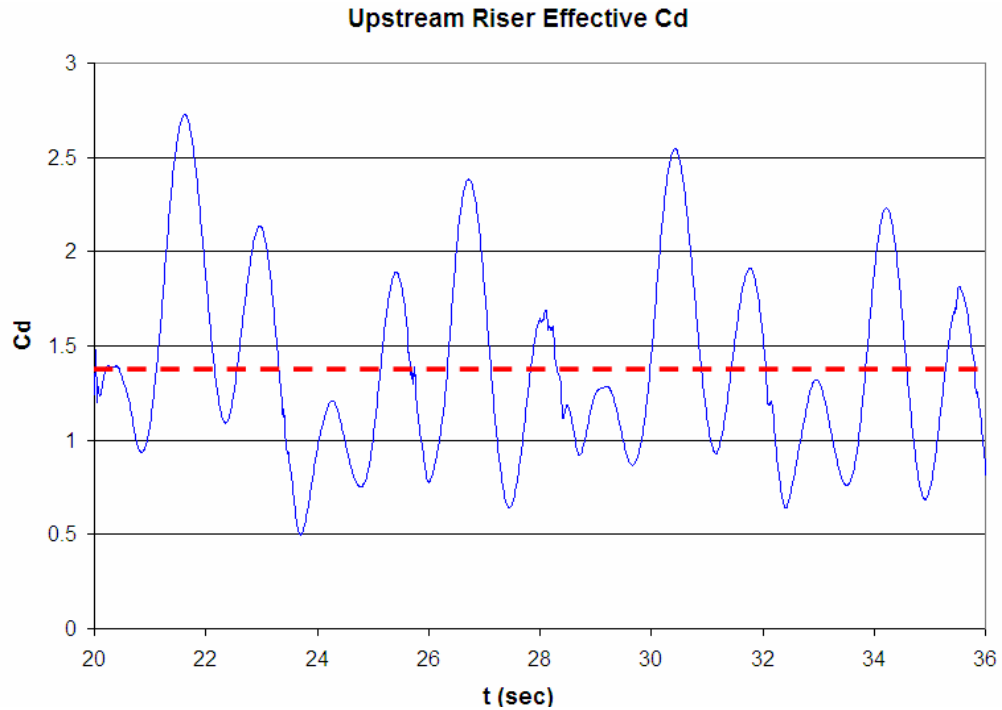


Figure 11. Effective Drag Coefficient for a Vibrating Riser

Riser Clearance Check Results

Riser clearance has been checked in a 10-yr loop current based on the methodology presented in the previous sections. The riser string is modeled with about 400 elements of different sizes. Fine elements have been used on the specialty joints and transitional sections. Figures 12 and 13 show the riser lateral displacements obtained from Huse's formula and the CFD method, respectively. It is found that for the same riser arrangement, Huse's formula predicts a negative clearance (collision occurs), while the CFD approach predicts a narrow positive clearance (no collision). This is critical since the potential collision is very difficult to avoid by simply increasing the riser spacing on the sea floor. Without using the CFD approach, it would be impossible to demonstrate the designed riser system has sufficient clearance up to 10-yr loop current conditions.

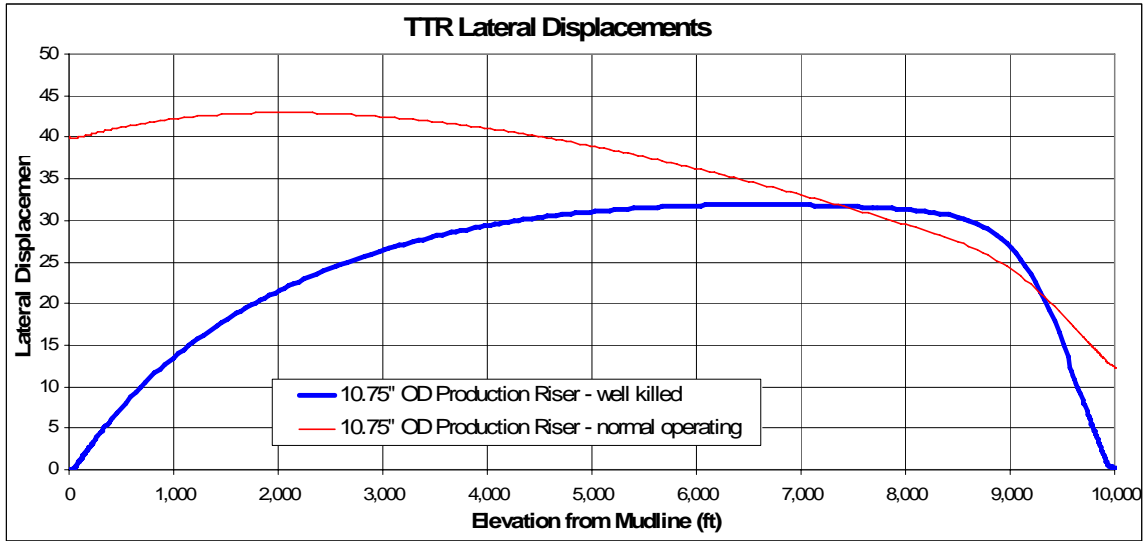


Figure 12. Riser Displacement along Riser – Huse’s Formula

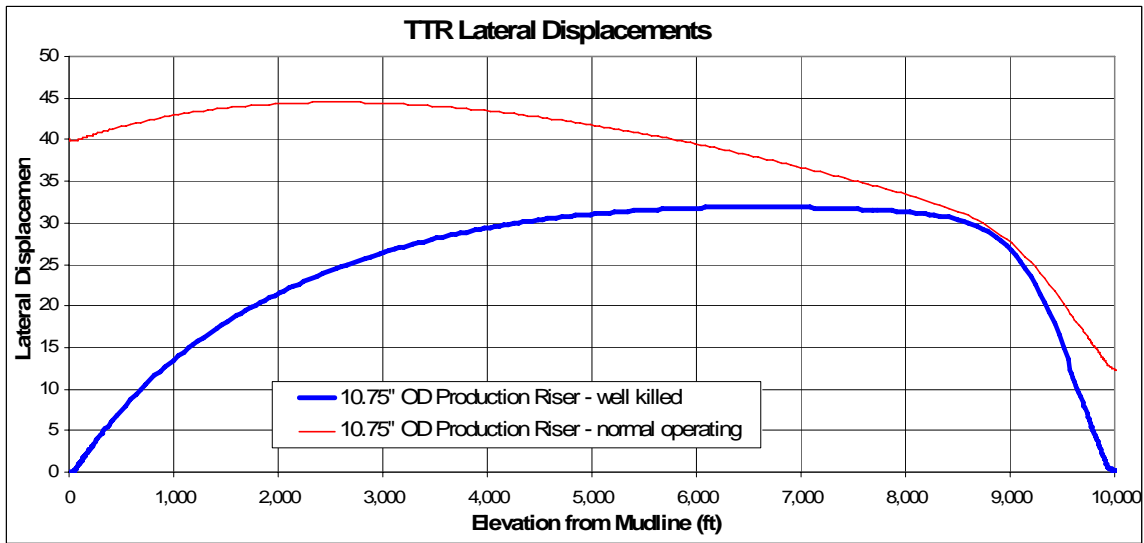


Figure 13. Riser Displacement along Riser – FANS

3.5 Discussion

This section preliminarily studied the ultra deepwater riser interference by using an unsteady, overset-grid (Chimera), incompressible Navier-Stokes (RANS) method. It is found that risers can have very large lateral deflections in strong and deep currents, and riser interference can impose serious challenges to riser system design. Under certain design conditions, such as the 10-yr loop current eddy studied in this section, the riser interference results are sensitive to drag coefficients. Therefore, accurate assessment of the effective drag

coefficients on both the upstream and downstream risers becomes critical. The CFD time domain simulation approach has predicted a narrow wake field and a high-speed zone outside the wake field. Both of these features positively affect the interference results. It is also indicated that the “no collision” design criteria may be satisfied up to 10-yr extreme current events in ultra deep water riser systems.

In conclusion, the FANS code can be applied to ultra deepwater riser interference analysis and its validity and effectiveness have been demonstrated through a case study.

4 3D VIV Simulations of a Horizontal Riser in Uniform Current

4.1 General Description

Recently experiments on a long riser ($L/D = 1400$) have been conducted at Marintek's Ocean Basin in Trondheim (Trim et al. 2005). Figure 14 is a schematic plan view of the test setup. The riser model has a mass ratio of 1.6 and a length of 38 m. It is towed through the wave basin to generate the desired current (relative velocity) condition. The testing was performed under two different current conditions: uniform and sheared current. Some experimental data are published in Trim's paper (2005). This VIV experiment has generated considerable interest since it provides detailed results of riser VIV with large L/D .

As the offshore oil and gas industry is progressing toward the development of ultra deepwater fields, it is of particular importance to disclose and understand the characteristics of long riser VIV for field development and riser system design. Model testing is generally a favorable approach to provide design data and verification. However, it does have its limitations too, such as facility availability and capacity limits, model scale limit, difficulty of current profile generation, cost concerns, etc. Under such conditions, CFD provides a valuable alternative to model testing.

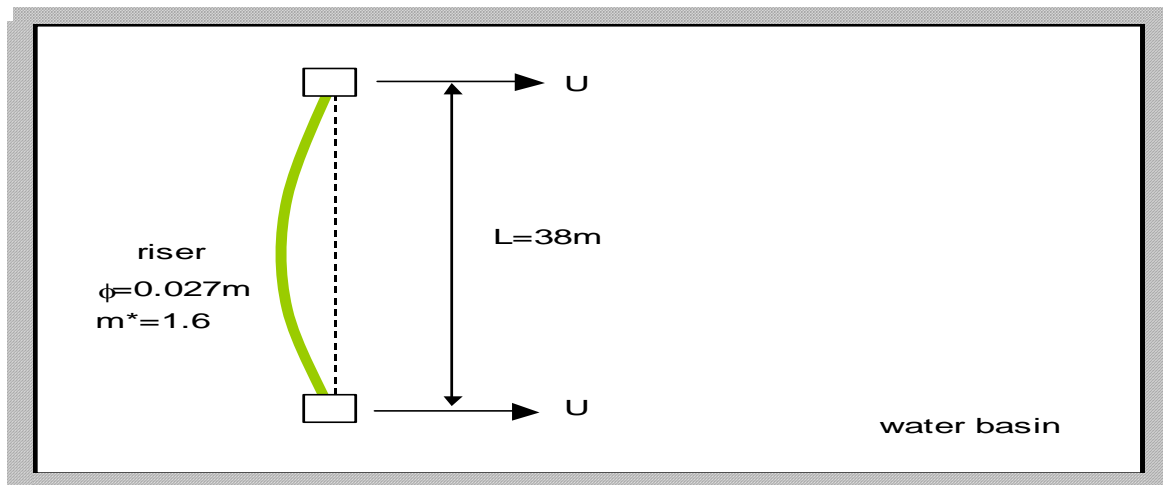


Figure 14. Plan View of Riser VIV Test Setup

Time-domain simulation of fully 3D riser VIV has been a formidable task due to the required computational effort. However, significant progress has been made recently with the help of ever increasing computational power and storage space. Currently a computational fluid domain with about 1 million elements can be practically handled by single processor personal computers, and clusters have also been used for large-scale simulations with significantly more elements. Some recent fully 3D CFD simulations of riser VIV (Holmes et al. 2006) have attempted to use element numbers in the order of 10 million. They have used unstructured data

grids, achieved reasonably good results, and demonstrated the possibility of calculating riser VIV using the full 3D CFD approach.

In this section we intend to further demonstrate that the VIV of a long riser can also be analyzed using the Chimera (overset grid) technique embedded CFD approach. This method has been previously validated and applied to different riser VIV studies (Pontaza, Chen & Chen, 2004, 2005a, 2005b; Pontaza, Chen & Reddy, 2005; Pontaza & Chen 2006). The Chimera technique is particularly well suited for computational fluid dynamics (CFD) simulation involving moving objects such as risers. A very fine data grid (body grid) is attached to the moving riser and embedded in a relatively coarse earth-fixed grid (background grid). When the riser moves, the body grid moves relative to the background grid. The data consistency between the body grid and the background grid in the overlapped region is enforced by data interpolation. Theoretically the data grids can be overlapped and nested in as many levels as desired. In this section, three layers of data grids are used: a body grid, a wake grid, and an artificial (phantom) background grid. By using the Chimera technique, the data grids can be generated with great attention to the details, such as the regions near the riser surface and in the vortex shedding and propagation area, yet without worrying about the re-generation of the data grid at each time step when the riser moves.

As noted earlier, the Finite-Analytic Navier-Stokes (FANS) code developed by Chen et al. (2006) is capable of handling fully 3D CFD problems for risers with L/D in the order of 10. In this section, the FANS code has been further generalized to include a tensioned beam dynamic response model in order to handle the fluid and slender structure interactions. Based on the flexible riser dynamic motion solver, we attempted to apply the FANS code to riser VIV with large L/D ($= 1,400$) in this study. However, to avoid excessive computational time and storage space, we used a fine mesh only at riser sectional planes, while a relatively coarse mesh was used in the riser axial direction. This will maintain the accuracy of the drag force and the lift force while sacrificing the 3D spanwise secondary flow details. In other words, we chose to trade off some of the detailed 3D flow characteristics for computing speed. The drag and lift forces thus obtained are equivalent to the spanwise averaged values for each riser segment. This is acceptable since the riser dynamic response is a global behavior and should be fairly insensitive to the small scale 3D flow details.

For this study the riser is positioned horizontally with uniform sectional properties and constant tension. Its two ends have pinned connection boundary conditions. In such a case the modal shapes of the riser follow sinusoidal functions and are well defined by simple analytic formulae. A uniform current of 0.4 m/s and 0.8 m/s are imposed on the riser respectively, and the riser response is then calculated in the time domain for sufficiently long durations. The simulation results are compared to the published experimental data and other CFD results. Some interesting phenomena regarding the transient flow and motion are also discussed.

It is concluded that the presented CFD analysis approach provides reasonable results of the riser VIV response. Therefore it is suitable for riser VIV analysis with large L/D .

4.2 Analysis Approach

The flow field around a riser is calculated by numerically solving the unsteady, incompressible Navier-Stokes equations. The turbulence flow is solved using Large Eddy Simulation (LES) with a Smagorinsky subgrid-scale turbulence model. The Reynolds numbers are 8×10^3 and 1.7×10^4 for $U = 0.4$ m/s and $U = 0.8$ m/s, respectively. The FANS code has been validated up to a Reynolds number of 1×10^7 (Pontaza, Chen and Reddy, 2005). A detailed description of the governing equations and numerical method used in the FANS code is given in Chen et al. (2006). The governing equations are transformed from physical (x, y, z) space into numerical (ξ, η, γ) space. The continuity equation is then solved by a finite-volume scheme. The transport equations are solved by the finite-analytic method of Chen, Patel and Ju (1990) assuming the pressure field is known. The pressure is then updated by a hybrid PISO/SIMPLER algorithm (Chen and Patel, 1989).

The non-dimensional time step used in the simulation is 0.01, which means the free stream fluid travels a distance of one riser diameter in 100 time steps. The dimensional time steps are about 0.0007 seconds for $U = 0.4$ m/s current, and half of that for $U = 0.8$ m/s current. Considering that both the vortex shedding frequency for the fixed riser and the vibrating frequency of the riser are less than 3 Hz, this time step is sufficiently small.

Overset Grid

The overset grid (Chimera) technique provides an effective way to handle riser movement. Figures 15 and 16 show the structured data grids used in this study. The body grid has a dimension of 182 (azimuthal) \times 41 (radial) \times 30 (elevations), the wake grid has a dimension of 200 (parallel to current) \times 101 (transverse to current) \times 30 (elevations), while the background grid is artificial (i.e., a phantom grid). The phantom background grid provides boundary conditions to the wake grid, but it is not involved in the numerical iterations, therefore it is not shown in the figures. The data grids have a total of slightly less than 1 million elements, and have been delicately generated with very fine grid sizes in the riser boundary layer and vortex shedding zones.

In this study, the wake grid is set to move with the riser, which eliminates the relative movement between the riser body grid and wake grid. As a result, the overlapping region depends only on the riser initial position, and the interpolation coefficients between these two grids need to be determined only once throughout the simulation. Figure 15 illustrates the data grids when the riser is at its initial position (not deflected) and when it is deformed due to current loading. Figure 16 shows the grid details around/along the riser surface.

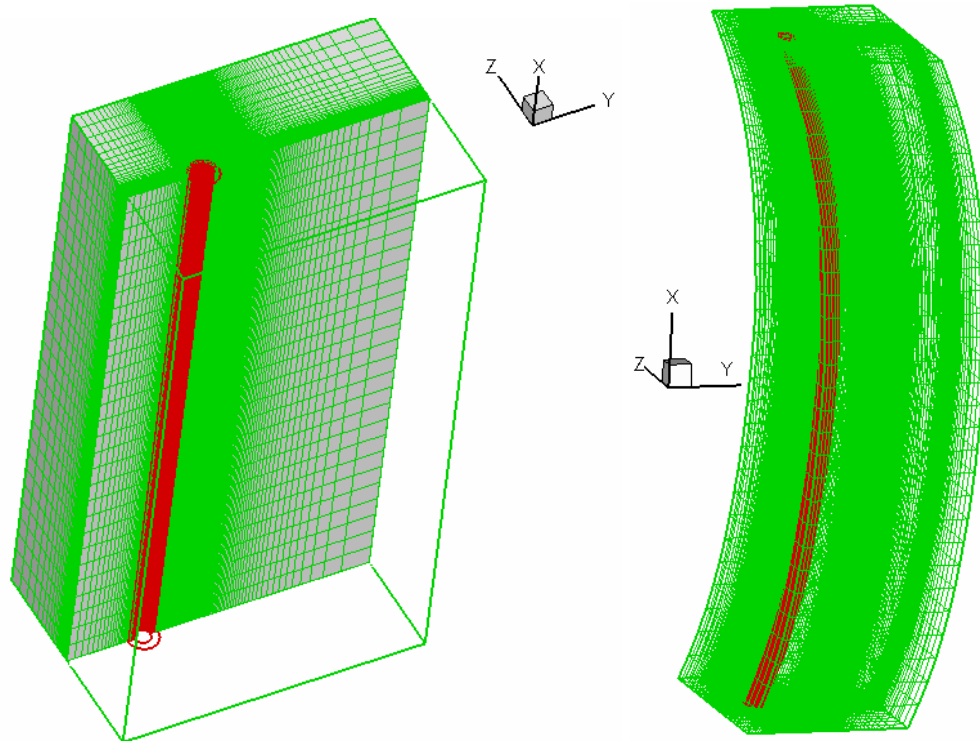


Figure 15. Data Grids in 3D, Left: Undeformed Riser, Right: Deformed Riser

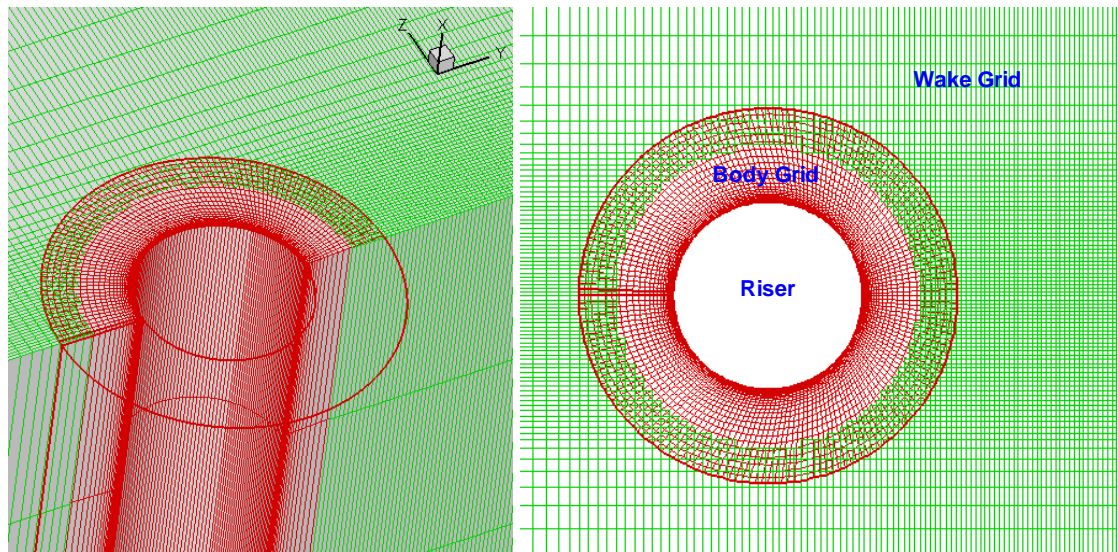


Figure 16. Data Grid near Riser Surface

The simulation starts with an initial uniform flow on the background data grid. The riser deflects toward the current direction until its internal restoring force overcomes the current drag force. After a certain period of transitional dynamics, it then oscillates about its equilibrium position. Both inline and cross flow motions are included in this study.

4.3 Simulation Results

We focused on the uniform current condition in this study, and started the riser VIV simulation with an initially straight riser. Because it is subject to the mean drag force, the riser deflects toward the downstream direction. The maximum riser deflections occur at the middle section, with values of approximately $5D$ and $20D$ for current speed 0.4 m/s and 0.8 m/s respectively. Figure 17 shows the evolution of these deflections and the corresponding vorticity fields around the riser. The results indicate that the riser approaches its equilibrium position after 6,000 time steps (current travels a distance of $60D$), and its inline vibration amplitudes are small compared to the riser mean deflections. The figure also shows the vortex shedding at different locations along the riser can be either in phase or out-of-phase. The majority of the vortex shedding shows a clear 2S pattern. Occasionally coalescence of vortices (C pattern) occurs near the top and bottom regions. This indicates that the riser is self-exciting most of the time throughout the whole riser span.

Figures 18 and 19 present riser and flow field vorticity contour snap shots for $U = 0.4\text{ m/s}$ and 0.8 m/s , respectively. Only 5 sectional planes are shown. The figures confirm that the vortex shedding at different riser sectional stations is synchronized with the riser motions. Furthermore, the figures also illustrate the riser VIV response in 3D, including in-line and cross flow vibrations. It is interesting to see the large riser mean deflections in the flow direction. We noticed that this in-line deflection could affect the riser VIV responses, both in-line VIV and cross flow VIV. To illustrate this, we plotted the 1st mode response time histories in Figure 20 and 21 for $U = 0.4\text{ m/s}$ and 0.8 m/s respectively. These figures show that:

1. The 1st mode amplitude approaches a large mean value, i.e. $5.2D$ for $U = 0.4\text{ m/s}$, and $23.3D$ for $U = 0.8\text{ m/s}$. Note that the mean value increases by approximately 4 times when the current velocity doubles, which is as expected since the current loading is proportional to the square of the speed. Also note that the 1st mode response is different from the riser response. The former is only a component of the latter.
2. The 1st mode amplitude decays very slowly, if it decays at all. It oscillates about its mean value with a standard deviation of $0.4D$ and $1D$ for $U = 0.4\text{ m/s}$ and 0.8 m/s , respectively. Therefore, it seems that the 1st mode dynamics are intrinsic and somewhat proportional to the incoming current speed. These standard deviations are of the same order of magnitude as the riser diameter, and obviously comparable to the in-line and cross flow VIV amplitudes.

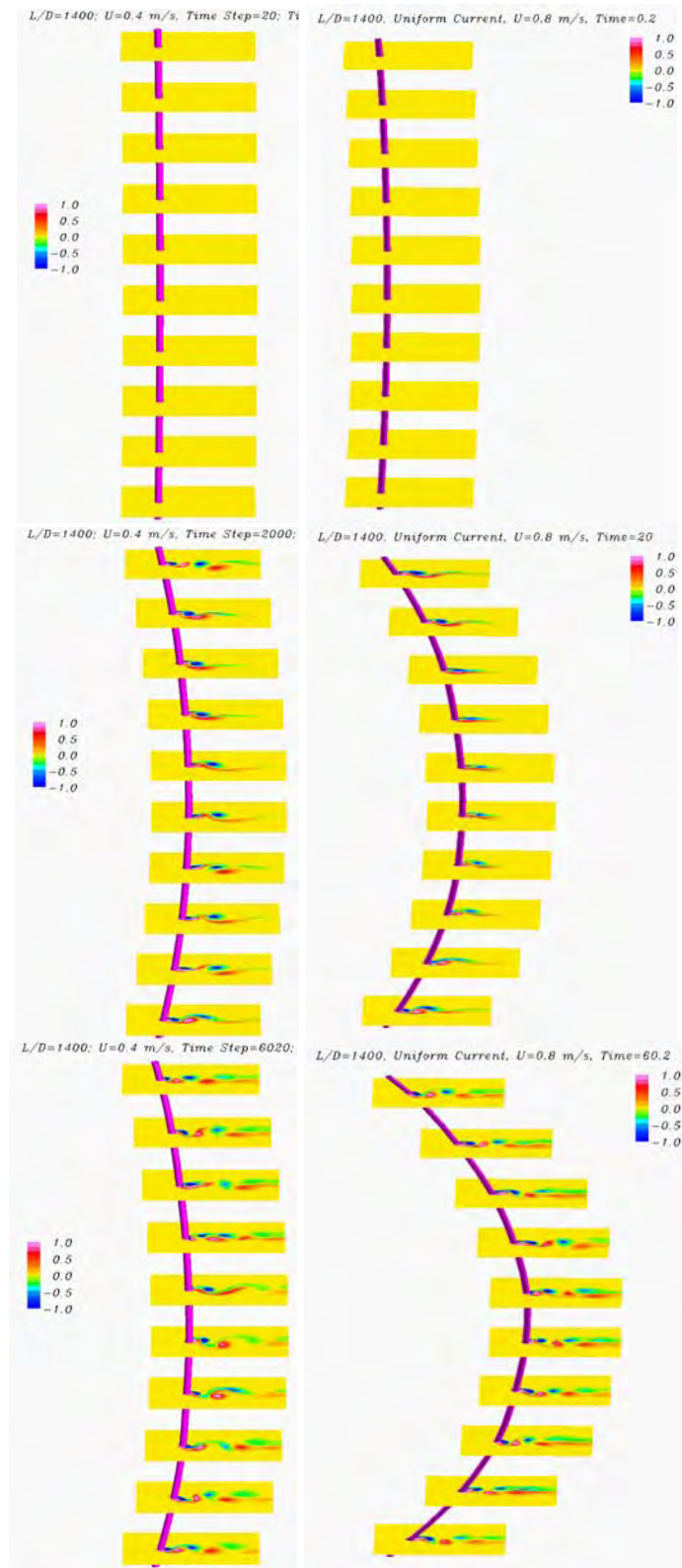


Figure 17. Horizontal Riser VIV Evolution in Uniform Current, Left: $U = 0.4$ m/s, Right: $U = 0.8$ m/s

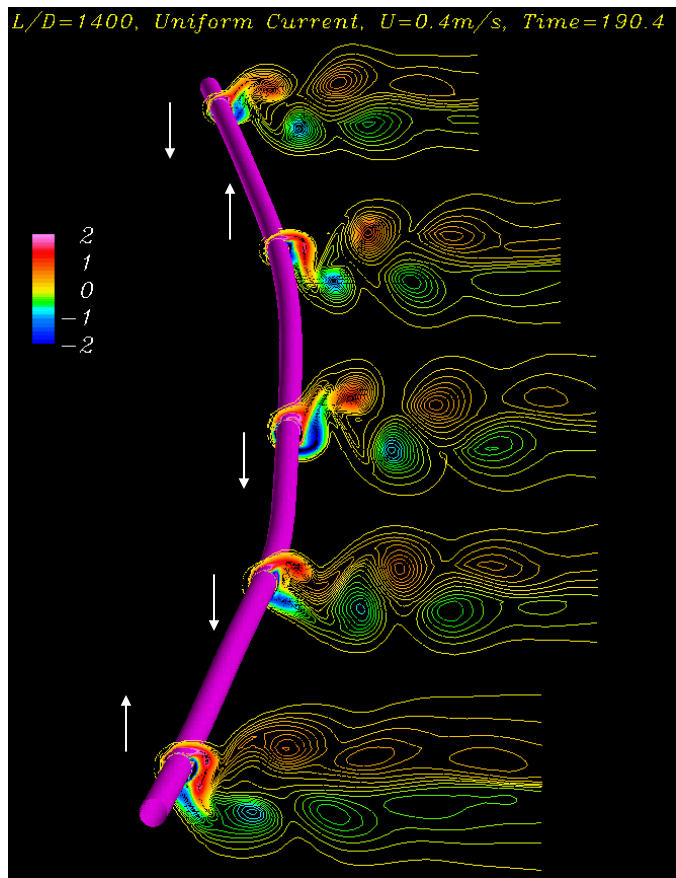


Figure 18. Horizontal Riser VIV Snap Shot - Uniform Current $U = 0.4 \text{ m/s}$

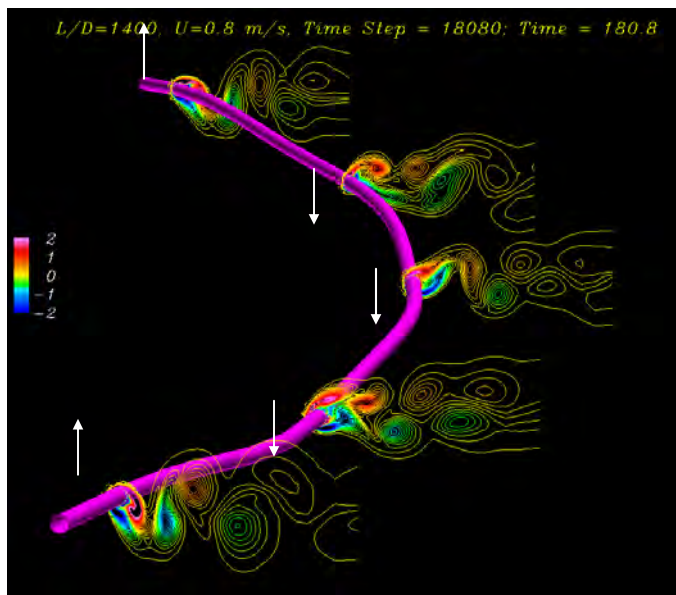


Figure 19. Horizontal Riser VIV Snap Shot - Uniform Current $U = 0.8 \text{ m/s}$

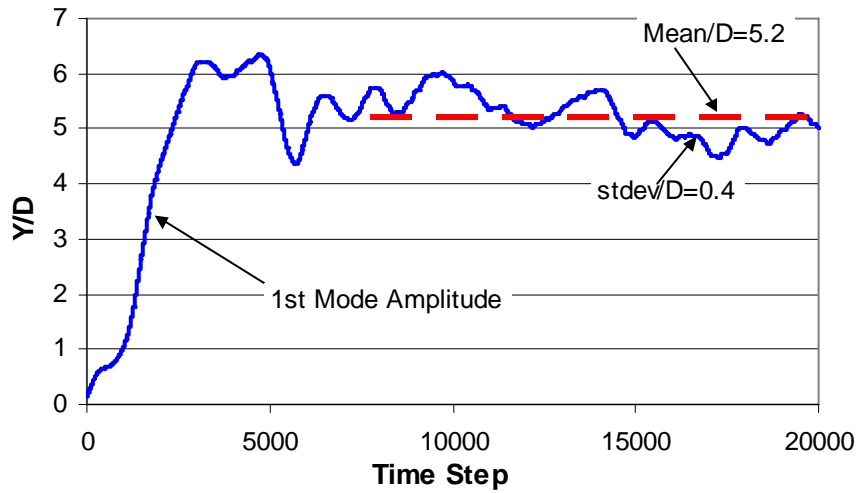


Figure 20. Horizontal Riser In-Line Modal Response – Uniform Current $U = 0.4$ m/s

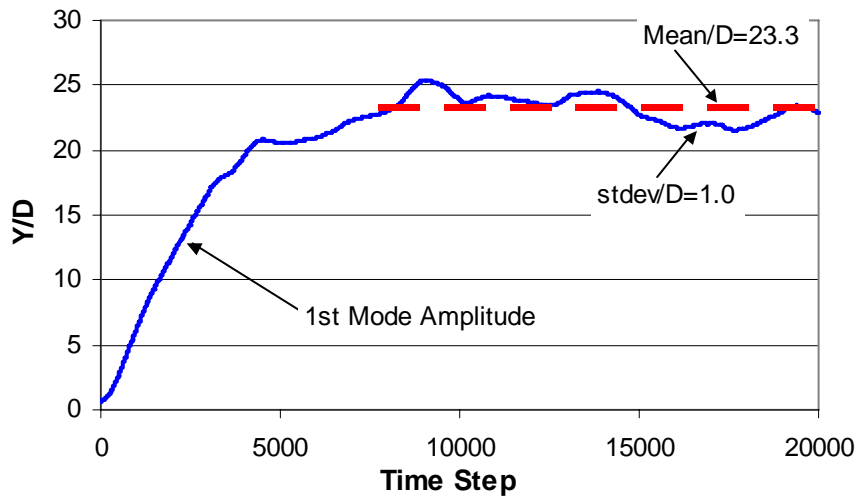


Figure 21. Horizontal Riser In-Line Modal Response – Uniform Current $U = 0.8$ m/s

Other low order modes, i.e. the 2nd and 3rd modes, also show a similar trend. The higher order the mode is, the lower its mean and standard deviation are. The existence of these low order modes complicates the riser VIV phenomenon. This also implies that the riser deflection will influence its own VIV. This effect can easily be studied and evaluated further with the time domain simulation approach.

Drag and Lift Coefficients

Drag and lift coefficients are calculated at each time step along the riser. Figure 22 shows the mean drag coefficient distributions. The drag coefficients are calculated based on the global current velocity and have mean values between 1 and 2.5. By comparing the mean C_d distributions to the riser cross flow VIV amplitude envelopes (shown in Figures 28 and 29), we find they are correlated to each other. The higher the cross flow VIV amplitude is, the higher the averaged C_d is. The results also show that higher current speed does not necessarily cause higher drag coefficients. More details on the effective drag coefficients for risers undergoing VIV can be found in Huang & Chen (2006).

Figure 23 shows the RMS lift coefficient distributions. The lift coefficients tend to have more evenly distributed, but lower, RMS values along the riser at higher current speed. This would explain the observation that the dominant mode response amplitude usually decreases when the current speed increases. In other words, higher order modes are excited in higher speed current, but likely with lower vibration amplitudes.

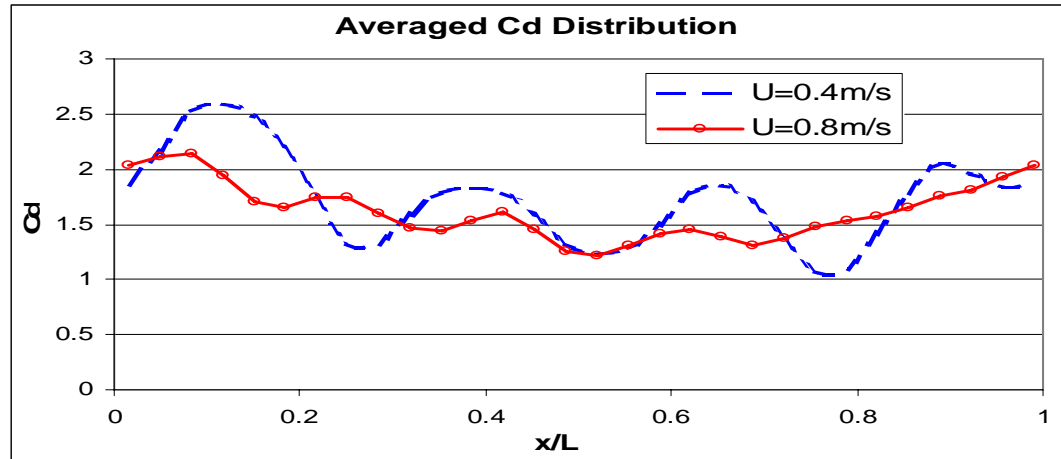


Figure 22. Mean Drag Coefficients for Horizontal Riser VIV in Uniform Current

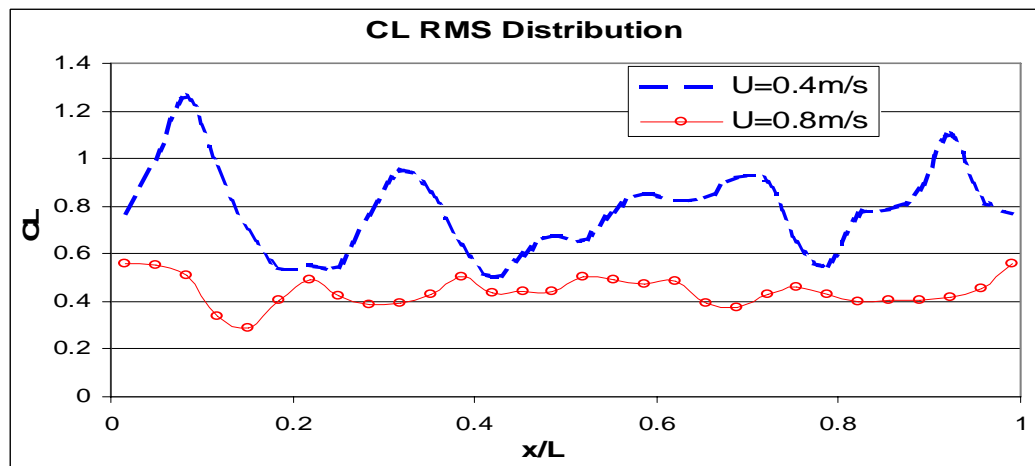


Figure 23. RMS of Lift Coefficients for Horizontal Riser VIV in Uniform Current

Riser Motion Trajectory

Figure 24 shows the riser motion trajectories at different elevations for $U = 0.4$ m/s and 0.8 m/s. The riser is first pushed downstream to a certain distance. It then oscillates laterally in both the in-line and cross flow directions. Note that the mean positions are different at different riser elevations.

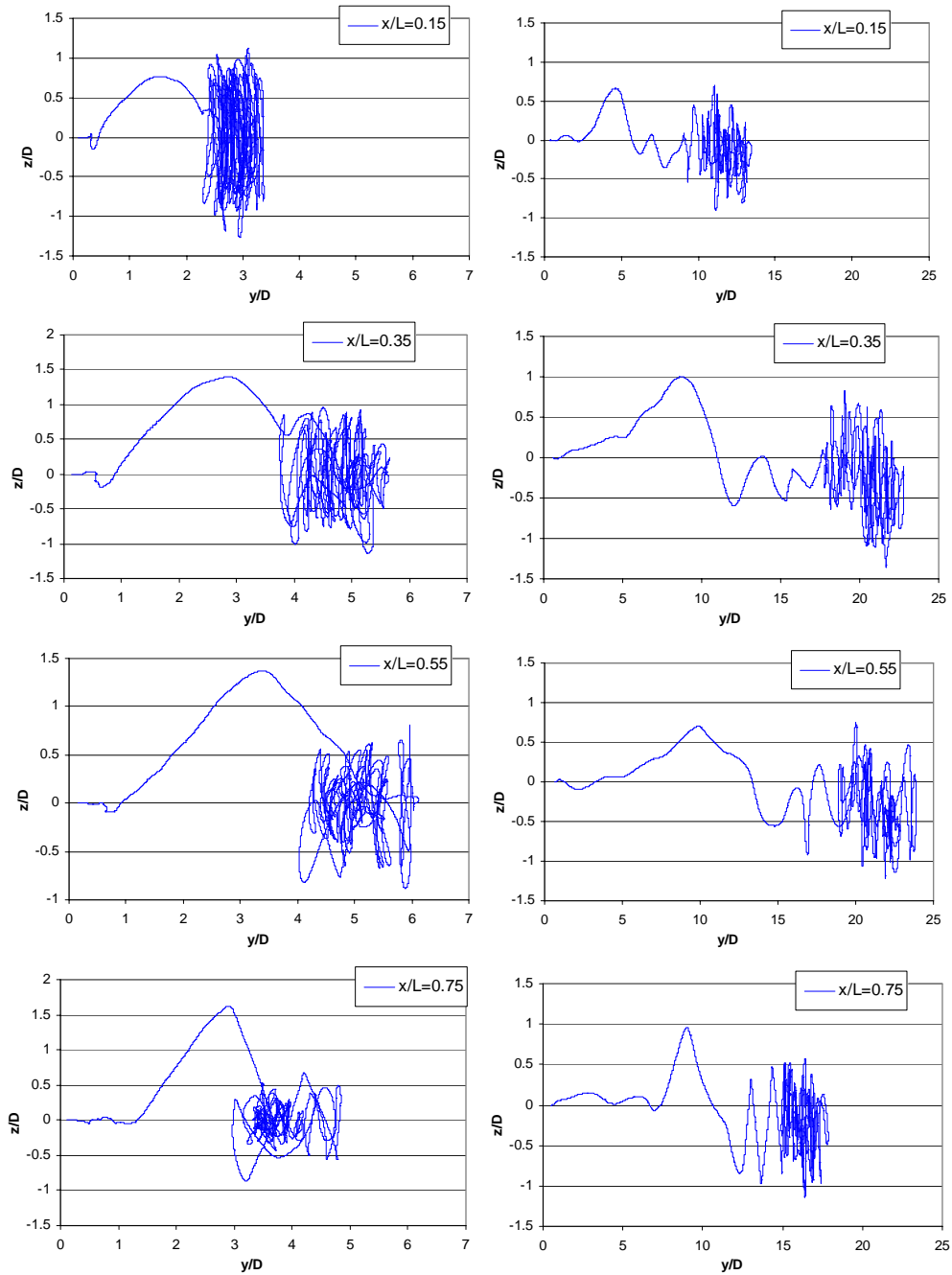


Figure 24. Horizontal Riser Motion Trajectory in Uniform Current, Left: $U=0.4$ m/s, Right: $U=0.8$ m/s

Figures 25 to 27 show the amplified views of the riser motions at $x/L = 0.15, 0.35$ and 0.55 for $U = 0.4$ m/s. The figure “8” movement pattern is clearly observed in the riser top and bottom regions ($x/L \approx 0$ or 1), and is less obvious in the riser middle sections ($x/L \approx 0.5$). A possible reason is the large riser deflection effect as discussed in previous sections. The figure “8” pattern is usually seen in 2D or 3D rigid cylinder VIV simulations, where the cylinder mean C_d is independent of the riser elevation. The mean C_d of a long and flexible riser depends also on the elevation, i.e. x/L . This introduces a more complex pattern of riser in-line movement. On the other hand, when the riser has a large lateral deflection, even a very slight change of drag force could cause the riser’s in-line deflection to fluctuate up to several diameters and break the figure “8” pattern. As a result, the riser motion trajectory pattern is complicated by the riser lateral flexibilities as well.

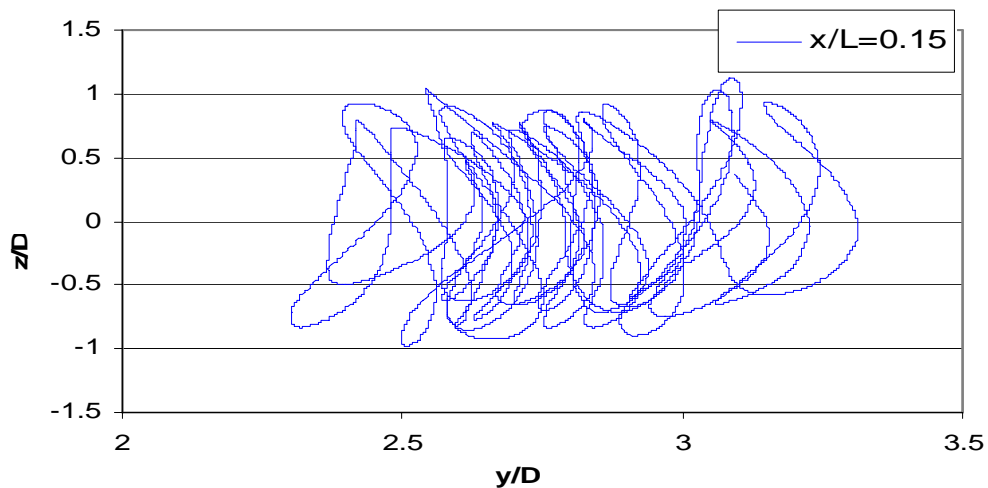


Figure 25. Horizontal Riser Motion Trajectory at $x/L=0.25$ in Uniform Current $U=0.4$ m/s

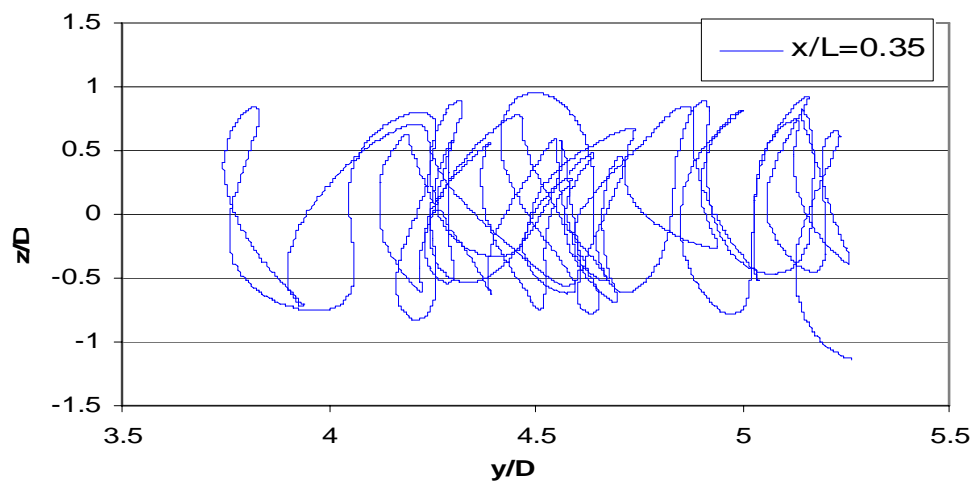


Figure 26. Horizontal Riser Motion Trajectory at $x/L=0.35$ in Uniform Current $U=0.4$ m/s

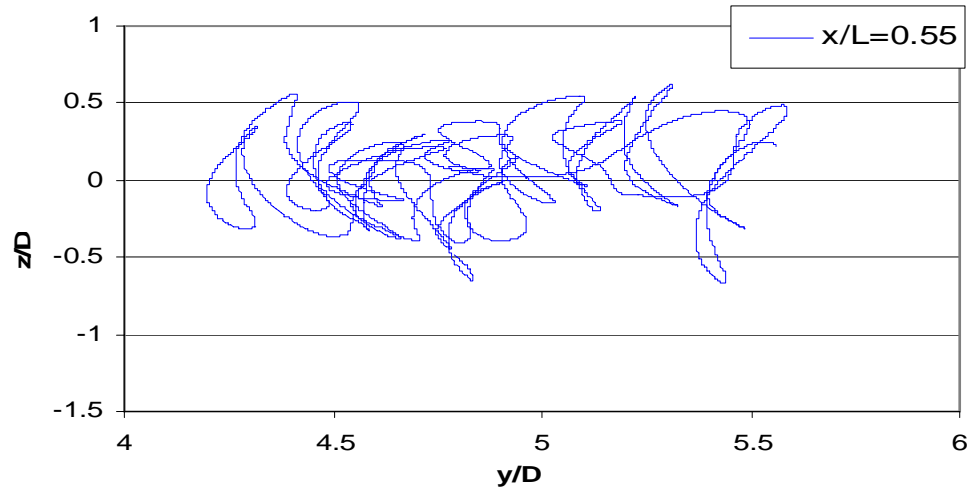


Figure 27. Horizontal Riser Motion Trajectory at $x/L=0.55$ in Uniform Current $U=0.4$ m/s

Riser Motion RMS a/D

Snap shots of the riser cross flow motion are plotted in Figures 28 and 29. They show the envelope of the dominant mode. The responses are not exactly symmetric. This could be due to the interference from the low-mode riser vibrations in both the in-line and cross flow direction, as discussed later in this section. We also plotted the riser motion RMS a/D in Figures 30 to 33, and compared the results to the experimental data (Trim et al. 2005) and other CFD results (Holmes et al. 2006). Generally, the comparisons show very good agreement to the experimental data. Some highlights are:

- For cross flow VIV the dominant modes are clear: the FANS code predicts the 4th mode is dominant for $U = 0.4$ m/s and the 6th mode is dominant for $U = 0.8$ m/s. The model tests indicate the 3rd mode is dominant for $U = 0.4$ m/s. One possible reason for the discrepancy would be the tension variation. In our calculation the tension within the riser is set to 5 kN, while in the model tests it varied in a range from 4 kN to 6 kN.
- For in-line VIV the dominant modes are not obvious in the FANS results. However, the model tests show the 5th mode is dominant for $U = 0.4$ m/s. Again this is likely due to the lower order mode dynamics. We suspect that in the model tests the weight of the riser played a role in the riser in-line VIV by acting as a restoring force. Further assessment is needed to confirm this.

The maximum cross flow rms a/D is compared to the experimental data at $U = 0.4$ m/s and 0.8 m/s in Figure 34, and it shows good agreement as well. We noticed that the locations of the maximum riser response are not at the riser middle section. Some of the maximum responses are near the two ends of the riser. This could be due to the “pinned” boundary conditions, where all the modes have zero curvature at the two ends, and the peak curvature values of the excited modes are most likely to add together near the ends.

Another interesting phenomenon is that the cross flow VIV is not symmetric along the riser. This is clearly shown in the experimental data; the rms has a trend of increasing at large x/L . We also found the same in our results. Further investigations disclose that the excitation of the 2nd in-line mode (and higher even order modes) could be the reason. We plotted the in-line motion time histories at $x/L = 0.25$ and 0.75 , took the difference between these two motions, and compare the difference to the 2nd in-line mode amplitude, as shown in Figure 35. The correlation between these two is clearly shown. Due to the existence of the even order in-line mode, the riser top and bottom section experience different relative fluid-riser velocities, hence different lift forces.

Overall, the FANS code has demonstrated the capability of being used for assessment of long riser VIV. Compared to another CFD tool, it is able to achieve similar results by using much fewer elements. The FANS code also has the potential to model more complex problems, such as realistic risers exposed to sheared currents.

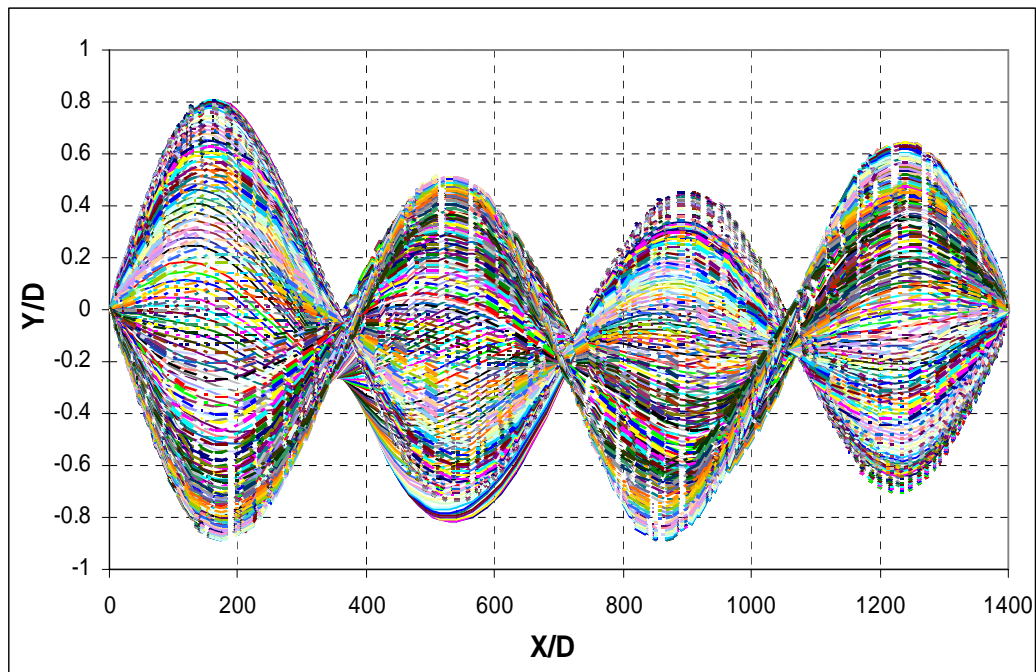


**Figure 28. Horizontal Riser Cross Flow Response Envelope in Uniform Current
 $U = 0.4$ m/s, $t = 193\sim 200$**

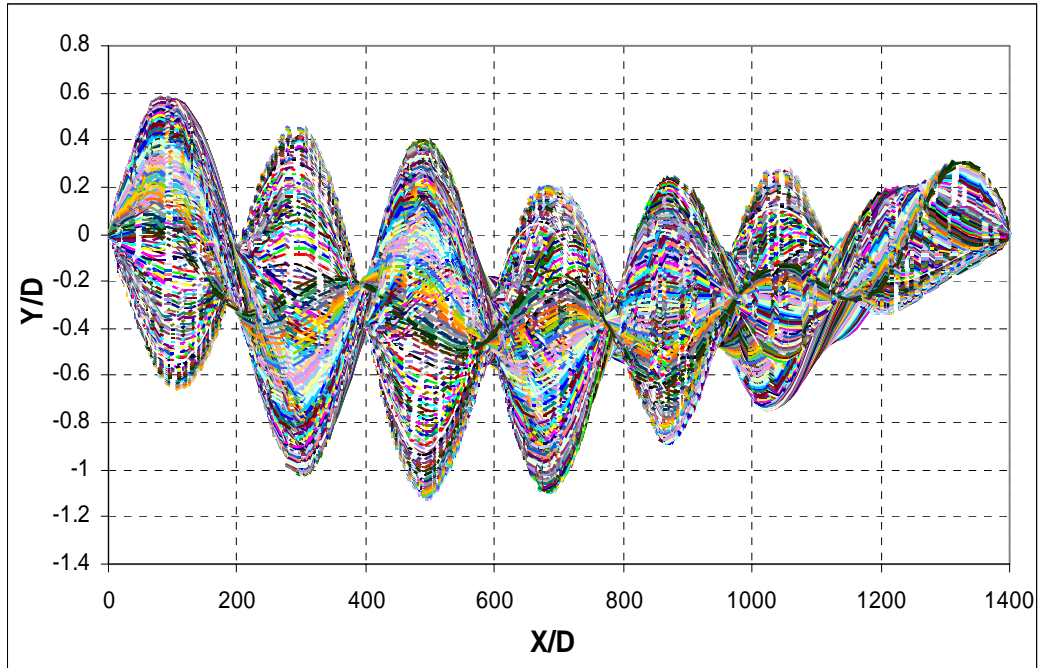


Figure 29. Horizontal Riser Cross Flow Response Envelope in Uniform Current $U = 0.8 \text{ m/s}$, $t = 193\sim 200$

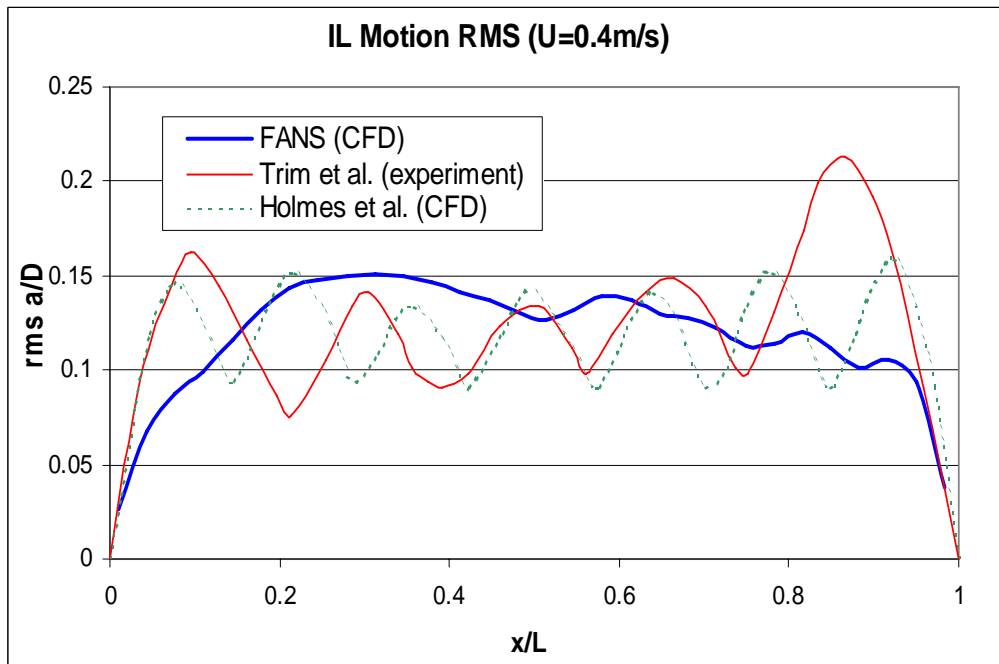


Figure 30. Horizontal Riser In-line VIV RMS a/D in Uniform Current $U = 0.4 \text{ m/s}$

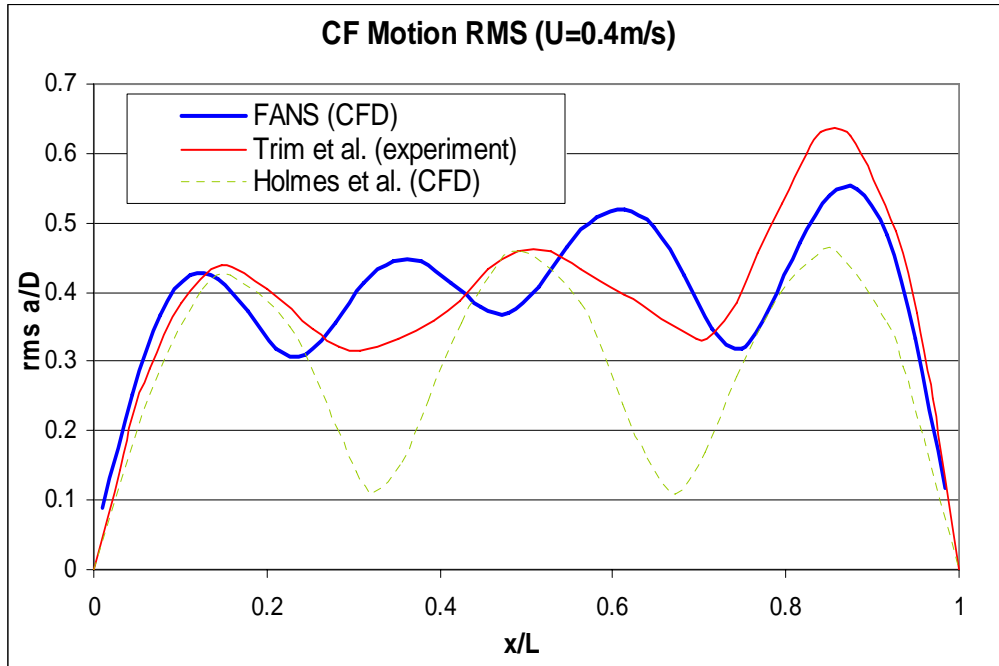


Figure 31. Horizontal Riser Cross Flow VIV RMS a/D in Uniform Current $U = 0.4 \text{ m/s}$

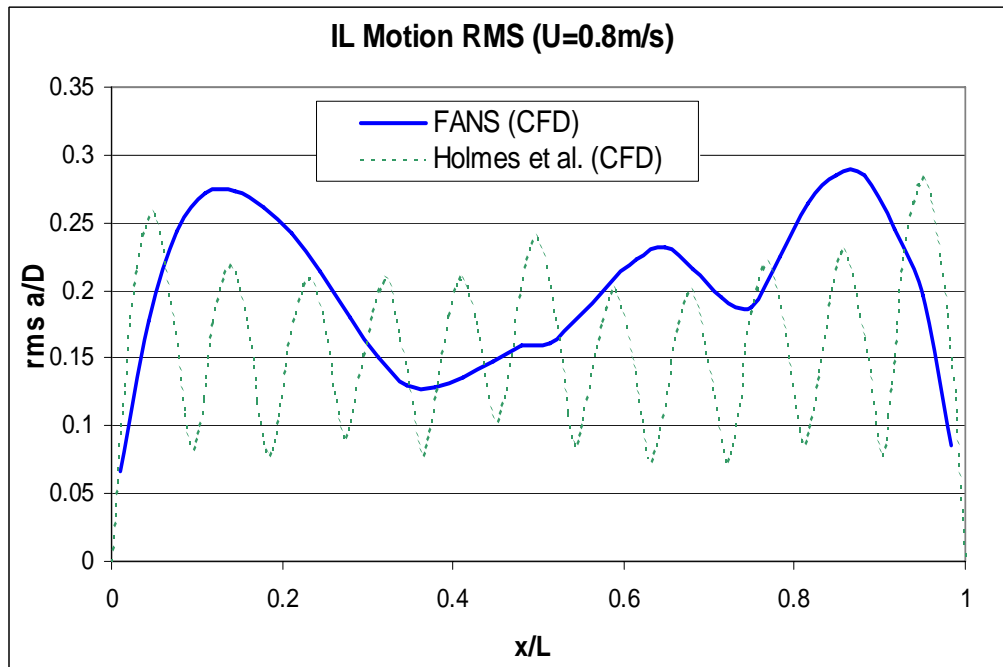


Figure 32. Horizontal Riser In-line VIV RMS a/D in Uniform Current $U = 0.8 \text{ m/s}$

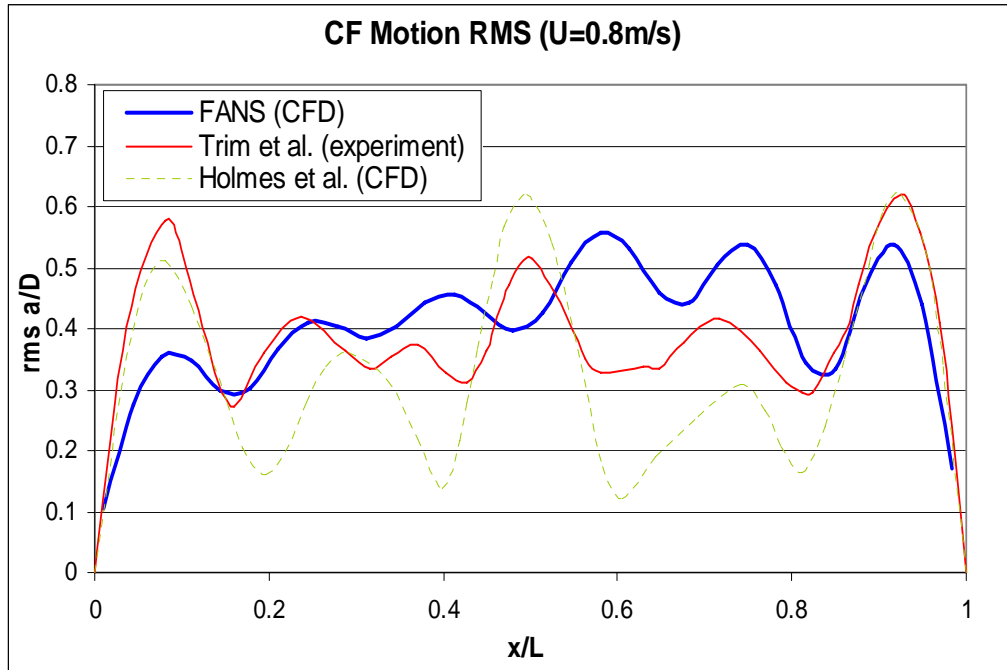


Figure 33. Horizontal Riser Cross Flow VIV RMS a/D in Uniform Current U = 0.8 m/s

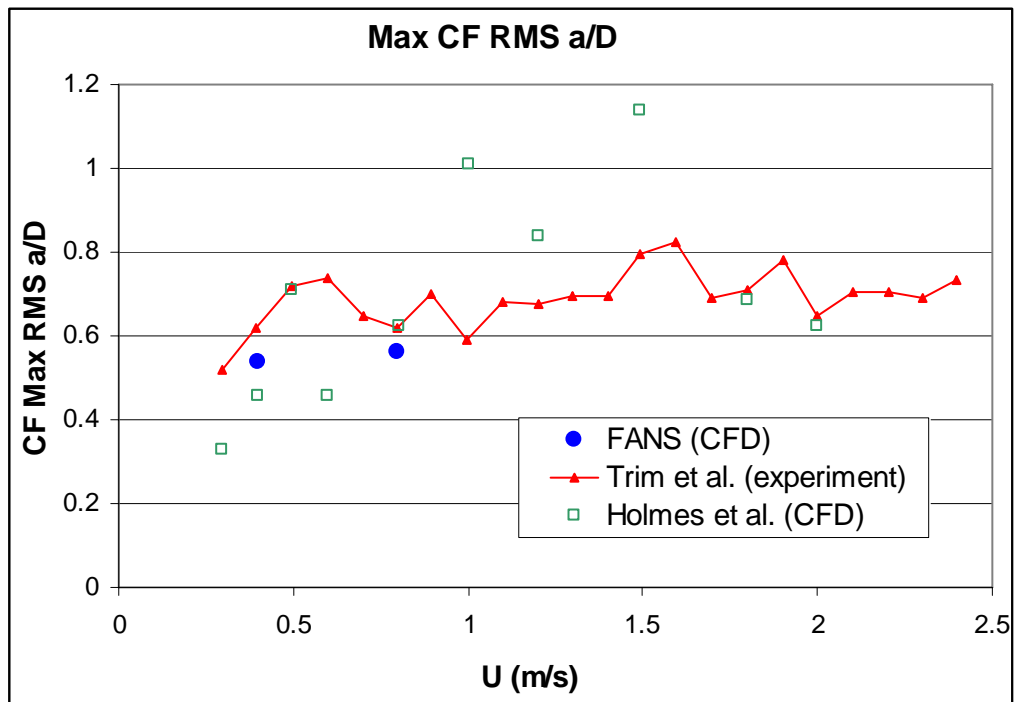


Figure 34. Horizontal Riser Cross Flow VIV Max RMS a/D in Uniform Current

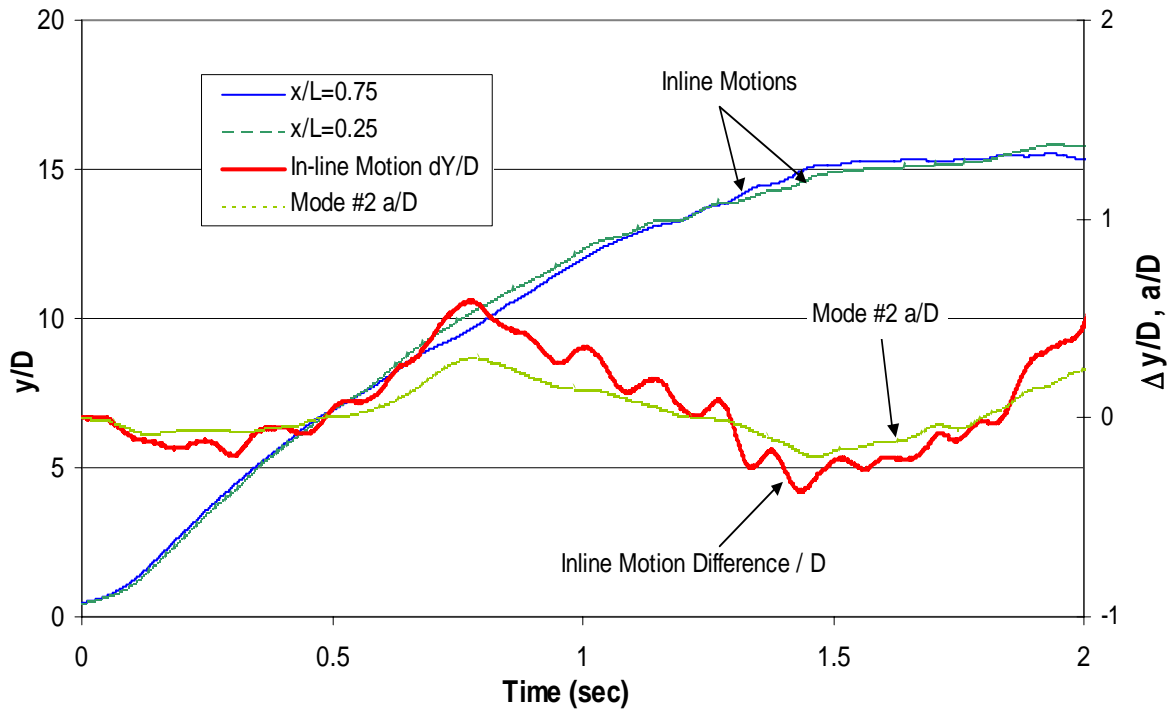


Figure 35. Horizontal Riser VIV Motions at $x/L=0.25$ and 0.75

4.4 Discussion

This section studied the VIV response of a long horizontal riser exposed to a uniform current by using an unsteady, overset-grid (Chimera), Navier-Stokes method. Two case studies were presented with 0.4 m/s and 0.8 m/s current, respectively. The total number of fluid domain elements used for the computation is less than 1 million, and the results are in good agreement with published experimental data. It is found that when constrained by the total number of grid elements, it is more efficient to focus on accurate prediction of the drag and lift forces than of the flow details in the spanwise direction. This suggests that in some cases the 2D strip method, as used in this study, is as effective as fully 3D simulations with coarse elements spreading out into the fluid domain. Nevertheless, more elements could have been used in the riser axial direction to provide better resolution, hence more accurate drag and lift force distributions. Deepwater risers can experience very high mode VIV when the current speed is high. Therefore, the data grid in the riser spanwise direction should be adequately fine to predict the high order VIV responses with acceptable accuracy.

In this study it also demonstrated that the time domain CFD approach is able to provide valuable details on the drag force, lift force, fluid velocities and vorticities, riser displacement and modal response time histories. The FANS code was used to uncover some interesting but unexplained phenomena in the experimental data. In conclusion, a CFD approach that could be applied to long marine riser VIV assessment has been presented. Its validity and effectiveness to predict long riser VIV in uniform current have been demonstrated through case studies and comparisons to published experimental data.

5 3D VIV Simulations of a Horizontal Riser in Sheared Current

5.1 General Description

In Section 4, we compared CFD simulation results to experimental data for riser VIV in uniform currents. In this section, we continue to use the same CFD approach and data grids to study the riser VIV response in sheared current. In order to facilitate a direct comparison with the experimental data of Trim et al. (2005), we have chosen two linearly sheared current profiles with maximum speeds of 0.4 m/s and 0.8 m/s, respectively. During the experiment, the riser was horizontally positioned under the water. One end of the riser was fixed, while the other end was towed in a circular movement at constant speed. This procedure simulates a linearly sheared current. The effect on VIV due to the riser's circular movement is expected to be small, as discussed in Holmes et al. (2006).

5.2 Simulation Procedures

Time domain simulations were performed using the Finite-Analytic Navier-Stokes (FANS) code, a previously validated program through various applications (Pontaza, et al., 2005a, 2005b, 2006, Huang and Chen 2006). It solves the unsteady Reynolds-Averaged Navier-Stokes equation with Large Eddy Simulation (LES) in the time domain. A non-dimensional time step of 0.01 is used in all the calculations. The overset grid (Chimera) technique was used to handle the riser movement. Validation of these data grids can be found in Pontaza et al. (2004).

The riser is 38 m in length and 0.027 m in diameter. In the simulations, the drag (C_d) and lift (C_L) coefficients are calculated along the riser at each time step. Then the riser motions are solved by a modal motion solver (Huang et al., 2007b) as if the drag and lift forces are constant. This is an explicit approach without iteration between the flow field and the riser motion. We used the 4th order Runge-Kutta method to integrate the equation of motion. Figure 36 summarizes the time domain simulation procedure.

The riser is modeled as a beam with a constant tension of 5 kN. Its two ends are assumed to have pinned connections. No structural or material damping has been included. It is estimated that the dominant mode should be less than the 10th mode. Therefore, the riser bending stiffness was expected to have very limited effect on the results, and was neglected in this study. The Reynolds number varies along the riser. It has a maximum value of 1.7×10^5 at $x/L = 1$ for the $U_{max} = 0.8$ m/s case.

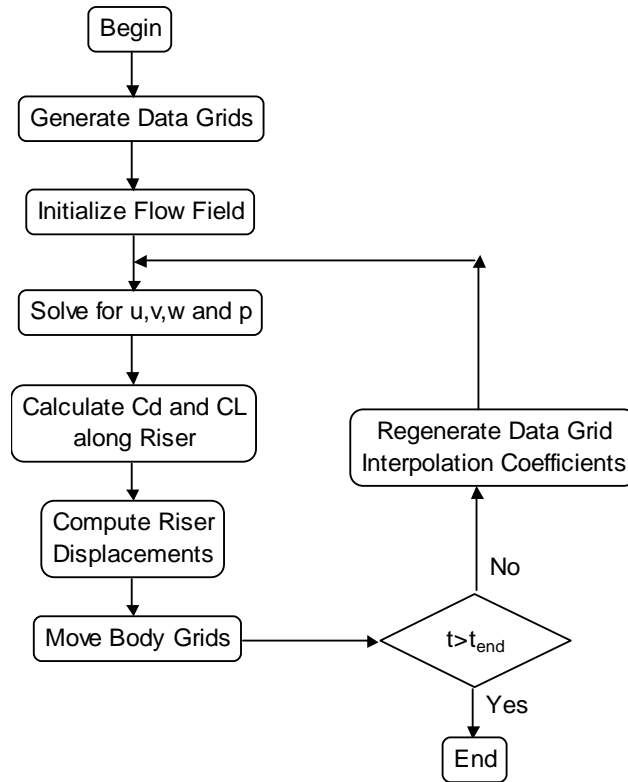


Figure 36. Riser VIV Simulation Procedure

5.3 Simulation Results

The riser VIV responses in two linearly sheared current profiles are analyzed. These two profiles are illustrated in Figure 37. We chose these two current profiles to facilitate a direct comparison of the simulation results with the experiment data and other numerical investigations. The present numerical method has been validated for high Reynolds number cases up to $Re = 1 \times 10^7$ (Pontaza, Chen and Chen, 2005a). Therefore, it is capable of handling a wide range of current speeds other than those used in this study.

We adopted fine meshes on the riser cross-sectional planes and coarse meshes in the riser spanwise direction. This reduces the total number of elements and allows the simulations to be performed on a single-processor personal computer. The numerical grid is the same as that shown in Figures 15 and 16 for the uniform current case. It has a total of slightly less than 1 million grid points. Although the fluid domain is solved using the fully 3D CFD approach, the spanwise grid spacing is too coarse to resolve the 3D flow interaction between adjacent grid layers in the spanwise direction. As a result, the predicted secondary flow velocity in the riser axial direction is fairly weak and the fully 3D simulation results are qualitatively similar to those obtained from a typical 2D strip method. Nevertheless, we are still able to achieve reasonably good prediction of riser VIV responses. The spanwise flow resolution can be improved by adding more grid layers along the riser axial direction and using a more powerful multi-processor computer cluster.

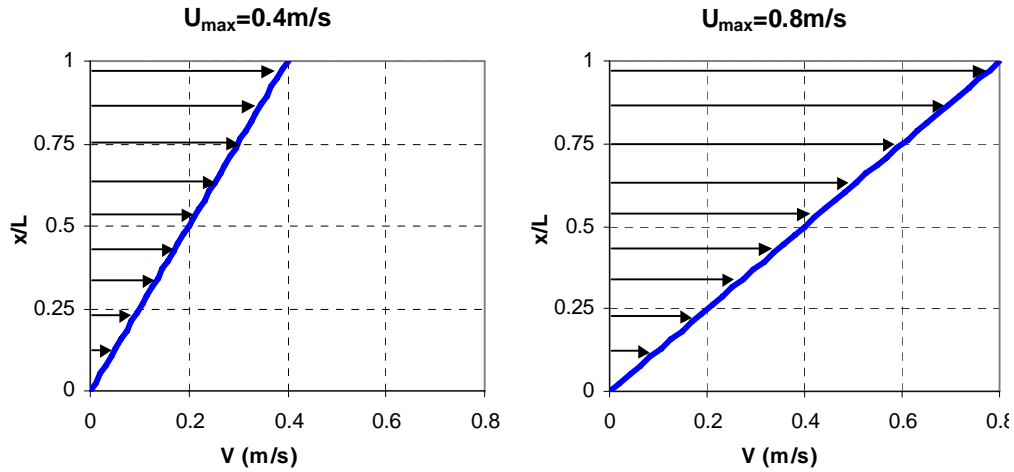


Figure 37. Linearly Sheared Current Profiles

The simulations started with an initially un-deformed riser. The riser begins to move after it is subjected to a sheared current, and deflects continuously until its internal restoring force is sufficiently large to overcome the drag forces. Theoretically, this motion is transient and subsides as the simulation continues. However, we found that the transient response decays rather slowly over the duration of the present simulations, which made it difficult to distinguish this transient motion from the riser in-line VIV.

The time domain simulations are carried out to a total of 20,000 time steps, or during which time the fluid travels a total distance of 200 OD (5.4 m) at $x/L = 1$ for the $U_{\max} = 0.4$ m/s case. Figure 38 shows the evolution of the riser VIV and vortex shedding under different current profiles. The left hand side riser is undergoing VIV in sheared current, while the right hand side riser is undergoing VIV in uniform current. Both risers start with an un-deformed configuration. After a period (approximately 4,000 time steps) of transient response, both risers reach nearly equilibrium positions. The maximum riser deflection occurs at the middle section for risers in uniform current, while it occurs at a slightly higher position in the sheared current. The maximum riser deflection amplitude in the uniform current is approximately four times that in the sheared current. This is reasonable since the averaged speed for the sheared current is half of that for the uniform current, and the drag force is proportional to the square of the current speed. The majority of the vortex shedding shows a clear 2S pattern, which is defined in Williamson et al. (1988). Coalescence of vortices (C pattern) also exists in both cases. It occurs near the top and bottom regions in the uniform current, and around the middle section in the sheared current. The cross flow VIV amplitudes are moderate and of the order of 1D. No obvious 2T patterns (Williamson and Jauvtis, 2004) have been observed in these two-degree-of-freedom simulations.

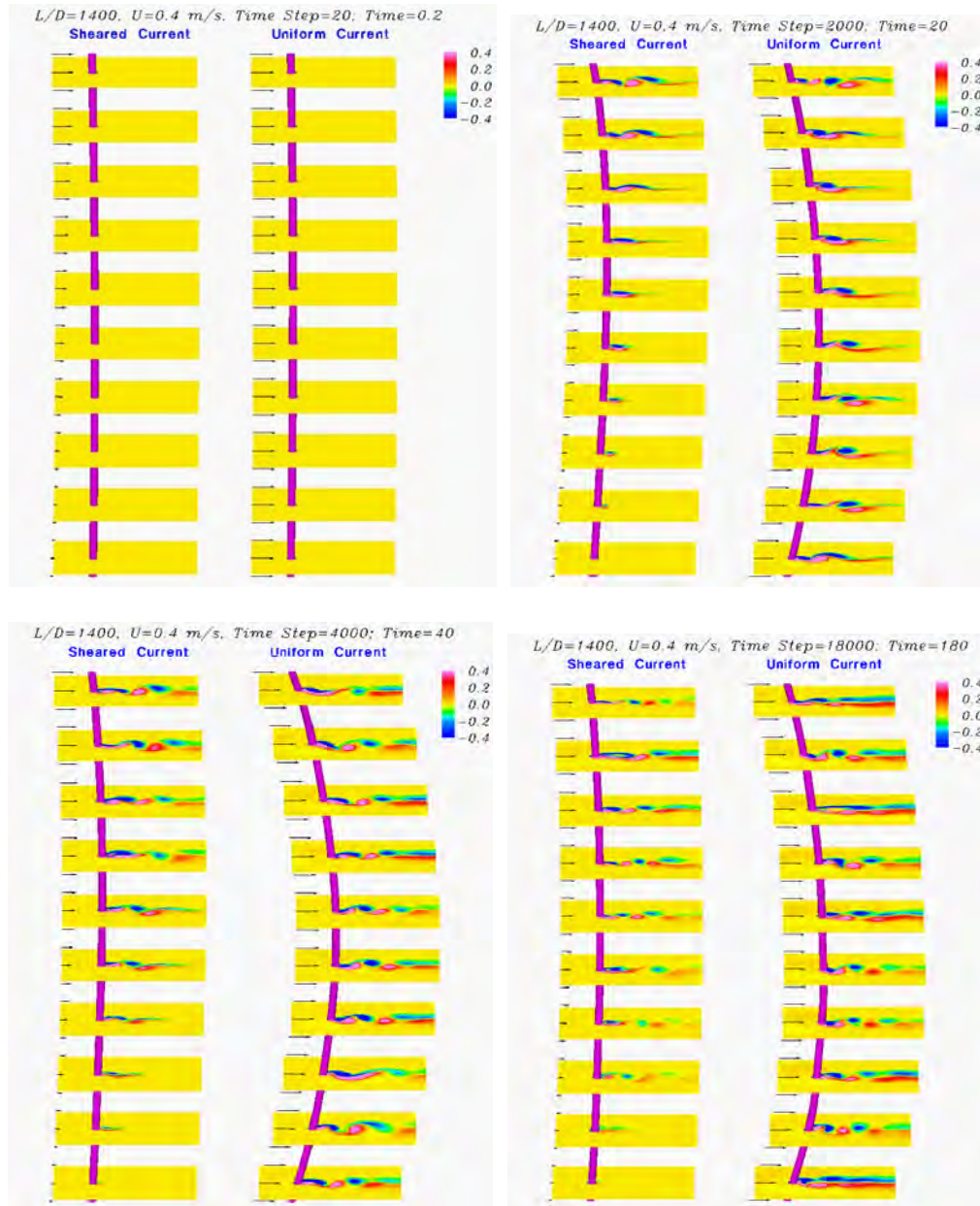
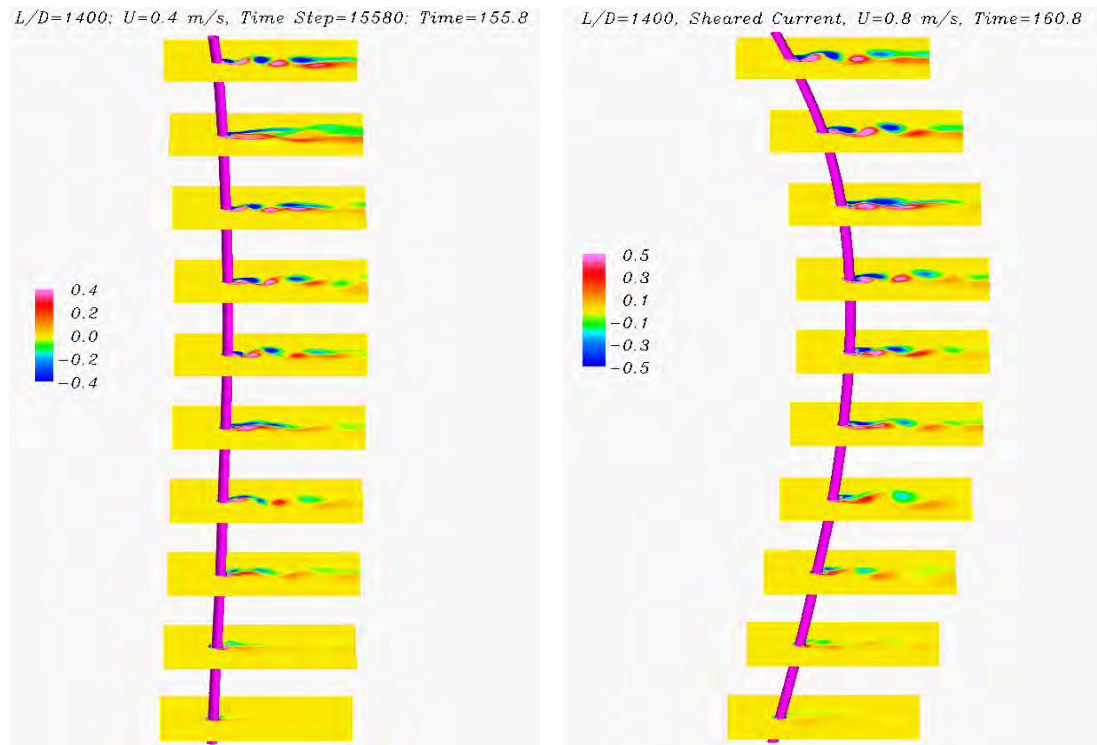


Figure 38. Vortex Shedding Patterns and Horizontal Riser Responses, $U_{max} = 0.4$ m/s, Left: Sheared Current, Right: Uniform Current

Figure 39 shows two snap shots of the vorticity fields for $U_{max} = 0.4$ m/s and 0.8 m/s, respectively. The riser maximum lateral deflection for the $U_{max} = 0.8$ m/s case is approximately 5~6 times the riser diameter. As expected, it is much larger than that for the $U_{max} = 0.4$ m/s case. It is also observed in both cases that the 2S pattern and C pattern are mixed along the riser. The C pattern indicates a possible power out region. Therefore, it is likely that the riser middle section is the power in region, while the riser top and bottom sections are the power out regions (Vandiver and Li, 2003).



**Figure 39. Snap Shots of Horizontal Riser VIV in Sheared Current,
Top: $U_{max} = 0.4$ m/s, Bottom: $U_{max} = 0.8$ m/s**

Figure 40 shows the vorticity contours for $U_{max} = 0.4$ m/s and 0.8 m/s, respectively, at selected time instants. For $U_{max} = 0.8$ m/s case, the dominant modal shape number (7th mode) is much higher than that (3rd mode) of the $U_{max} = 0.4$ m/s case.

Drag and Lift Coefficients

The drag and lift coefficients are calculated at each time step. Figures 41-44 show the comparisons of the drag and lift coefficients between the uniform and the sheared current cases. The comparisons show that the drag coefficients are in similar ranges for all cases, with minor variations due to different dominant modes, while the lift coefficients for the sheared current are generally lower than those for the uniform current. This could be related to the riser vibration mode dominant level and amplitudes in these two current profiles. It is not surprising to see that the single mode dominant is more likely to occur in uniform current than in sheared current, and with higher a/D rms values.

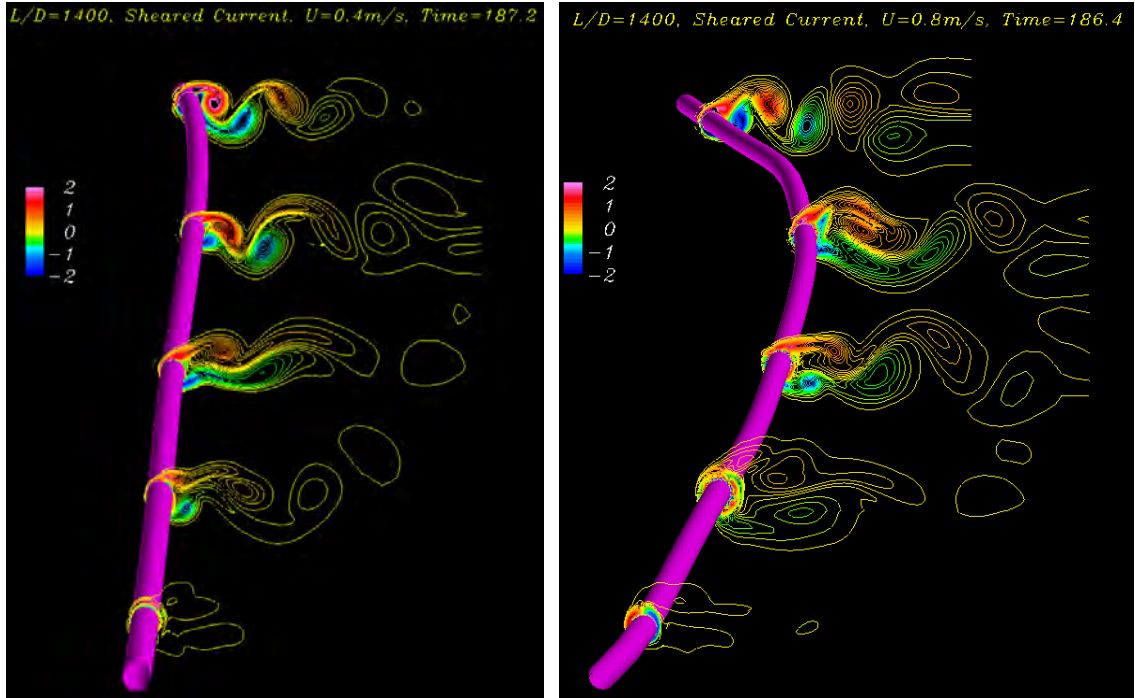


**Figure 40. Vorticity Contours in Sheared Current, Top: $U_{max} = 0.4$ m/s,
Bottom: $U_{max} = 0.8$ m/s**

The lift coefficients also show variations along the riser that corresponds to the dominant mode shapes. The higher the current speed, the higher the dominant mode number becomes. Hence more peaks and troughs are observed in the lift coefficients for the $U = 0.8$ m/s case. The results also show that the lift coefficients have a rms value of 0.2~0.4 in sheared current profiles. The averaged lift coefficient values for sheared current cases are 0.34 for $U_{max} = 0.4$ m/s, and 0.32 for $U_{max} = 0.8$ m/s. On the other hand, the averaged rms values of the lift coefficient are 0.78 for $U = 0.4$ m/s and 0.44 for $U = 0.8$ m/s in the uniform current cases. Although the exact values are case dependent, it seems that the lift coefficients are less sensitive to the current speed under sheared current condition.

The drag coefficients are slightly higher in the riser top and bottom regions in the uniform current cases. One possible reason could be due to the vortex shedding pattern near the top and bottom boundaries (C pattern). Note that the mean drag coefficient is related to several factors, including Reynolds number, riser vibration amplitudes and frequencies. Therefore, high velocity does not necessarily result in high drag coefficient, as shown in the sheared current cases. However, the actual drag forces are significantly larger for the high velocity case ($U = 0.8$ m/s) since the drag force is proportional to U^2 .

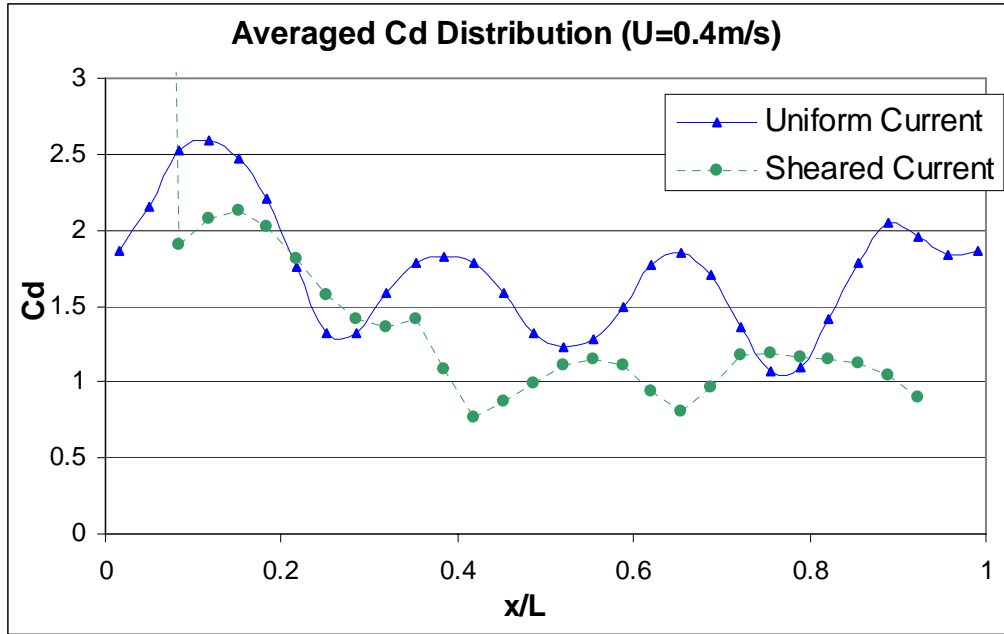


Figure 41. Drag Coefficient Distributions for Horizontal Riser, $U_{max} = 0.4 \text{ m/s}$

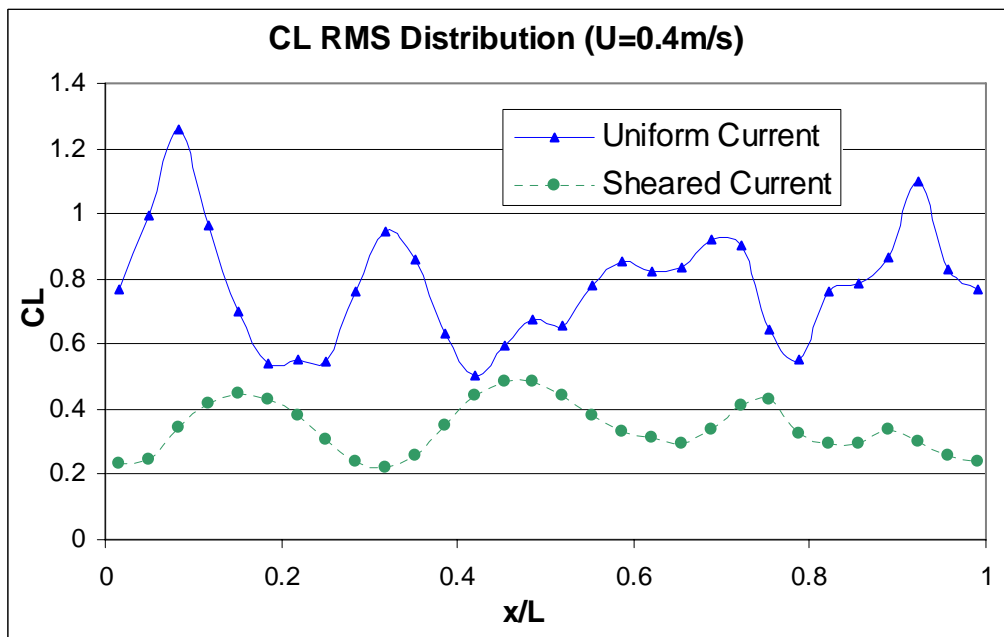


Figure 42. Lift Coefficient Distribution for Horizontal Riser, $U_{max} = 0.4 \text{ m/s}$

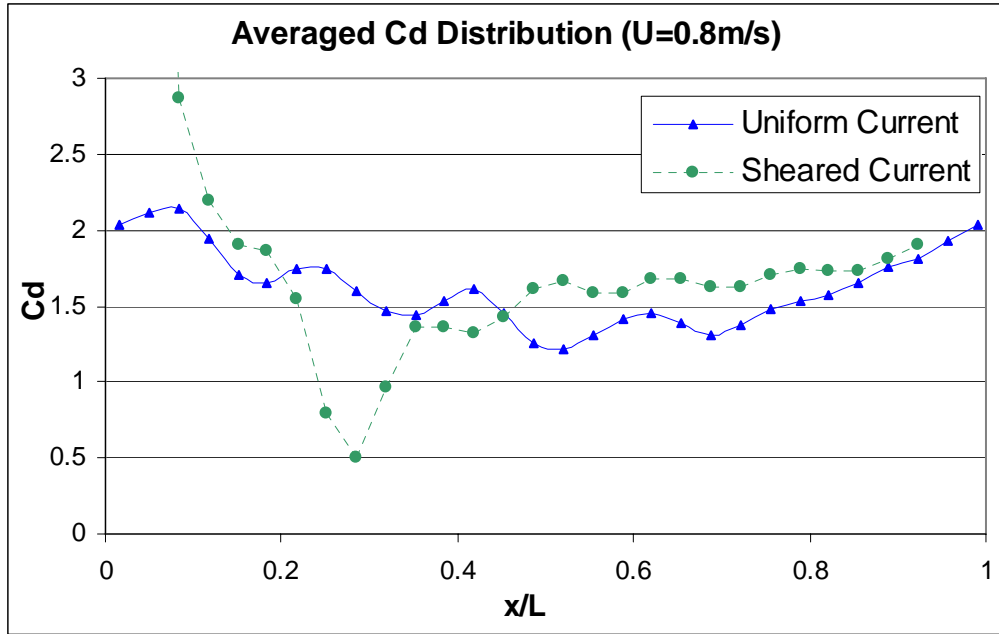


Figure 43. Drag Coefficient Distribution for Horizontal Riser, $U_{max} = 0.8$ m/s

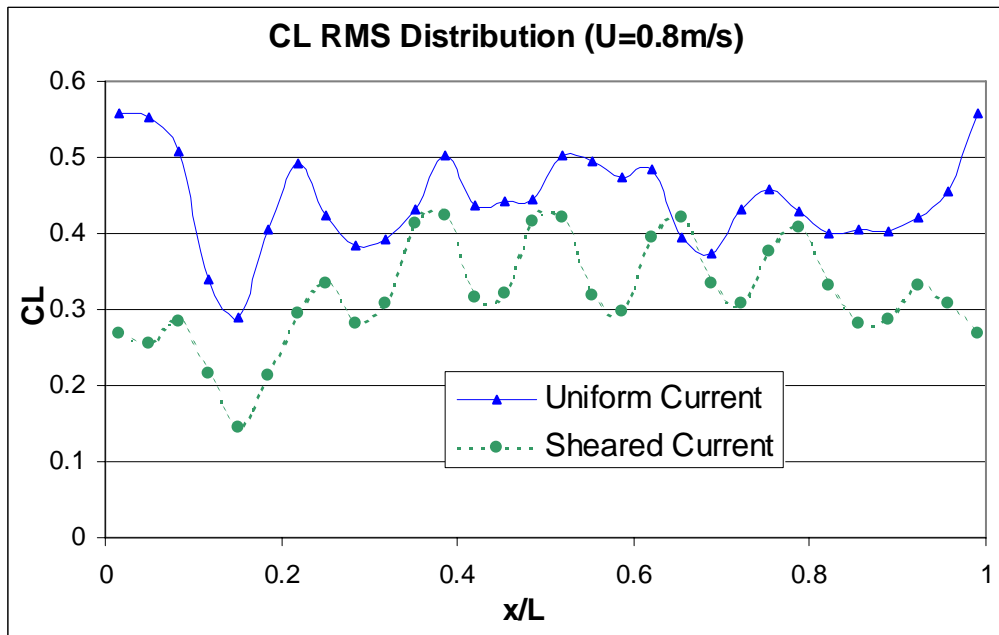


Figure 44. Lift Coefficient Distribution for Horizontal Riser, $U_{max} = 0.8$ m/s

Riser Motion RMS a/D

The riser response rms a/D is of particular interest in the riser VIV simulations. Figures 45 and 46 show the comparison between the simulation results and experimental data for cross flow VIV. The experimental data are plotted in straight lines since only the mean and maximum values are given in Trim et al. (2005). The CFD simulation results predict similar maximum and mean values as the experimental data for the slower sheared current case ($U_{max} = 0.4$ m/s), while they under-predict the VIV in the higher sheared current case ($U_{max} = 0.8$ m/s). Figure 47 shows the comparison of maximum rms a/D.

In general the CFD approach tends to underestimate the riser VIV peak response. The in-line riser VIV rms a/D is not presented since it is dominated by the transient motions as noted in the earlier discussion. Hence, it is difficult to distinguish the in-line VIV from the overall dynamic motions.

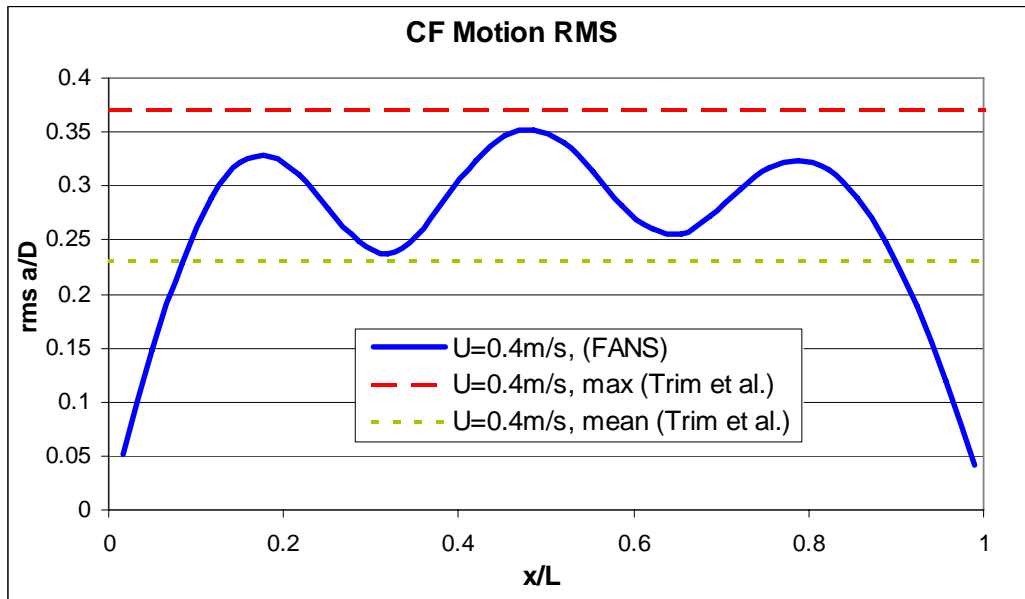


Figure 45. Horizontal Riser Cross Flow VIV RMS a/D, $U_{max} = 0.4$ m/s

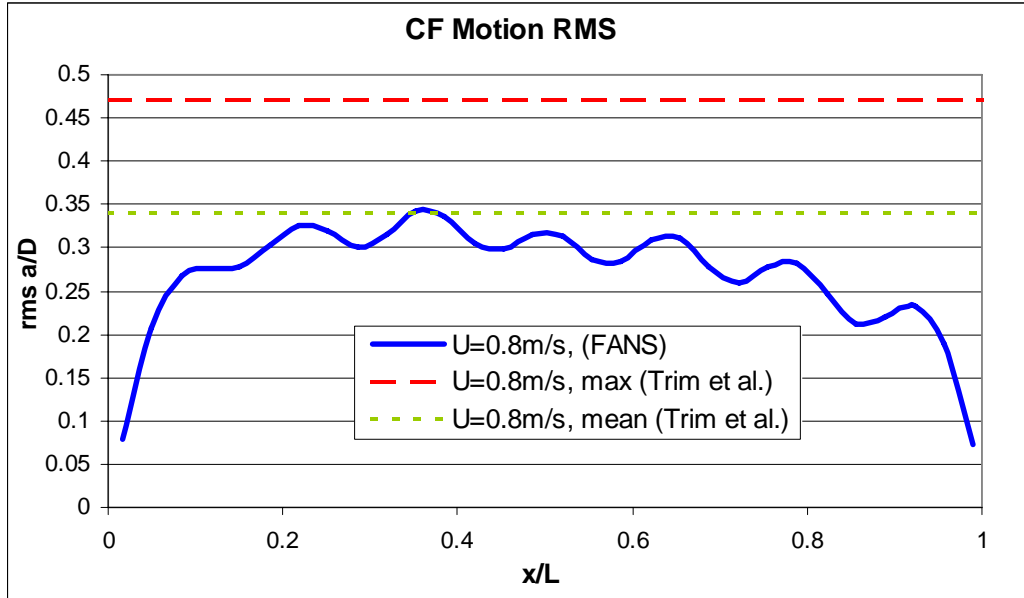


Figure 46. Horizontal Riser Cross Flow VIV RMS a/D, U_{max} = 0.8 m/s

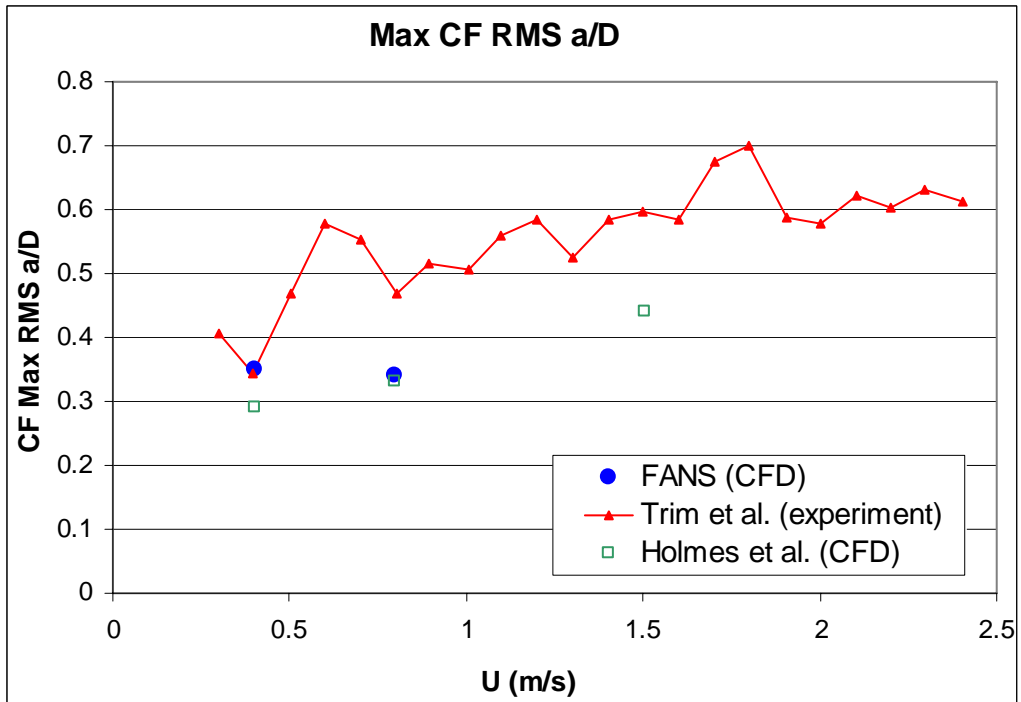


Figure 47. Horizontal Riser Cross Flow VIV Max RMS a/D

Riser Motion Trajectory

For completeness, the riser motion trajectories for both the sheared and uniform currents are also shown in Figures 48 and 49 for $U_{max} = 0.4$ m/s and 0.8 m/s cases, respectively.

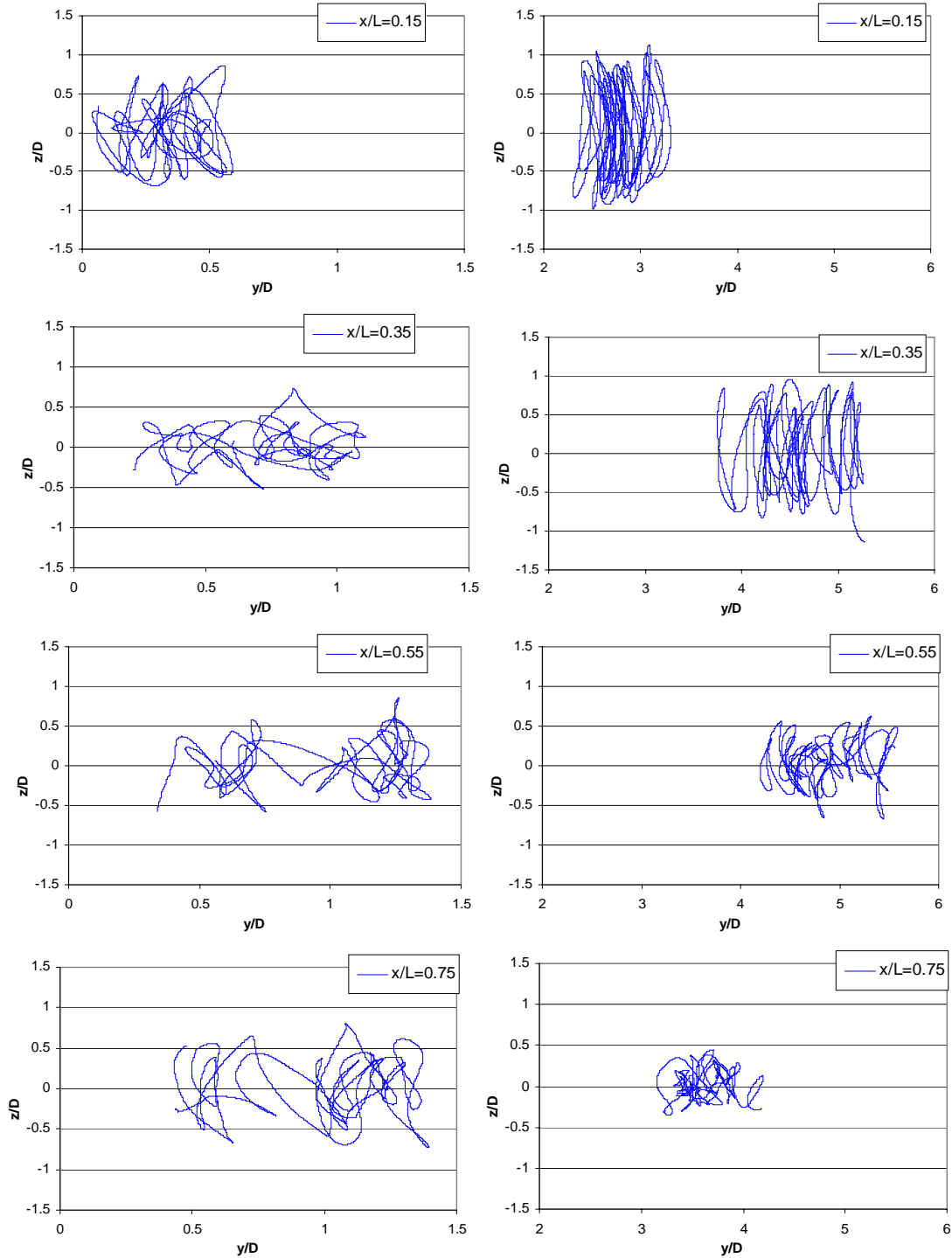


Figure 48. Horizontal Riser Motion Trajectory Comparison, $U_{max} = 0.4$ m/s, Left: Sheared Current, Right: Uniform Current

The figure “8” pattern is clearly shown only when the in-line motion is small, and the dominant mode number is low, i.e. $x/L = 0.15$ and $U_{max} = 0.4$ m/s. Otherwise, the riser movement does not necessarily take any simple shapes.

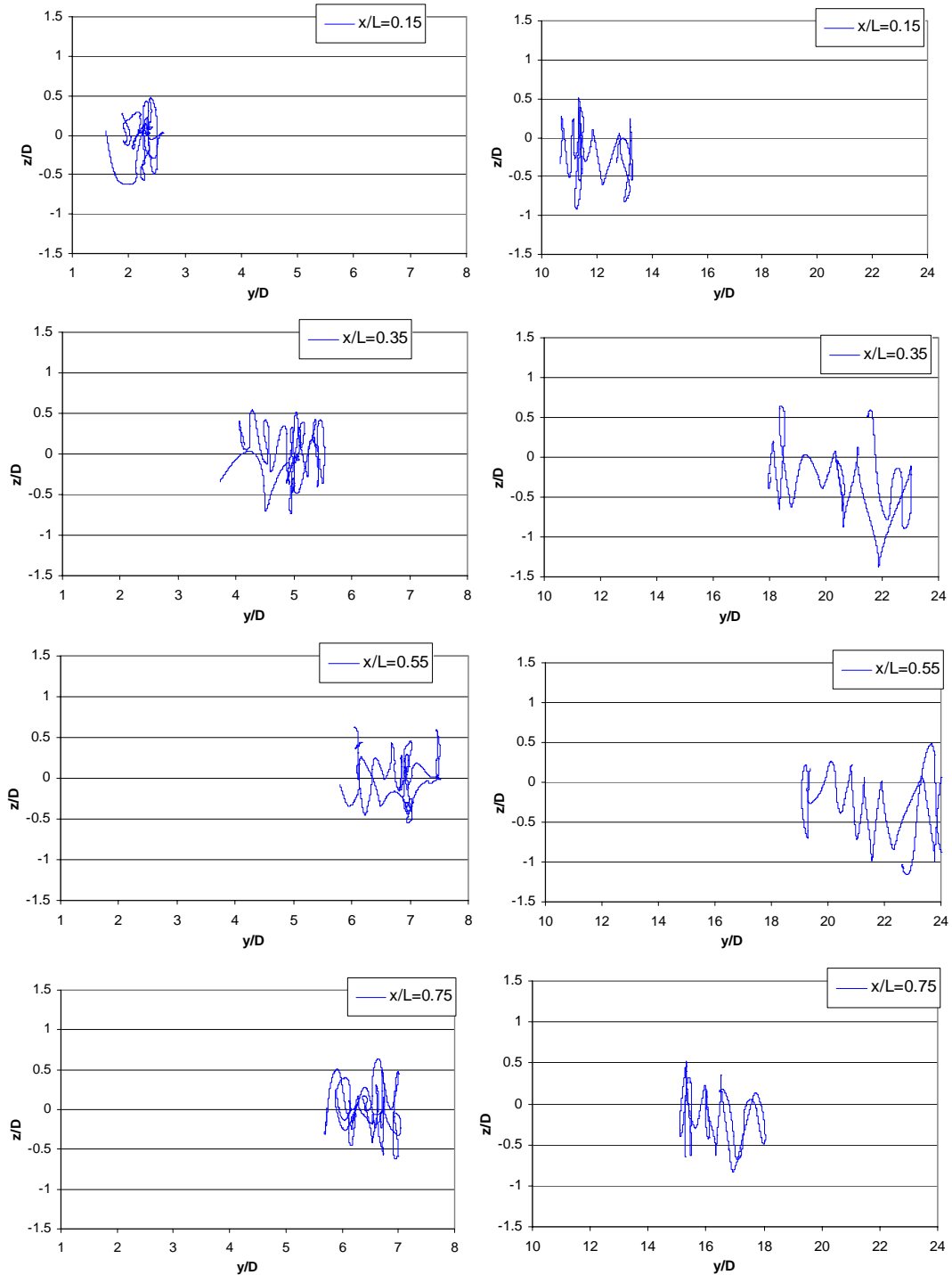


Figure 49. Horizontal Riser Motion Trajectory Comparison, $U_{max} = 0.8$ m/s, Left: Sheared Current, Right: Uniform Current

Riser VIV Modal Decomposition

The riser in-line and cross flow motion responses are calculated through modal superposition. The rms a/D of each modal component is plotted in Figures 50 and 51 for in-line and cross flow motion, respectively. The response includes both the riser transient dynamic motions due to its initial positions and velocities, and the steady VIV. The transient response is usually low frequency and involves low modes, as shown in Figure 50. We did not attempt to split the transient response and steady VIV in this section. Further investigation is needed in order to separate the transient response from the steady VIV.

In order to measure the dominant level of an excited modal shape, we normalized the modal energy by the total response energy. In other words, we looked at the modal energy percentage of each mode. Figure 52 shows the results for in-line motion, which is dominated by the 1st mode. As discussed earlier, this 1st mode is mainly due to the transient effect. Figure 53 shows the modal energy percentages of cross flow motion. For each case studied, there is a single mode that contributes at least 40% of the total vibration energy. This single mode is the dominant mode that is of particular concern for VIV-induced fatigue. However, we also see a number of non-dominant modes that each contribute 10% to 20% of the total energy. The importance of these non-dominant modes and their impact on the riser VIV and VIV-induced fatigue remain to be determined.

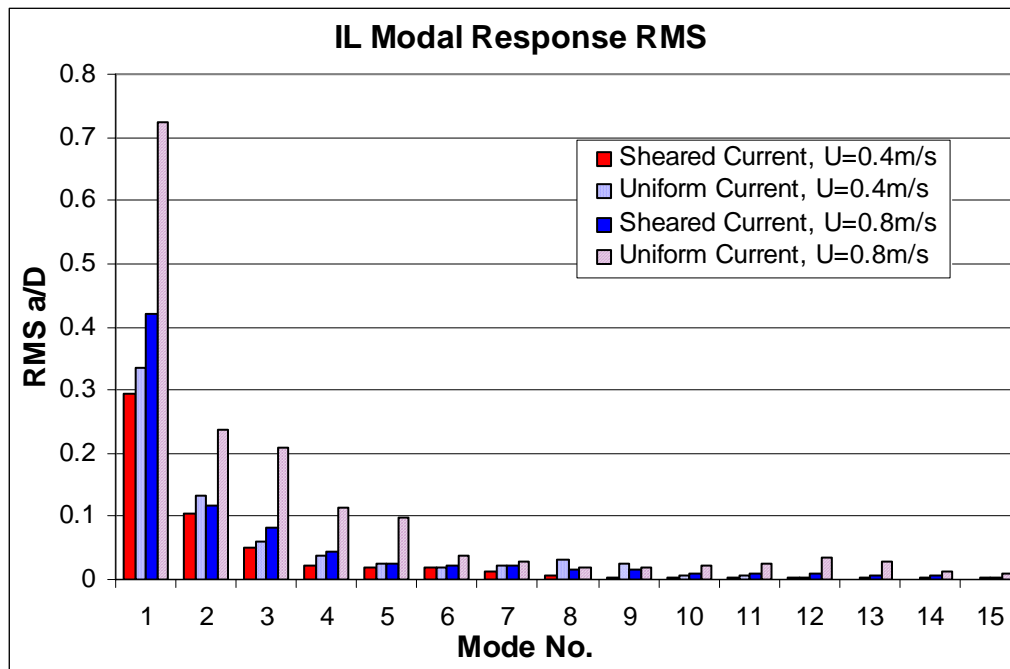


Figure 50. Horizontal Riser In-line VIV Modal Response Amplitude

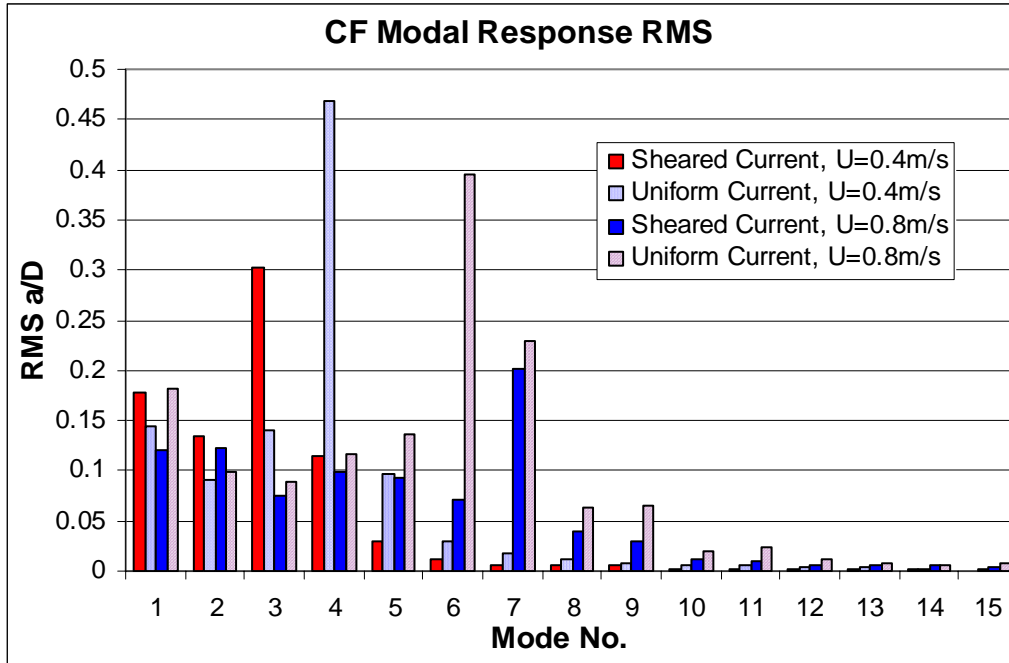


Figure 51. Horizontal Riser Cross Flow VIV Modal Response Amplitude

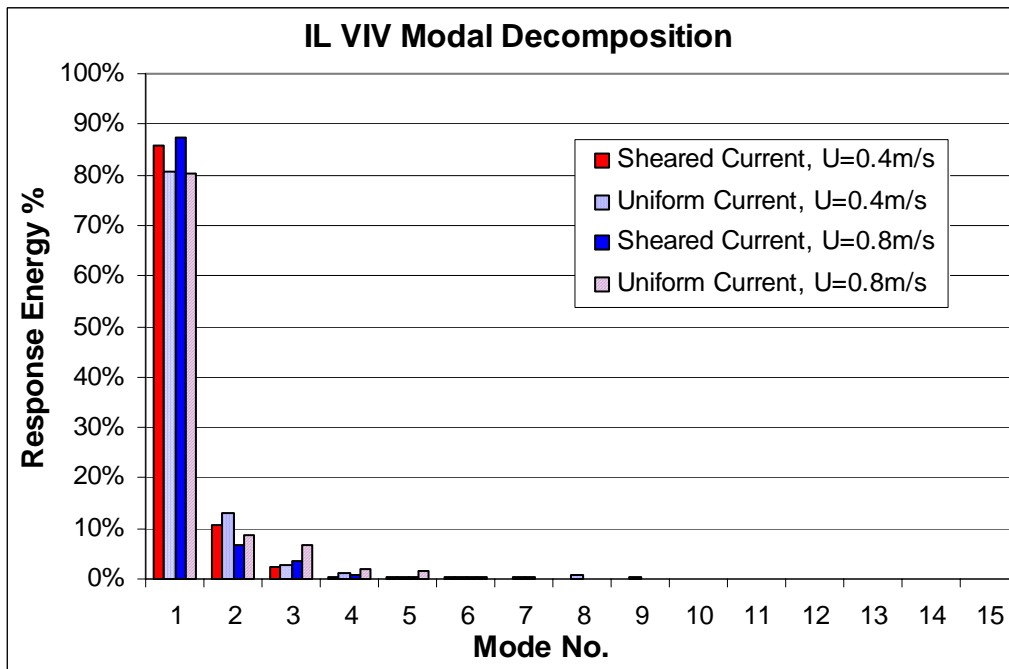


Figure 52. Horizontal Riser In-line VIV Modal Response Energy

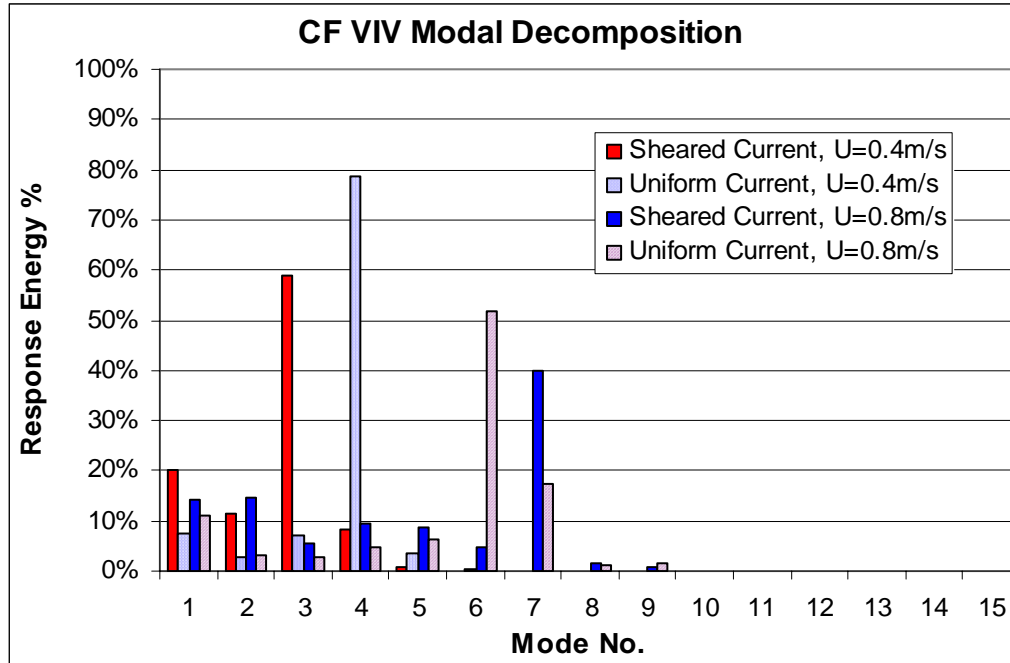


Figure 53. Horizontal Riser Cross Flow VIV Modal Response Energy

5.4 Discussion

In this section two case studies were presented of a horizontal riser exposed to a sheared current speed of 0.4 m/s and 0.8 m/s at $x/L = 1.0$. The results are within the ranges of published experimental data. They indicate that the FANS code is capable of predicting reasonable VIV results for long risers using a fairly coarse grid in the riser axial direction. It is worthwhile to note that FANS can be readily generalized to handle much more complex current conditions, such as a highly sheared current and a submerged current. Some findings of the study are:

1. The vortex shedding pattern in the sheared current is different from that in the uniform current. In the uniform current case, the riser motion and vortex shedding are usually synchronized. In the sheared current case, the mixture of 2S and C vortex shedding patterns may suggest the existence of power-in and power-out zones along the riser.
2. Mode lock-in could occur in the sheared current. However, its dominant level (in terms of the energy percentage) is lower than that of the uniform current.

A long marine riser could have large mean lateral deflection when subject to a strong current. It seems that this mean lateral deflection is more than a static value that could be subtracted during the riser VIV simulation. It is partly the result of the fluid-structure interaction. Hence it could influence the in-line and cross flow VIV by altering the flow field.

6 3D VIV Simulations of a 3000 ft Vertical Riser

6.1 General Description

This section studies the VIV of a typical 10 ¾” single casing top tensioned riser. The riser is sized for 3,000 ft water depth and its dynamic response under both uniform and sheared currents is simulated in 3D. The fluid-riser interaction effect is included through instantaneous drag and lift forces. The riser inline and cross flow responses, including a/D , modal shapes and frequencies, and VIV induced stresses, are studied in detail as well.

It is demonstrated that the CFD approach provides reasonable results. It is also found that further improvements, for example, refined data grids in the riser spanwise direction and additional coupled terms in the riser modal equations, are essential for riser VIV assessment in more complex current profiles and riser conditions.

6.2 Description of CFD Approach

The flow field around a riser is calculated by numerically solving the unsteady, incompressible Navier-Stokes equations in conjunction with the Smagorinsky subgrid scale model for large eddy simulation (LES). Time-domain simulations of riser dynamic responses are performed using the FANS code (Chen et al., 2006; Pontaza et al., 2005) for both the uniform current with $U = 0.4$ m/s, and the linearly sheared current with $U_{max} = 0.4$ m/s. The Reynolds number based on the maximum current speed and riser diameter is 8×10^4 . The non-dimensional time step used in the simulation is 0.01, which means the free stream fluid travels a distance of one riser diameter in 100 time steps. This time step is typical for analysis of similar riser VIV problems, and is sufficiently small for stable time domain simulations.

The fluid domain around the riser is meshed with structured data grids, which consist of a phantom background grid, a wake grid, and a riser body grid. The data grids are structured for easy implementation of higher order numerical schemes. Since this is a very long riser with L/D of 3,350, the element number would be on the order of 10 billion if were to mesh the riser span direction with similar resolution as in the current direction. That is beyond the available computational power we can have access to. Therefore, we chose to have a relatively coarse grid in the riser span direction. It is estimated that the highest mode that could be excited in a 0.4 m/s current (slightly less than 1 knot) is the 12th mode. In order to represent this mode, we used 30 data grids in the riser spanwise direction. The total element number is kept below 1 million, so the computation can be performed on a single processor PC. More data grids would certainly improve the riser simulation accuracy, at the expense of computational speed and resources. During the simulation the wake grid and body grid move together with the riser. Therefore, there is no need to re-generate the data grids at each time step.

Top Tensioned Riser and its Modal Analysis

The riser studied is a 10 ¾” single casing top tensioned riser for 3,000 ft water depth. It has a nominal top tension of 400 kips, submerged weight of 121 lb/ft, and mass ratio of 4.0. The riser string consists of steel bare joints without external insulation or strakes. For simplicity, specialty joints, such as the stress joint and the tension joint, are assumed to have the same sectional properties as the standard joint. The riser top and bottom boundary conditions are also simplified as pinned connections.

The riser has a fundamental frequency of 38 seconds in seawater. The riser modal shapes have been calculated up to the 40th mode through a separate finite element analysis (FEA) program. However, preliminary reduced velocity screening shows the dominant mode is likely to have a frequency between the 8th and 12th mode. Therefore, these modes are shown in Figure 54. Note that the modal shapes are normalized to unit maximum amplitude, which is usually located near the riser bottom.

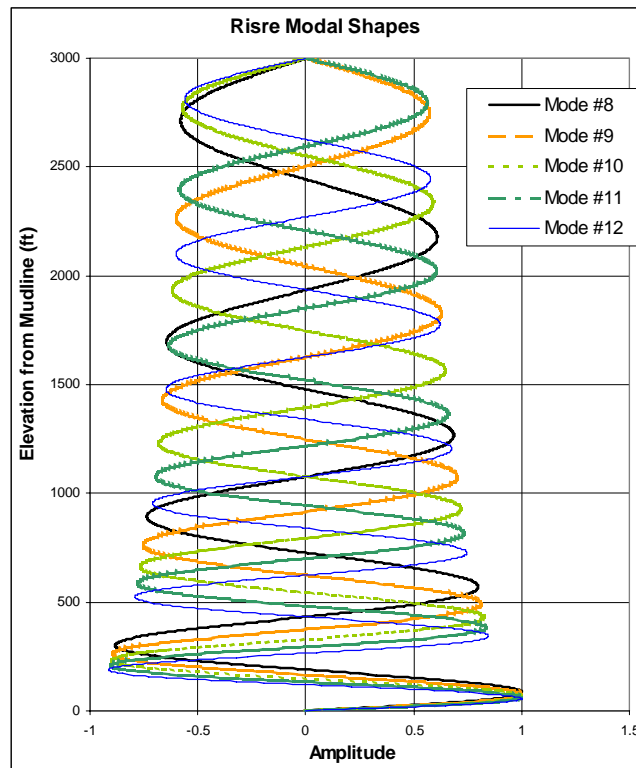


Figure 54. Vertical Riser Modal Shapes

For deepwater risers, the effective tension near the subsea wellheads is minimum, while it increases to its maximum at the top. Therefore, the peak values of its modal shapes are not constant along the riser. Lower effective tension results in higher vibration amplitudes. This leads to an interesting observation: in deepwater applications, the current profiles usually have their maximum speed near the ocean surface, however, the worst riser VIV response is well

below that region, and it occurs near the bottom, where the current speed is nearly zero, or there is no current at all.

It is also worthwhile to note that a typical production riser has slightly more complicated top and bottom boundary conditions than the pinned connection; the bottom stress joint/tieback connector is nearly rigid, the riser top section is constrained by the floater, and possibly other lateral constraints exist from a keel joint. While all these details could also be modeled in the proposed CFD approach, we start with the pinned connection case for illustration purposes. After all, when the riser is as long as 3,000 ft, the boundary conditions are less likely to have significant impact on the riser global dynamic response.

6.3 Simulation Results

The simulations have been performed for 20,000 time steps, which correspond to a period of 140 seconds. Figure 55 shows the evolution of the riser dynamic motion. The risers are initially straight and have no external force except gravity. At time $t = 0$, the risers are subject to a uniform or sheared current. They deflect to a new equilibrium position and vibrate back and forth. The in-line motions are dominated by transient dynamics. It is not that straightforward to filter out the in-line transient motions. That is also one reason we mainly focused the study on cross flow VIV. Another reason is that the expected dominant mode for in-line VIV is very high (twice of the dominant mode in cross flow VIV), and it may be beyond the riser axial resolution of the data grid we used. It should be noted, however, that the in-line transient motion could also be important to riser VIV in a sense that: (1) it could influence the riser VIV through disturbing the flow field and changing the initial conditions for vortex shedding, and (2) in the physical world the current condition changes continuously. In other words, the transient response would always exist in real world and might also deserve some attention as well. Some observations from the snapshots are:

- During the startup phase, the vortices develop slower in the riser middle section than in the regions near the ends. Since the riser is fixed at its two ends, the relative velocity in those regions is close to the incoming current velocity, and vortices are able to develop and shed as if flowing around fixed cylinders. In the middle section the riser segment has no lateral constraint during the initial period and moves downstream with the current, which results in small relative velocity. As a result, the drag coefficients near the riser ends are larger than those in the middle section.
- In the sheared current, the riser top section is subject to higher current speed than the lower section. Its initial deflection corresponds to the current profile, i.e. larger riser deflection in the higher speed region. However, as the riser deflects more, its own characteristics take effect as well. The riser has much higher effective tension in the top section than in the bottom section. From the riser equation of motion we know that the higher the tension, the stiffer the riser is in the lateral direction. Therefore, even though the riser lower section is subjected to lower current speed, it has much more lateral flexibility, hence it has more lateral excursion.

- The vortex shedding in the wake of the riser exhibits different patterns at different times. Initially the 2S pattern is clearly seen along the entire riser. When the riser reaches near its maximum deflection, coalescence of vortices (C pattern) occurs at the top and bottom regions. In the sheared current case, the C pattern occurs only at the top region where the current speed is the maximum. The vortex shedding maintains the 2S pattern below a transitional section from the C pattern to the 2S pattern. In the uniform current case, we found that the C pattern could continue propagating into the middle section of the riser, until it covers the entire riser. Due to the reduced drag force on the riser for the C pattern vortices, the riser reduces its lateral deflections dramatically, as indicated by the arrow in the figure. After that, the 2S pattern recovers in the middle section and pushes the riser back toward its equilibrium position. Figures 56 and 57 show the vorticity contour snapshots where the vortex pattern could be clearly identified.

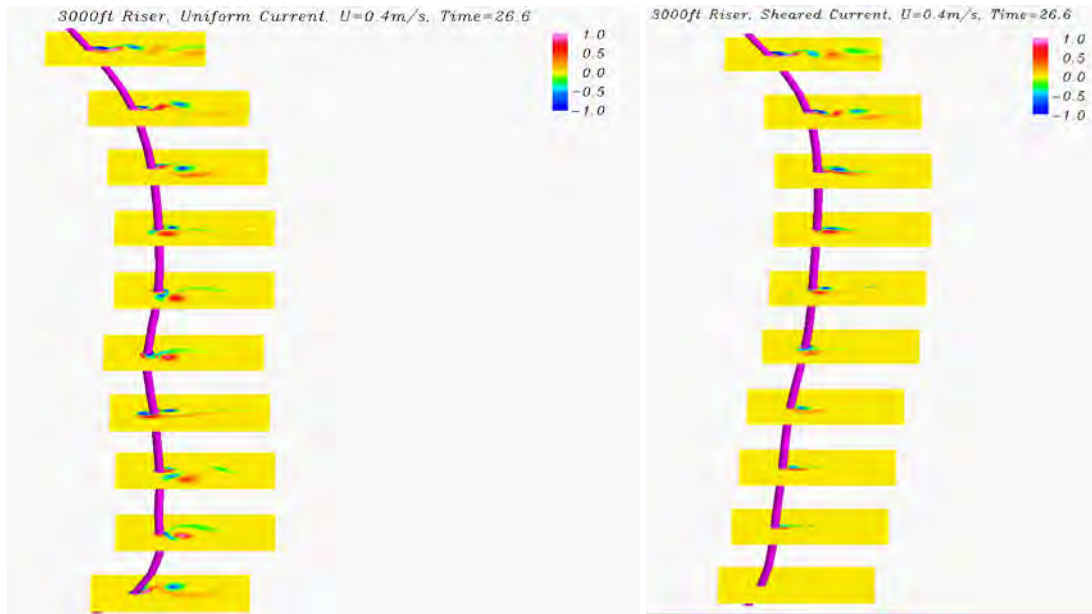


Figure 55. Vertical Riser VIV Comparison, Left: Uniform Current 0.4 m/s, Right: Sheared Current 0.4 m/s

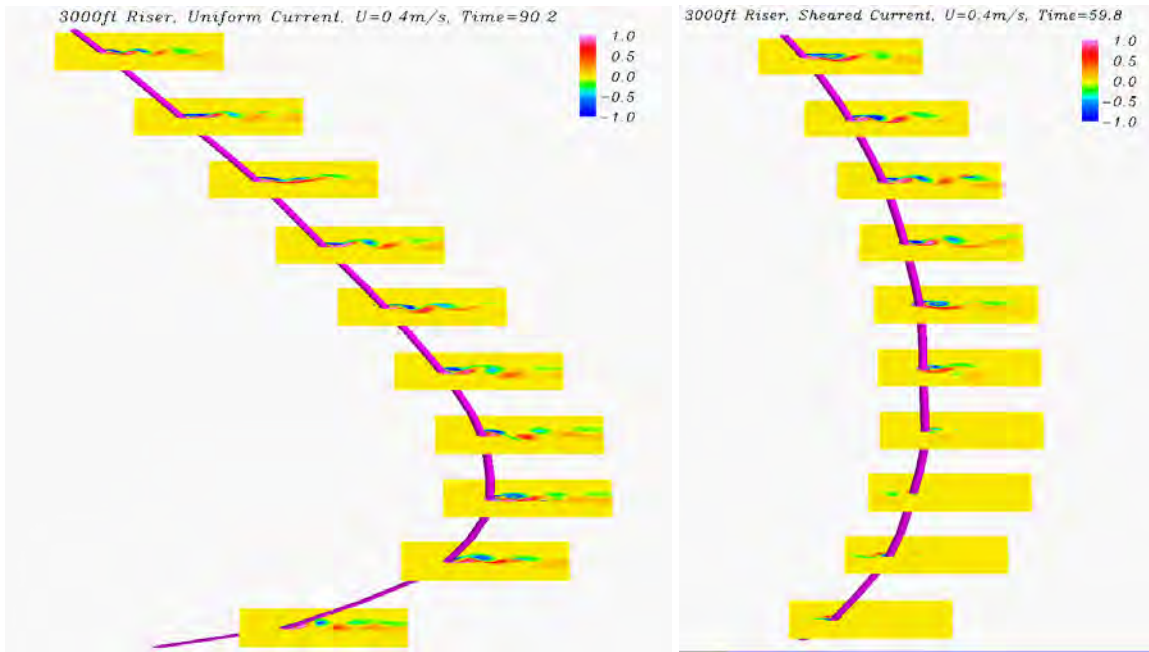
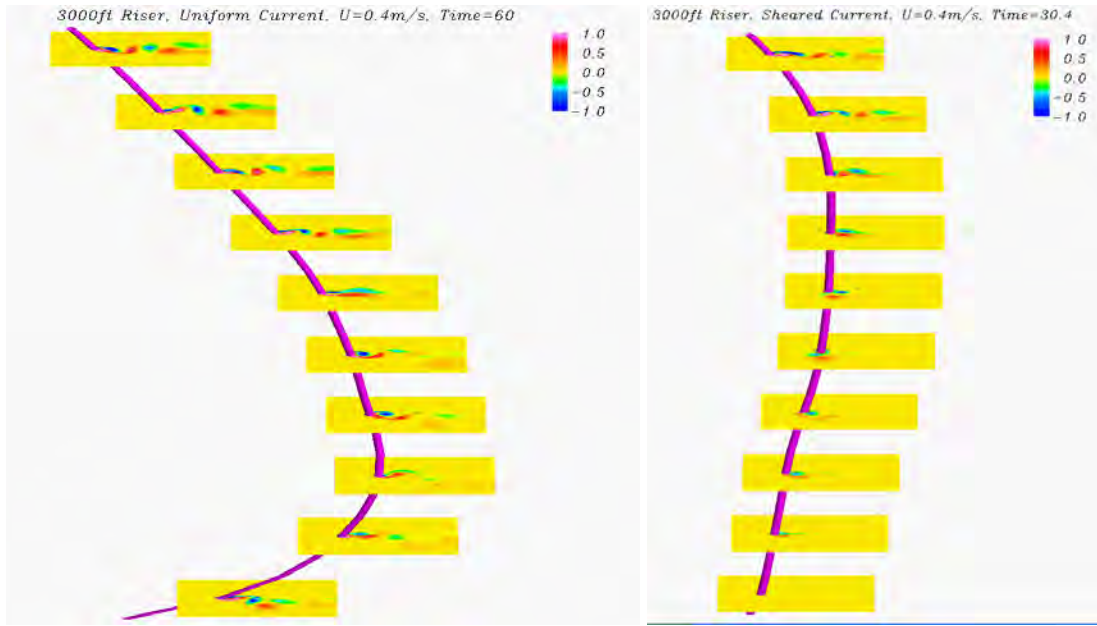


Figure 55. Continued

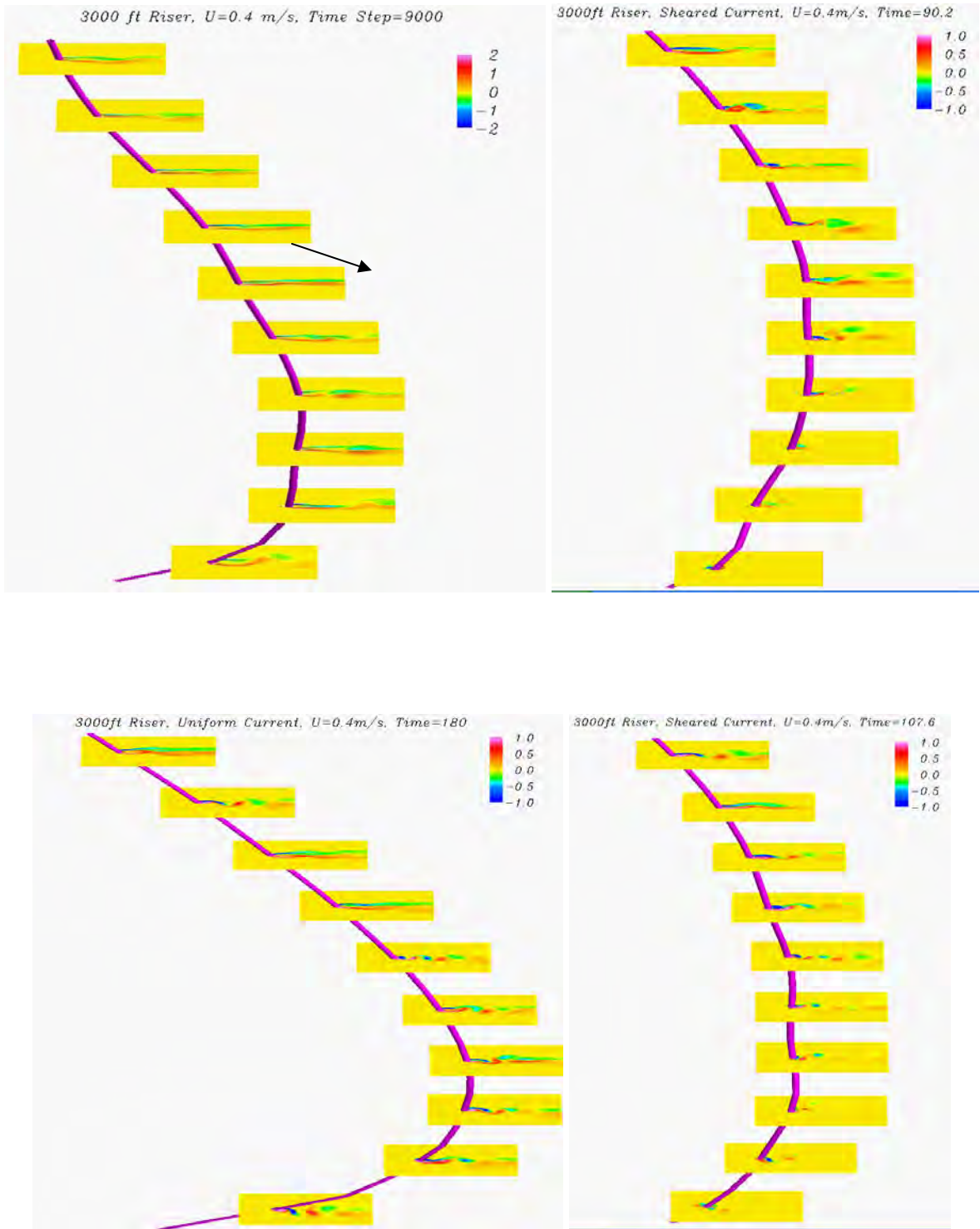


Figure 55. Continued

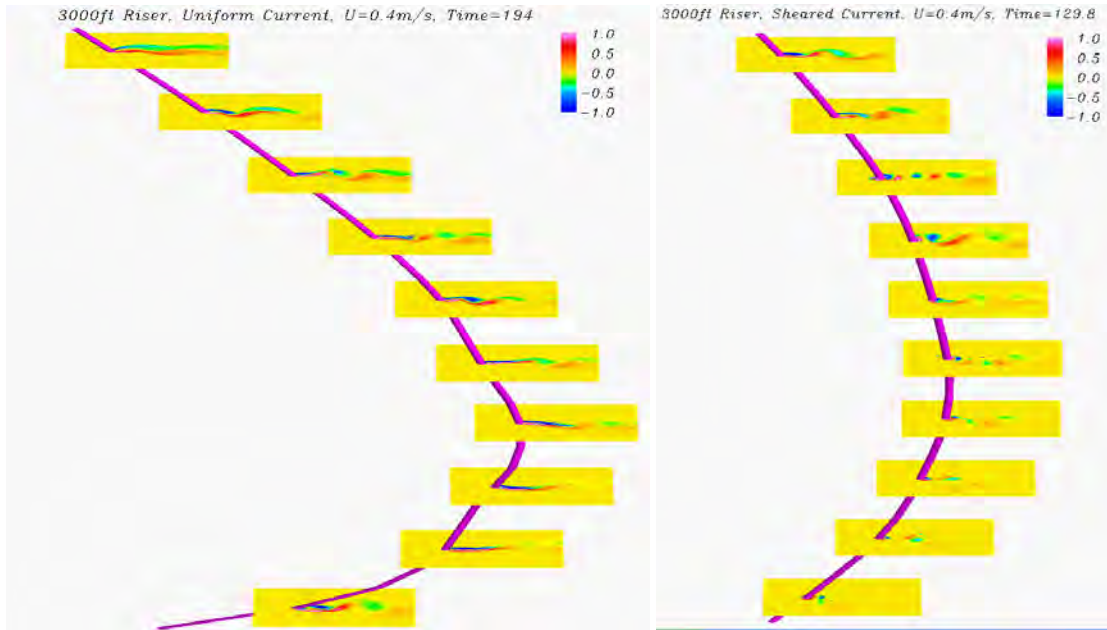


Figure 55. Continued

Overall, the riser exhibits strong flexibility. The cross flow VIV amplitudes are also shown in Figures 56 and 57 for sheared and uniform current, respectively. As expected, the sheared current causes much less drag force, hence lateral excursion on the riser than the uniform current. The figures also show that the riser lateral deflection is coupled with the vortex shedding, and it could introduce complicated dynamic cross flow response, even in a simple uniform current.

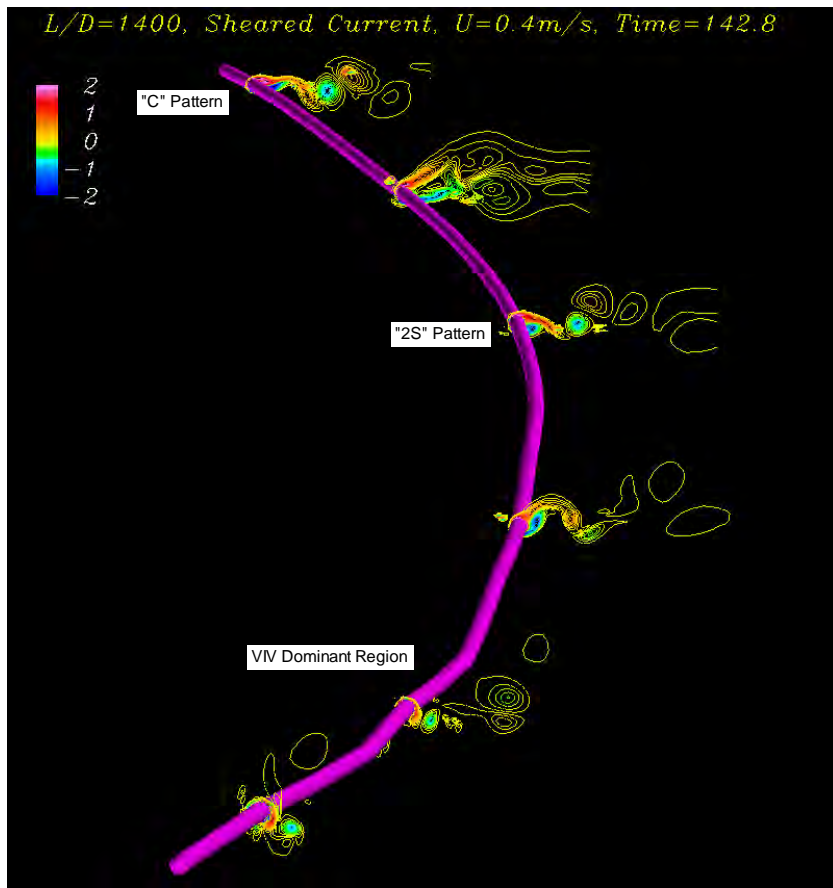


Figure 56. Vertical Riser VIV Snapshot, Sheared Current



Figure 57. Vertical Riser VIV Snapshot, Uniform Current

The cross flow modal responses are plotted in Figure 58. For clarity the modal responses below 7th mode and above 12th mode have been filtered out during the post-processing. The results show the dominant mode for the sheared current is the 9th mode, while both the 11th and 12th modes have significant contribution to the VIV response for the uniform current case.

We compared the rms a/D predicted by FANS to the results from Shear 7 in Figures 59 and 60 for the uniform and sheared currents, respectively. Shear 7 (Vandiver et al., 2003) is a riser VIV analysis tool developed by MIT, and it is based on the frequency domain modal superposition approach and use of empirical lift coefficients. The figures show the results are comparable for the sheared current, while the FANS code predicts lower response in the uniform current. This is clearly related to the number of dominant modes. It is worthwhile to point out that other CFD simulations (Willden and Graham, 2004) also showed that the VIV in uniform current is multi-modal, i.e. several modes with similar frequencies are excited at the same time through added mass adjustment. Note that we have simplified the riser equation of motion and neglected the modal damping and stiffness coupling terms. It is unclear that inclusion of these terms would help or impede the multi-mode VIV. Further evaluation is required to address this issue.

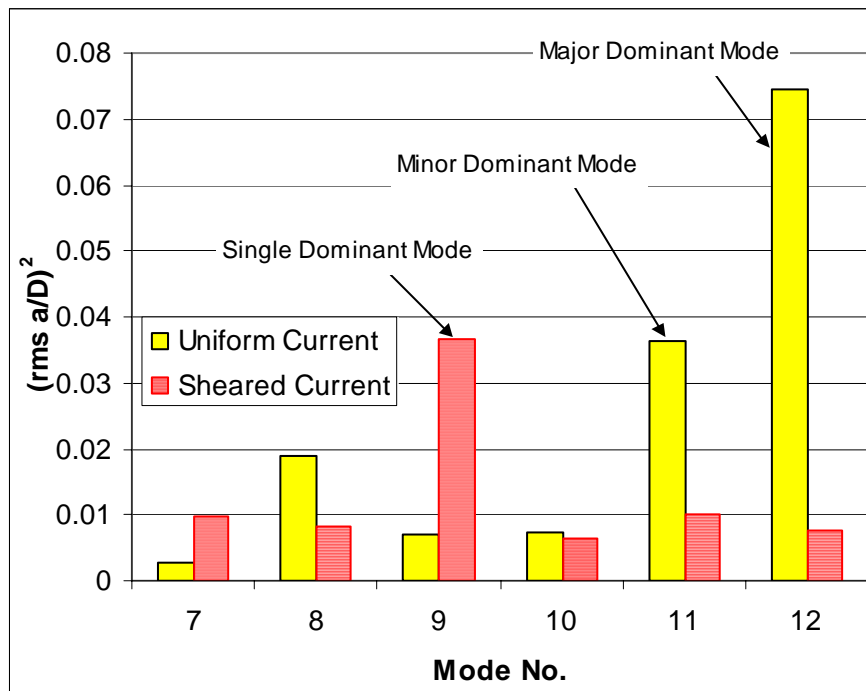


Figure 58. Vertical Riser Cross Flow VIV Modal Response

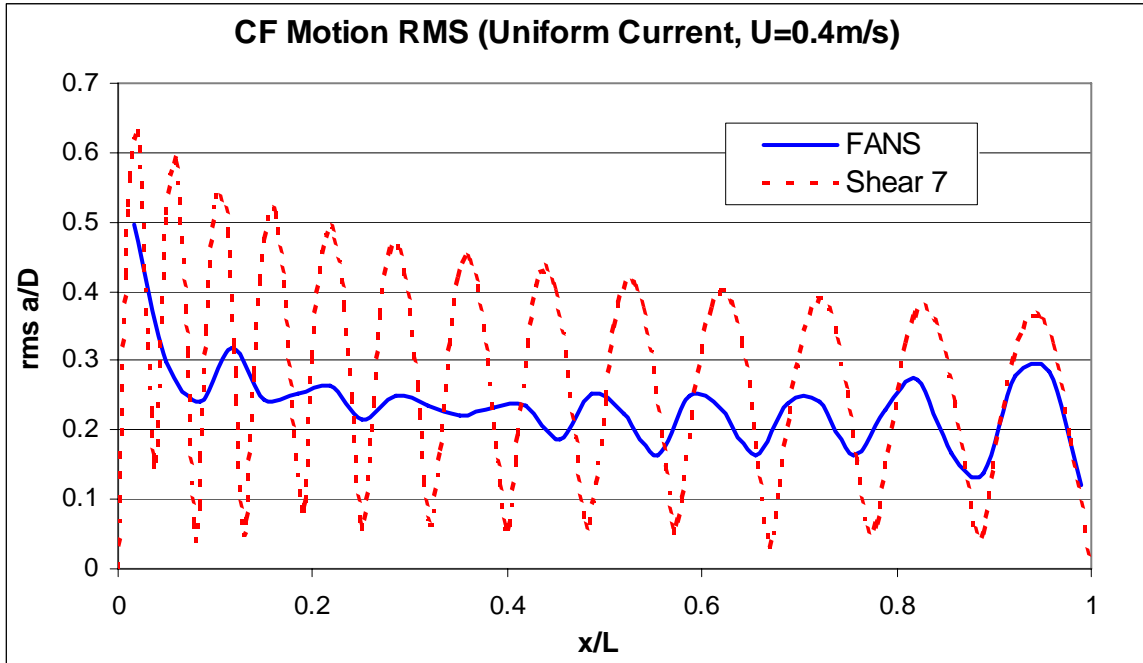


Figure 59. Vertical Riser Cross Flow VIV RMS a/D - Uniform Current

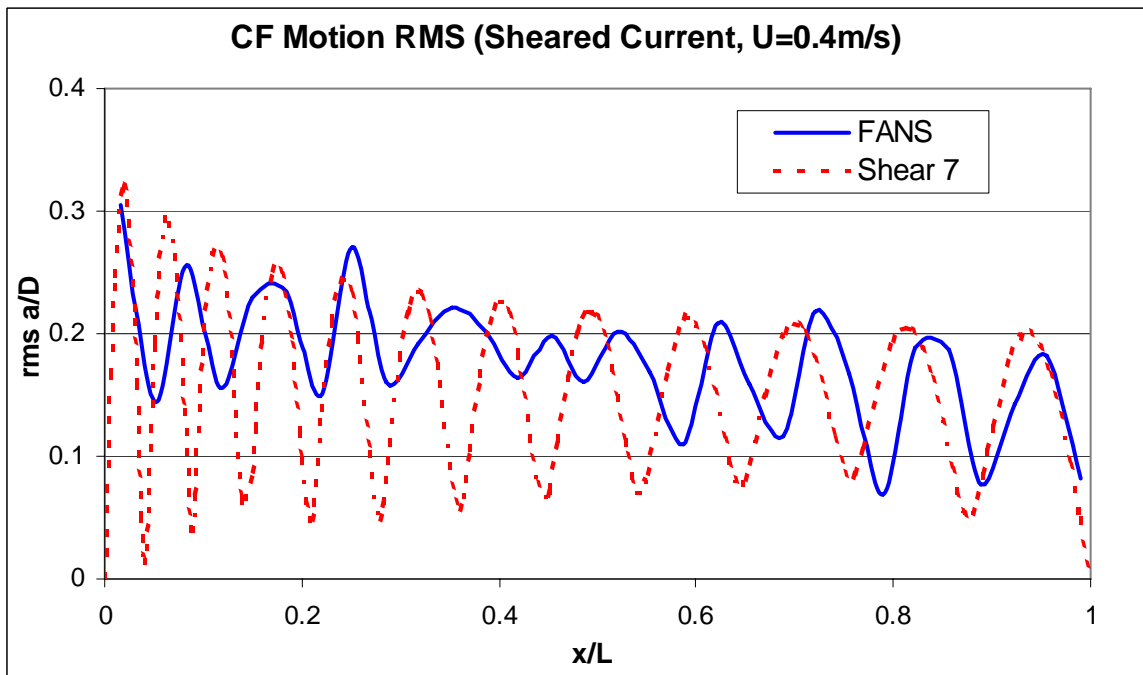


Figure 60. Vertical Riser Cross Flow VIV RMS a/D - Sheared Current

VIV Induced Stress

The rms stress distributions in the riser for the uniform and sheared current cases are presented and compared to Shear 7 in Figures 61 and 62, respectively. The comparisons are in general agreement. They show in both cases that the worst stress is near the lower end of the riser. This is due to the lower effective tension in the riser bottom portion. This is interesting since in sheared current the current has high speed at the top, while the VIV-induced fatigue damage at this location is minimum. In contrast, there is no current near the bottom, while the fatigue damage in this region is the worst.

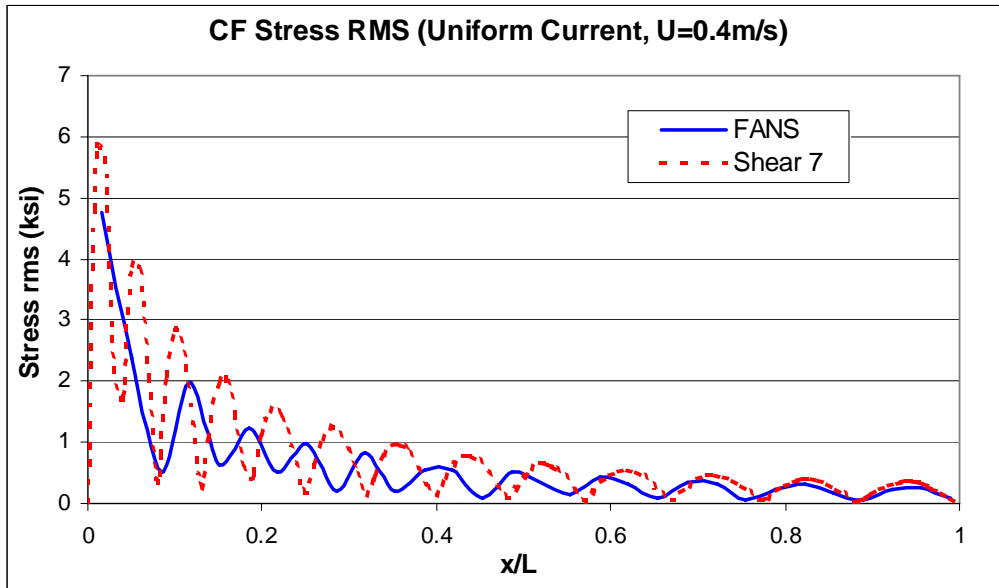


Figure 61. Vertical Riser Cross Flow VIV Induced Stress – Uniform Current

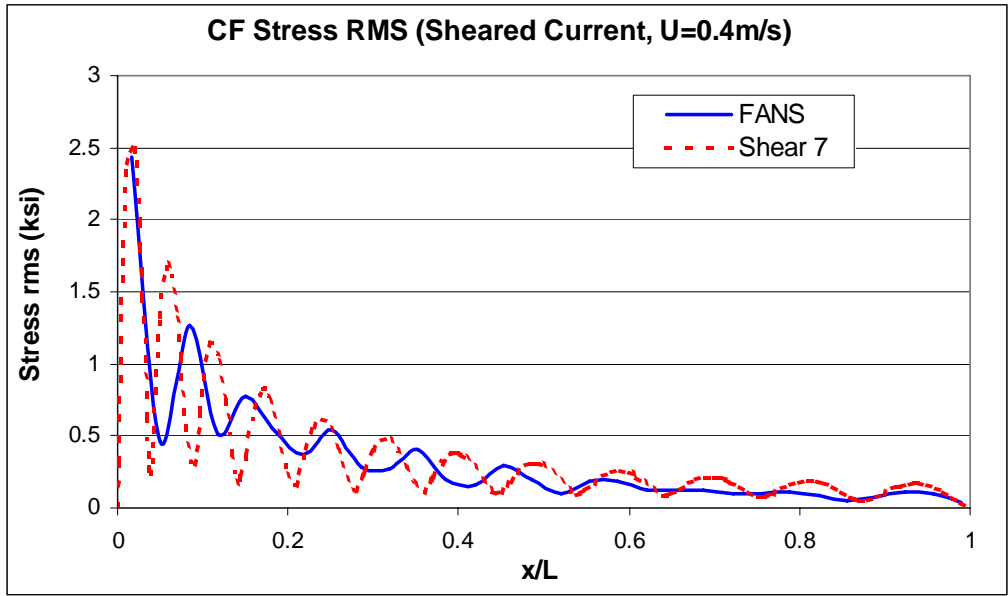


Figure 62. Vertical Riser Cross Flow VIV Induced Stress – Sheared Current

6.4 Discussion

In this section we have studied the VIV of a 3,000ft vertical riser under both uniform and sheared current conditions. The fluid-riser interactions are simulated in the time domain. The riser 3D motion and vortex shedding pattern are examined in detail. We also calculated the cross flow VIV amplitudes and rms stress along the riser, and compared with the results obtained from Shear 7. It is found that the riser could experience multi-mode VIV in uniform current. It is also found that the CFD approach provides reasonable results. Hence it is feasible to use CFD tools for deepwater riser VIV assessment. Further work is recommended in the following areas:

1. riser initial condition and its transient effect on VIV, and
2. riser modal coupling effect on VIV.

In conclusion, an effective CFD approach has been presented and applied to practical riser VIV assessment.

7 3D VIV Simulations Using Direct Integration Riser Motion Solver

7.1 General Description

In our previous studies (Huang et al. 2006, 2007a, 2007b, 2007c), we successfully employed a fully 3D CFD approach for deepwater riser VIV simulations in uniform and sheared current profiles. For simplicity, a modal solver with pre-defined modal shapes was used for the riser structural deformation in our earlier investigations. In this study, we present an alternative riser motion solver that integrates the tensioned beam motion equation directly, and apply it to long riser VIV simulations.

We first present the riser structural response equation in discretized form, and assess its von Neumann stabilities. Numerical simulations are then carried out for long riser VIV for the following four cases:

- Case 1: the riser is horizontally positioned, and has a length of 38 m ($L/D = 1,400$) and a mass ratio of 1.6. The riser is constantly tensioned at 5 kN. The current profile is uniform with $U = 0.4$ m/s.
- Case 2: the riser configuration is the same as Case 1, but the uniform current speed is increased to $U = 0.8$ m/s.
- Case 3: the riser configuration is the same as Case 1, but the current profile is linearly sheared with $U_{max} = 0.4$ m/s at the top end and $U_{min} = 0$ m/s at the bottom.
- Case 4: the riser is a practical single casing 10 ¾" top tensioned vertical riser for 3,000 ft water depth. It has a top tension of 220 tonne, and all bare joints without VIV suppression devices.

The simulation results for the first three cases will be compared with the experimental data of Trim et al. (2005) to evaluate the accuracy of the present CFD approach. For completeness, the results obtained from different riser motion solvers will also be examined in the following sections to determine the validity of the new motion solver.

7.2 CFD Approach

The flow field around a riser is calculated by numerically solving the unsteady Navier-Stokes equations with a Smagorinsky subgrid-scale turbulence model. The Reynolds numbers are 8×10^3 for Cases 1 and 3, 1.6×10^4 for Case 2, and 8×10^4 for Case 4.

The non-dimensional time step used in the present simulations is 0.01, which means the free stream fluid travels a distance of one riser diameter in 100 time steps. The dimensional time steps are about 0.0007 seconds for Cases 1 and 3, 0.0004 seconds for Case 2, and 0.007 seconds

for Case 4. These time steps are sufficiently small since the vortex shedding frequency for the fixed riser and the vibration frequency of the riser is on the order of 1 Hz.

The simulation procedures are:

1. generate the data grids and obtain the interpolation coefficients between the overlapping data grids,
2. specify boundary and initial conditions on the data grids,
3. solve the unsteady Navier-Stokes equation using large eddy simulations,
4. once the fluid velocity and pressure field are determined, the drag and lift forces are obtained from the integration of the pressure and shear stresses on the riser surface,
5. determine the riser lateral accelerations and velocities, and solve for the new positions at the next time step, and
6. move the data grids attached to the riser and update the interpolation coefficients between overlapping data grids.

The non-dimensional time step is selected to be 0.01, which is sufficiently small to avoid possible numerical instabilities.

7.3 Simulation Results – Cases 1 and 2

In Cases 1 and 2, the riser is horizontally positioned with 5 kN constant tension. It is subjected to a uniform current with speed 0.4 m/s and 0.8 m/s, respectively. The riser OD is 0.023 m and its mass ratio is 1.6. The model test prototype has a length of 38 m ($L/D = 1,400$). Figures 63 and 64 show the movement of the riser for Case 1 after it is exposed to the current. The plots also show the vortex development and intensity in the riser wake field. Most of the vortices are shed in a single and distinct pattern (2S). A maximum riser deflection of approximately 15 ODs occurs in the middle section of the riser. Case 2 also shows similar riser VIV behavior except that the inline motion is considerably larger due to the higher current speed.

Figures 65 and 66 show the riser cross flow VIV rms a/D comparisons with the experimental data and our previous results (Huang, Chen and Chen, 2007c) obtained by the riser motion modal solver. The FANS code with the direct riser solver predicts similar cross flow VIV response as the modal solver. In Case 1, both the modal and direct solvers predict that the 4th mode is dominant, which is slightly different from the 3rd mode, as measured in the experiments of Trim et al. (2005). In Case 2, both riser motion solvers predict that the 7th mode is dominant, which is slightly different from the 6th mode, as measured in the experiments. The observed discrepancy may be attributed to different tension setting within the riser. In the model test the riser tension varies from 4 kN to 6 kN, while in our CFD simulations it is set to a constant value of 5 kN. Overall, the comparisons show good agreement between FANS predictions and the experimental data.

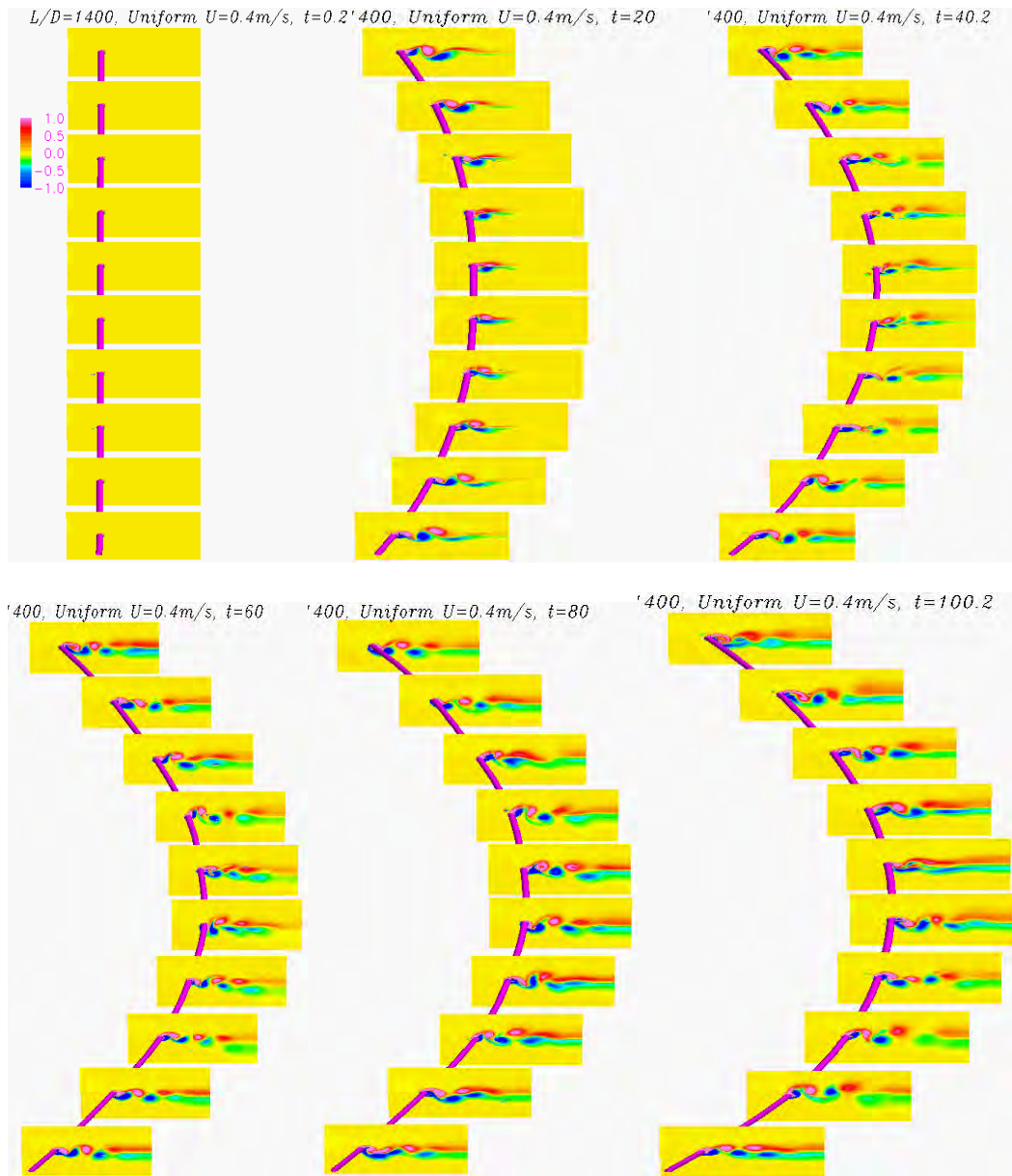


Figure 63. Riser VIV Snapshots from Simulations with Direct Solver – Case 1, Elevation View

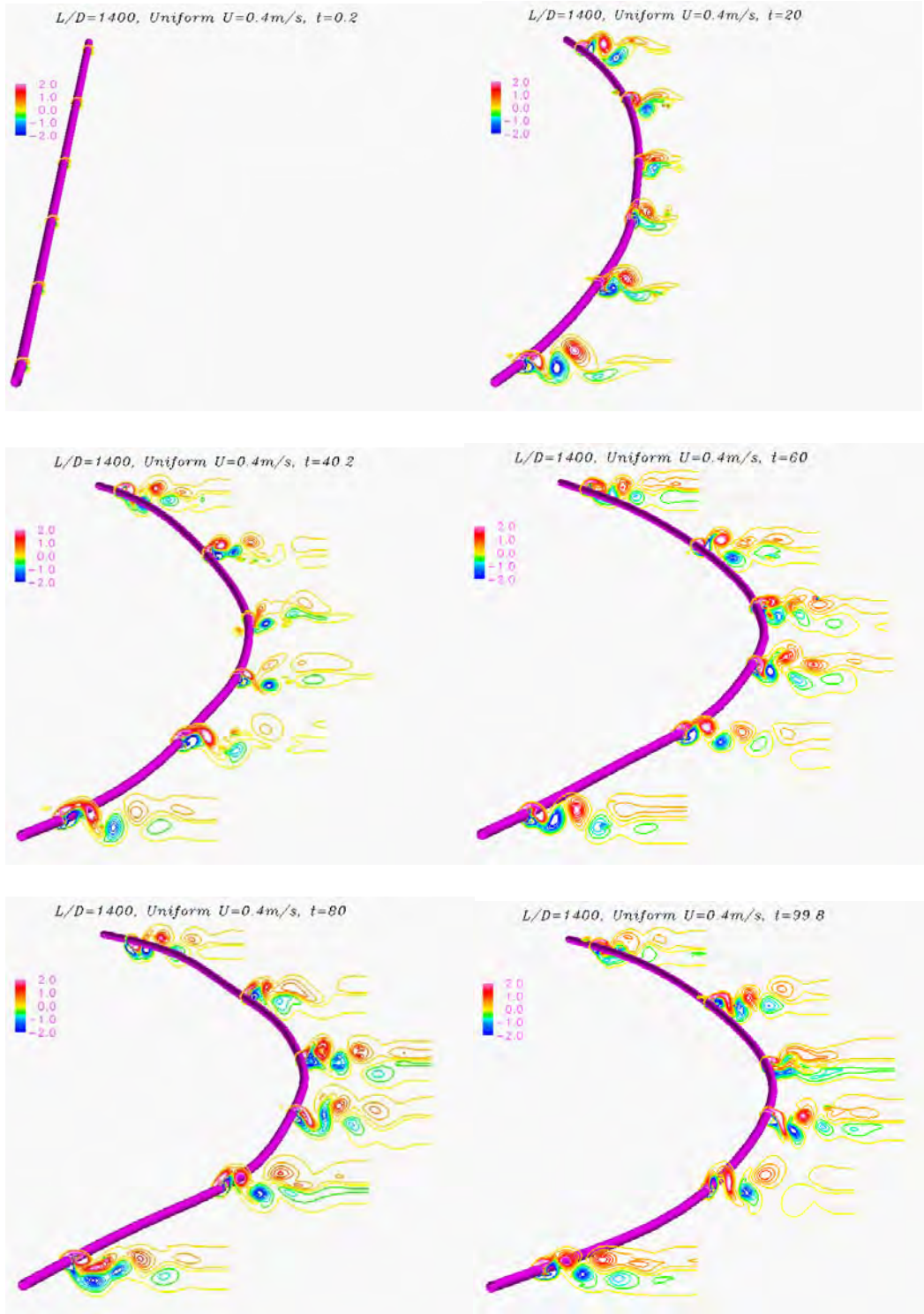


Figure 64. Riser VIV Snapshots from Simulations with Direct Solver – Case 1, Top View

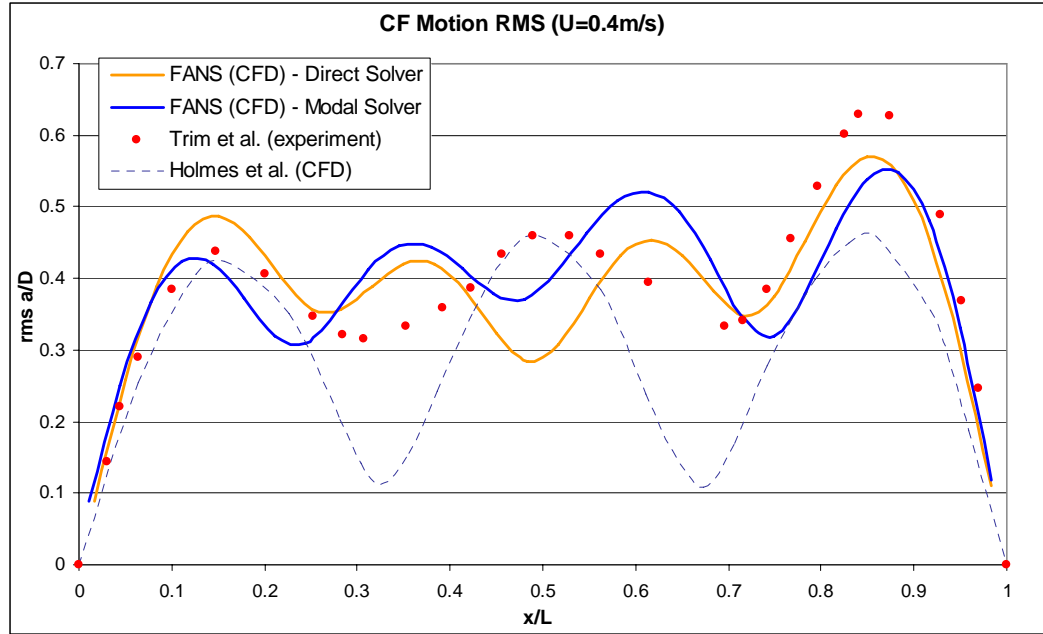


Figure 65. Comparison of Riser Cross Flow VIV RMS a/D – Case 1

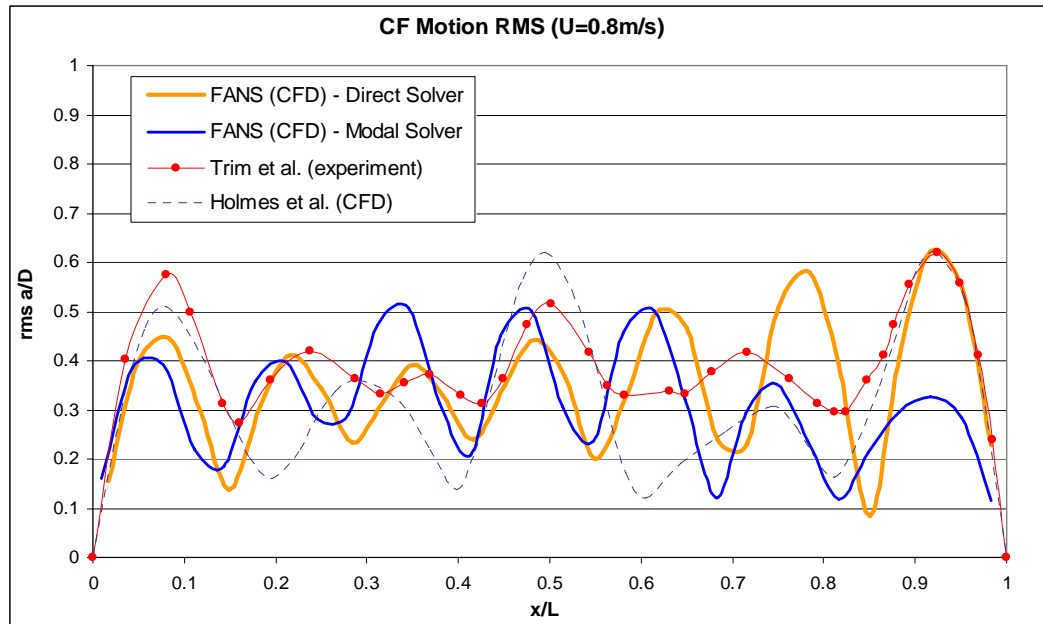


Figure 66. Comparison of Riser Cross Flow VIV RMS a/D – Case 2

7.4 Simulation Results – Case 3

In Case 3 the riser is exactly the same as Case 1, except that it is subjected to a linearly sheared current with 0.4 m/s surface speed. Figure 67 shows typical snapshots of the riser deflection and flow field vorticity contours.

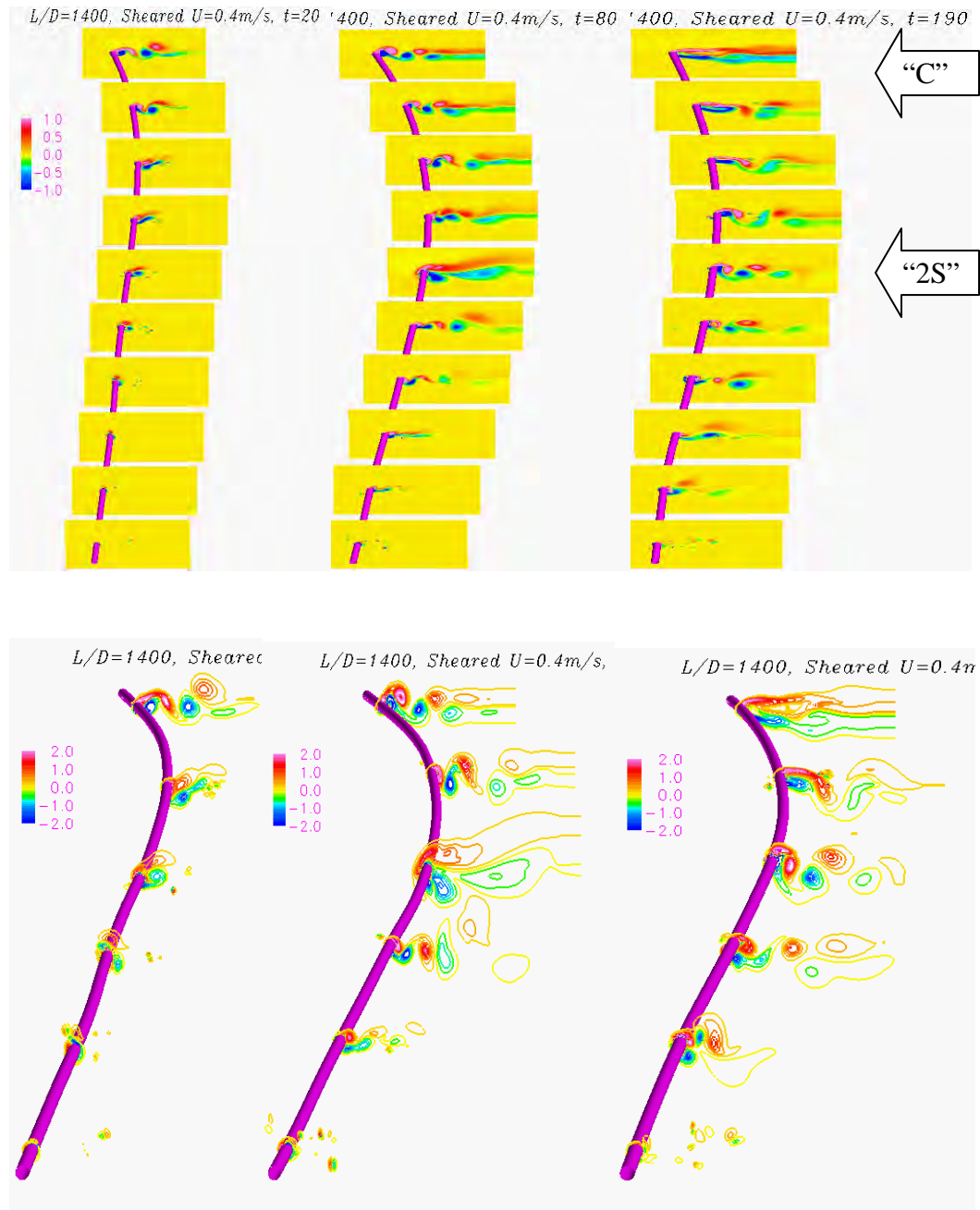


Figure 67. Riser VIV Snapshots from Simulations with Direct Solver– Case 3, Top: Elevation View, Bottom: Top View

Due to the higher current speed near the surface, the vortices are shed much faster in the surface region than the bottom region. The vortex shedding in the riser middle-upper section shows a clear “2S” pattern, while the vortex near the surface eventually breaks down into the “C” pattern. As noted in Huang, Chen and Chen (2007b), this suggests that the riser middle section is the power in zone, while the top section is likely to be the power out zone. The maximum riser deflection is approximately 5 ODs, and occurs in the riser middle-upper portion.

Figure 68 shows the riser cross flow VIV rms a/D comparisons. It shows the 3rd mode is dominant, and its amplitudes are consistent between the two FANS results with modal superposition and direct riser solver. It also shows that the maximum and mean values of the predicted rms a/D are comparable to the experimental data.

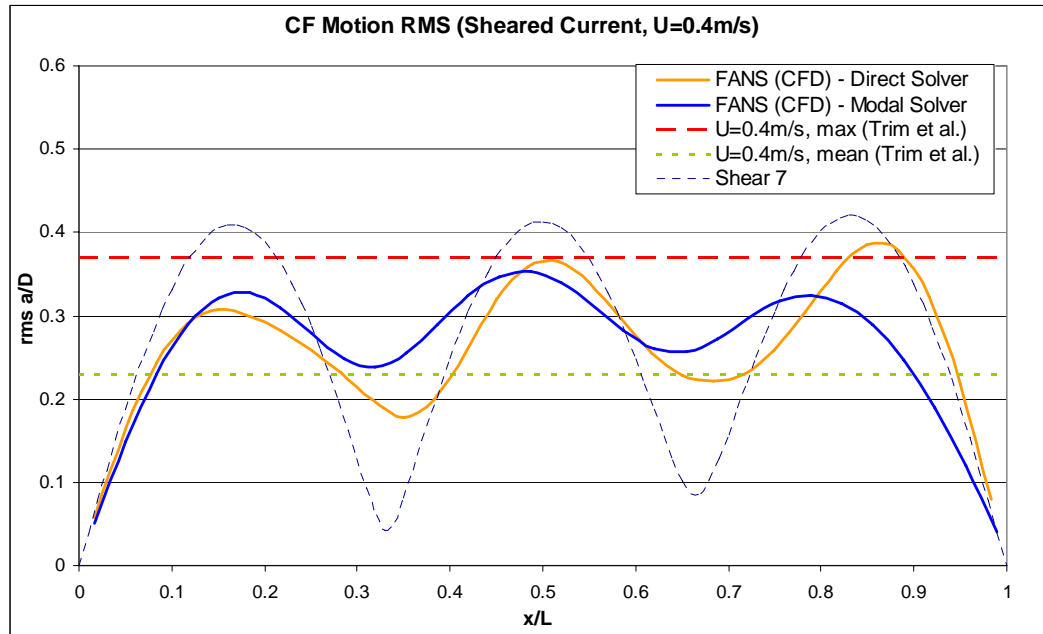


Figure 68. Comparison of Riser Cross Flow VIV RMS a/D – Case 3

7.5 Simulation Results – Case 4

In Case 4 the riser is a 3,000 ft vertical top tensioned riser with top tension of 220 tonne. It is subjected to a 0.4 m/s uniform current. Its OD is 0.23 m (10 3/4”), and its unit weight is 121 lb/ft. Figure 69 shows typical snapshots of the riser deflections and flow field vorticity contours. Due to the lower effective tension on the riser bottom section, the maximum lateral displacement occurs in the lower portion of the riser. The maximum riser deflection is approximately 20 ODs.

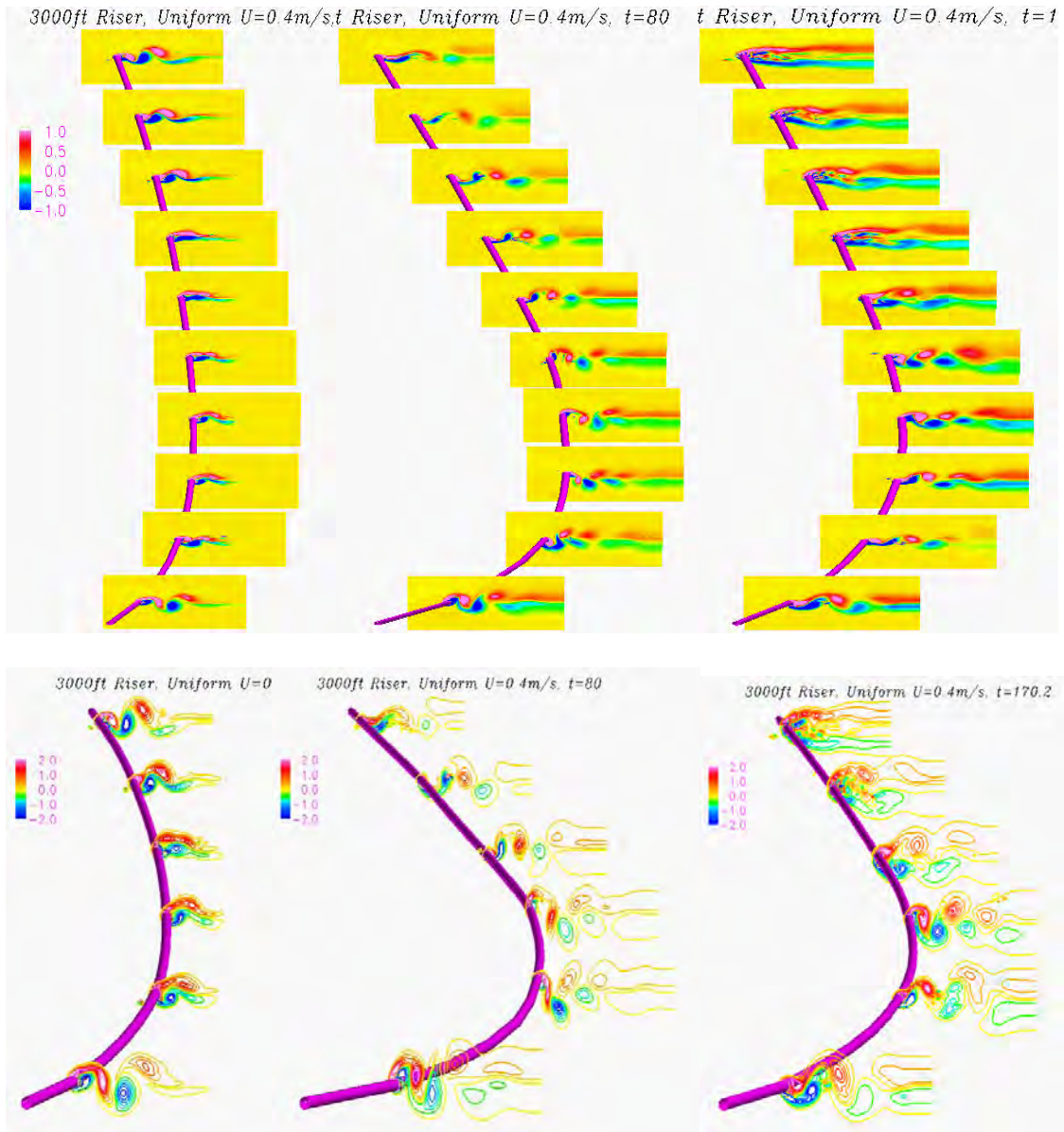


Figure 69. Riser VIV Snapshots from Simulations with Direct Solver – Case 4, Top: Elevation View, Bottom: Top View

The riser cross flow VIV rms a/D is compared to the Shear 7 results in Figure 70. In this case, Shear 7 (Vandiver et al., 2003) predicts single mode lock-in at the 13th mode. In general, the comparisons show a similar trend for the VIV amplitudes, i.e. higher VIV amplitudes near the riser bottom area. However, the FANS code predicts that the VIV is multi-mode. This seems more reasonable since:

1. The modes are coupled for top tensioned risers, especially for long risers. In other words, the existence of one mode will transfer its energy to other modes (Huang, Chen and Chen, 2007a).
2. Non-linear damping could have a strong effect on the riser VIV as well.

The fluid induced damping coefficient in the higher VIV amplitude region could be much higher than that in the lower VIV amplitude region. This is an area that deserves further assessment. This effect is also likely to be the reason that the FANS code with the direct riser solver predicts slightly lower cross flow VIV response near the riser bottom than the modal solver, where the riser motion is solved by modal superposition. The FANS code with the direct riser solver is expected to be more effective in dealing with any non-linear damping effect in the time domain. Nevertheless, the comparisons confirm a similar trend between the CFD and Shear 7 results, and disclose a possible course of future study that could have significant potential for industrial applications.

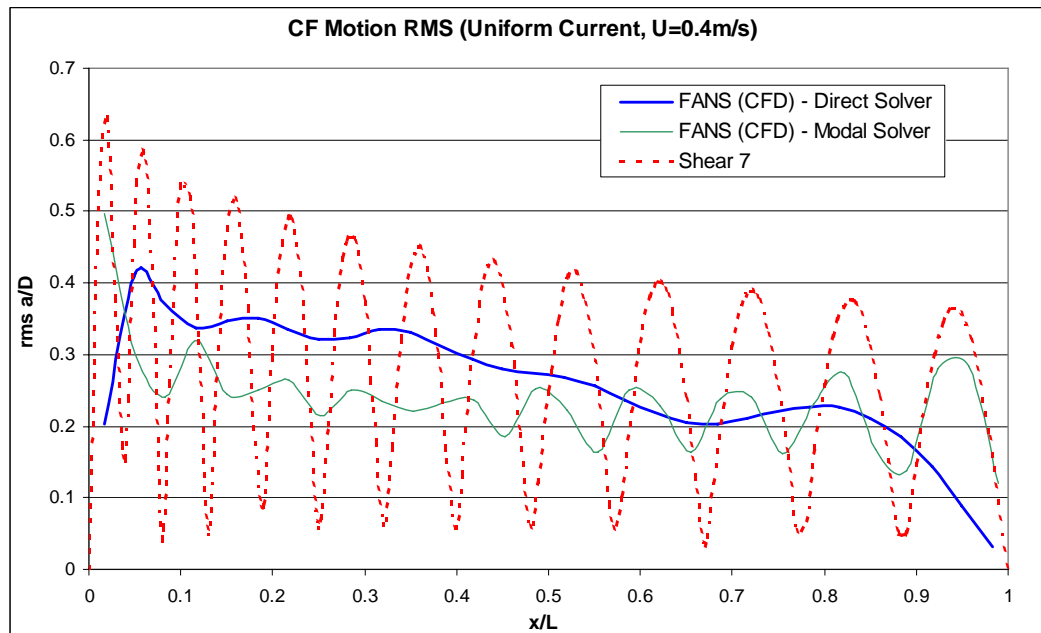


Figure 70. Comparison of Riser Cross Flow VIV RMS a/D – Case 4

7.6 Discussion

This section provided four case studies on long riser VIV response based on the unsteady, incompressible Navier-Stokes equations in conjunction with a large eddy simulation (LES) model. We used a direct riser motion solver to calculate the riser lateral displacements for two different types of risers in uniform current and/or sheared currents. The results are in good agreement with the corresponding experimental data and other analytic results, and consistent with the simulations we have developed by using a riser modal motion solver. Some findings of the study are:

- The asymmetry of the riser VIV response in the uniform current suggests that: (1) the cross flow VIV is influenced by the in-line riser motion, and (2) the VIV response

likely consists of several modal shapes, even though one of them is more dominant than the others.

- The vortex shedding pattern in the sheared current is different from that in the uniform current. In the uniform current case, the riser motion and vortex shedding are synchronized along the riser. In the sheared current case, the existence of the “C” pattern indicates a clear power-out zone at the riser top section.
- For a long marine riser, the maximum VIV response is near the riser bottom, where the effective tension is the minimum. The FANS results confirm this phenomenon. However, it also demonstrated that the VIV response could be over-predicted if the non-linear damping is not considered appropriately, especially in the high-amplitude response region.

Some of the areas that could be further investigated are:

1. Riser high mode VIV under strong current and high Reynolds number. This requires more grid elements in the riser axial direction, hence more powerful computer resources.
2. VIV suppression devices, such as fairings and strakes.
3. Deepwater riser non-linear damping effect on VIV.
4. Riser VIV in complex current conditions, such as submerged current or bottom current.

In conclusion, a three dimensional CFD approach for deepwater riser VIV simulation with a direct integration riser motion solver has been presented. The validity and effectiveness of the FANS code to predict long riser VIV in uniform and sheared current have been demonstrated through case studies and comparisons to the published experimental data.

8 Summary and Conclusions

This report documents a study of CFD simulation of long riser VIV responses in uniform and sheared currents. First, the 2D flow field around a fixed and a vibrating riser, was simulated and compared to the flow field predicted by Huse's empirical formula (based on experimental data). The simulation results show good agreement, which confirms the effectiveness of both the FANS code and data grids. At the same time, the "high speed" zone behind the riser was investigated and its influence on the interference of deepwater risers was illustrated. We then extruded the data grid in the axial direction, and applied the same data grids to a long riser VIV simulation. To facilitate the comparison to published experimental data, this riser was chosen as horizontally positioned and with $L/D = 1,400$. We chose to discretize the cross-sectional flow plane with delicately generated fine elements, while using relatively coarse elements in the spanwise direction to keep the total number of elements in the fluid domain less than 1 million, which is within the computational capability of a regular single-processor PC. In order to calculate the riser deflections, a riser modal motion solver was developed that calculates the riser lateral motions based on instantaneous drag and lift coefficients. The riser VIV response rms a/D showed general agreement with the model test results. We then further demonstrated the capability of the FANS code through riser VIV simulations in sheared currents. The results show that the riser has much less lateral displacement in the sheared current than the corresponding uniform current, and the power-in and power-out zones could also be easily identified by examination of the vortex shedding pattern.

After successful simulations of the constantly tensioned horizontal riser, we proceeded with CFD simulations of a typical vertical riser for 3,000 ft water depth. This top tensioned riser has much lower tension at the bottom than the top because of its own weight. In general, the riser bottom has much higher VIV response amplitudes than the rest of the riser. This is expected since lower tension is usually associated with higher lateral flexibility. The VIV simulation results are similar to those obtained by Shear 7 under the same flow conditions. Realizing that the riser modal solver is based on specified modal shapes, which sometimes are difficult to obtain, we provided a riser direct integration solver that could be more accurate and convenient than the modal solver. All the simulations were repeated with the new motion solver and the results were benchmarked as well.

In general, this research not only demonstrated that the FANS code is capable of long riser time domain VIV simulations, but it also disclosed a number of valuable insights on long riser VIV phenomena. Some highlights of the findings are as follows:

- The CFD time domain simulation approach has predicted a narrow wake field and a high-speed zone outside the wake field. Both of these features positively affect the riser interference results.
- The asymmetry of the riser VIV response in uniform current suggests that (1) the cross flow VIV is influenced by the in-line riser motion, and (2) the VIV response likely consists of several modal shapes, even though one of them is more dominant than the others.

- The vortex shedding pattern in the sheared current is different from that in the uniform current. In the uniform current case, the riser motion and vortex shedding are usually synchronized. In the sheared current case, the mixture of 2S and C patterns may suggest the existence of power-in and power-out zones along the riser.
- Mode lock-in could occur in the sheared current. However, its dominant level (in terms of the energy percentage) is lower than that in the uniform current.
- In the sheared current case, the existence of “C” vortex patterns indicates a clear power-out zone at the riser top section.
- For a long marine riser, the maximum VIV response is near the riser bottom, where the effective tension is the minimum. The FANS results confirmed this phenomenon. However, it also demonstrated that the VIV response could be over-predicted if the non-linear damping is not considered appropriately, especially in the high-amplitude response region.

Some of the areas that could be further investigated are:

1. Riser high mode VIV under strong current and high Reynolds number.
2. VIV suppression devices, such as fairings and strakes.
3. Deepwater riser non-linear damping effect on VIV.
4. Riser VIV in complex current conditions, such as submerged current or bottom current.

In conclusion, a three dimensional CFD approach for deepwater riser VIV simulation with different riser motion solvers has been presented. The computation of the VIV response of long risers is based on the unsteady, incompressible Navier-Stokes equations in conjunction with a large eddy simulation (LES) model. The validity and effectiveness of the FANS modeling approach to predict long riser VIV in uniform and sheared current have been demonstrated through case studies and comparisons to published experimental data.

Acknowledgements

The project was sponsored in part by the Department of Interior, Minerals Management Service (MMS) and in part by industry funding through the Offshore Technology Research Center (OTRC) under a project titled “VIV of Deepwater Risers”. Some computations were performed using resources from the Texas A&M University supercomputing facilities. Their support is also acknowledged.

References

- ASME B 31.4, "Pipeline Transportation Systems for Liquid Hydrocarbon and Other Liquids", 2002 Edition, August, 2002.
- ASME B 31.8a, "Gas Transmission and Distribution Piping Systems", 2001 Edition, November, 2001.
- API RP 1111, "Design, Construction, Operation, and Maintenance of Offshore Hydrocarbon Pipelines", 3rd Edition, July, 1999.
- API RP 2RD, "Design of Risers for Floating Production Systems (FPSs) and Tension-Leg Platforms (TLPs)", June, 1998
- API Specification 5L, "Specification for Line Pipe", 42nd Edition, January, 2000.
- API Bulletin 5C3, "Bulletin on Formulas and Calculations for Casing, Tubing, Drill Pipe, and Line Pipe Properties", 6th Edition, November, 1994
- Blevins, R.D. (1990), "Flow-Induced Vibrations", 2nd Edition. Van Nostrand Reinhold, ISBN 0-442-20651-B.
- Chen, H.C. and Patel, V.C. (1989), "The Flow around Wing-Body Junctions", *Proceedings of the 4th Symposium on Numerical and Physical Aspects of Aerodynamic Flows*, Long Beach, CA, 16-19 January.
- Chen, H.C., Patel, V.C. (1988), "Near-wall Turbulence Models for Complex Flows Including Separation", *AIAA Journal*, Vol 26, pp 641-648.
- Chen, H.C., Patel, V.C. and Ju, S. (1990), "Solutions of Reynolds-Averaged Navier-Stokes Equations for Three-Dimensional Incompressible Flows", *Journal of Computational Physics*, Vol. 88, No. 2, pp 305-336.
- Chen, H.C., Chen, C.R., Mercier, R., Pontaza, J.P. (2006), "CFD Simulation of Riser VIV", MMS and OTRC Project Final Report.
- Chaplin, J.R., Bearman, P.W., Cheng, Y., Fontaine, E., Graham, J.M.R., Herfjord, K., Huera, F.J., Isherwood, M., Lambrakos, K., Larsen, C.M., Meneghini, J.R., Moe, G., Pattenden, R.J., Triantafyllou, M.S., Willden, R.H.J. (2005), "Blind Prediction of Laboratory Measurements of Vortex-Induced Vibrations of a Tension Riser", *Journal of Fluids and Structures* 21, pp 25-40.
- Dong, S. Karniadakis, G.E. (2005), "DNS of Flow Past a Stationary and Oscillating Cylinder at $Re=10000$ ", *Journal of Fluids and Structures*, Vol 20, pp 519-531.
- E. Huse (1993), "Interaction in Deep Sea Riser Arrays", *Proc. of the Offshore Technology Conference*, OTC 7237, Houston, TX.
- E. Huse (1996), "Experimental Investigation of Deep Sea Riser Interaction", *Proc. of the Offshore Technology Conference*, OTC 8070, Houston, TX.
- Govardhan, R. Williamson, C.H.K. (2000), "Modes of Vortex Formation and Frequency Response of a Freely Vibrating Cylinder", *Journal of Fluids Mechanics*, Vol 420, pp 85-130.

- Holmes, S., Oakley, O.H., Constantinides, H. (2006), "Simulation of Riser VIV Using Fully Three Dimensional CFD Simulations," *OMAE 2006-92124, 25th International Conference on Offshore Mechanics and Arctic Engineering*, Hamburg, Germany.
- Huang, K., Chen, H.C. (2006), "Ultra Deepwater Riser Interference Analysis by Using a Time Domain Simulation Approach with VIV Effect", *Proceedings of D.O.T XVIII (2006) Conference*, Houston.
- Huang, K. Chen, H.C., Chen, C.R. (2007a), "Deepwater Riser VIV Assessment by Using A Time Domain Simulation Approach", *Proceedings of the Offshore Technology Conference*, OTC 18769, Houston, TX.
- Huang, K. Chen, H.C., Chen, C.R. (2007b), "Riser VIV Analysis by a CFD Approach", *Proceedings of the 17th International Offshore and Polar Engineering (ISOPE) Conference*, Lisbon, Portugal.
- Huang, K., Chen, H.C., Chen, C.R. (2007c), "Time-Domain Simulation of Riser VIV in Sheared Current", *Proceedings of 26th International Conference on Offshore Mechanics and Arctic Engineering (OMAE) Conference*, OMAE 29363, San Diego, California.
- Huang, K., Chen, H.C., Chen, C.R. (2007d), "A Three Dimensional CFD Approach for Deepwater Riser VIV Simulation", *Proceedings of 9th International Symposium on Fluid Control, Measurement and Visualization (FLUCOME)*, Tallahassee, Florida.
- Lucor, D. Mukundan, H, Triantafyllou, M.S. (2006), "Riser Modal Identification in CFD and Full-scale Experiments", *Journal of Fluids and Structures*, Vol 22, pp 905-917.
- Pontaza, J.P., Chen, C.R., Chen, H.C. (2004), "Chimera Reynolds-averaged Navier-Stokes simulations of vortex-induced vibration of circular cylinders", *Proceedings of the International ASCE Conference: Civil Engineering in the Oceans VI*, pp 166-176.
- Pontaza, J.P., Chen, C.R., Chen, H.C. (2005a), "Simulations of High Reynolds Number Flow Past Arrays of Circular Cylinders Undergoing Vortex-induced Vibrations", *Proceedings of the 15th International Offshore and Polar Engineering (ISOPE) Conference*, pp 201-207.
- Pontaza, J.P., Chen, H.C., Chen, C.R. (2005b), "Numerical Simulations of Riser Vortex-induced Vibrations", *Proceedings of the 2005 Society of Marine Engineers and Naval Architects (SNAME) Conference*, D52, pp 1-12.
- Pontaza, J.P., Chen, H.C., Reddy, J.N. (2005c), "A Local-analytic-based Discretization Procedure for the Numerical Solution of Incompressible Flows", *International Journal for Numerical Methods in Fluids* Vol 49, pp 657-699.
- Pontaza, J.P., Chen, H.C. (2006), "Three-dimensional Numerical Simulations of Circular Cylinders Undergoing Two Degree-of-freedom Vortex-induced Vibrations", *OMAE 2006-92052, 25th International Conference on Offshore Mechanics and Arctic Engineering*, Hamburg, Germany.
- Pontaza, J.P., Menon, R.G. and Chen, H.C. (2007), "Three-Dimensional Numerical Simulations of Flow Past Smooth and Rough/Bare and Helically Straked Circular Cylinders, Allowed to Undergo Two Degree-of-Freedom Motions", *OMAE 2007-29366, Proceedings of 26th International Conference on Offshore Mechanics and Arctic Engineering*, June 10-15, San Diego, California, USA.

- Pontaza, J.P., Chen, H.C. (2007), "Three-Dimensional Numerical Simulations of Circular Cylinders Undergoing Two Degree-of-Freedom Vortex-Induced Vibration", *ASME Journal of Offshore Mechanics and Artic Engineering*, Vol. 129, No. 3, pp 158-164.
- Trim, A.D., Braaten, H., Lie, H., Tognarelli, M.A. (2005), "Experimental Investigation of Vortex-induced Vibration of Long Marine Risers", *Journal of Fluids and Structures*, Vol 21, pp 335-361.
- Willden, R.H.J., Graham, J.M.R (2004), "Multi-modal Vortex-Induced Vibrations of a Vertical Riser Pipe Subject to a Uniform Current Profile", *European Journal of Mechanics B/Fluids*, Vol 23, pp 209-218.
- Willden, R.H.J., Graham, J.M.R (2006), "Three Distinct Response Regimes for the Transverse Vortex-Induced Vibrations of Circular Cylinders at Low Reynolds Number", *Journal of Fluids and Structures*, Vol 22, pp 885-895.
- Williamson, C.H.K., Roshko, A. (1988), "Vortex Formation in the Wake of an Oscillating Cylinder", *European Journal of Mechanics B/Fluids*, Vol 2, pp 355-381.
- Williamson, C.H.K., Jauvtis, N. (2004), "A High-amplitude 2T Mode of Vortex-Induced Vibration for a Light Body in XY Motion", *European Journal of Mechanics B/Fluids*, Vol 23, pp 107-114.
- Vandiver, J.K. (1993), "Dimensionless Parameters Important to the Prediction of Vortex-Induced Vibration of Long, Flexible Cylinders in Ocean Currents", *Journal of Fluids and Structures*, Vol. 7, pp 423-455.
- Vandiver, J.K., Li, L. (2003), "Shear7 V4.3 Program Theoretical Manual".

Publications under Project

Conference papers:

1. Huang, K., Chen, H.C. (2006), “Ultra Deepwater Riser Interference Analysis by Using a Time Domain Simulation Approach with VIV Effect”, *Proceedings of D.O.T XVIII (2006) Conference*, Houston, Texas.
2. Huang, K. Chen, H.C., Chen, C.R. (2007a), “Deepwater Riser VIV Assessment by Using a Time Domain Simulation Approach”, *Proceedings of the Offshore Technology Conference*, OTC 18769, Houston, Texas.
3. Huang, K. Chen, H.C., Chen, C.R. (2007b), “Riser VIV Analysis by a CFD Approach”, *Proceedings of the 17th International Offshore and Polar Engineering (ISOPE 2007) Conference*, Lisbon, Portugal.
4. Huang, K., Chen, H.C., Chen, C.R. (2007c), “Time-Domain Simulation of Riser VIV in Sheared Current”, *Proceedings of 26th International Conference on Offshore Mechanics and Arctic Engineering (OMAE) Conference*, OMAE 2007-29363, San Diego, California.
5. Huang, K., Chen, H.C., Chen, C.R. (2007d), “A Three Dimensional CFD Approach for Deepwater Riser VIV Simulation”, *Proceedings of 9th International Symposium on Fluid Control, Measurement and Visualization (FLUCOME)*, Tallahassee, Florida.
6. Pontaza, J.P., Menon, R.G. and Chen, H.C. (2007), “Three-Dimensional Numerical Simulations of Flow Past Smooth and Rough/Bare and Helically Straked Circular Cylinders, Allowed to Undergo Two Degree-of-Freedom Motions”, OMAE 2007-29366, *Proceedings of 26th International Conference on Offshore Mechanics and Arctic Engineering*, San Diego, California, USA.

Journal papers:

7. Pontaza, J.P. and Chen, H.C. (2007), “Three-Dimensional Numerical Simulations of Circular Cylinders Undergoing Two Degree-of-Freedom Vortex-Induced Vibration”, *ASME Journal of Offshore Mechanics and Arctic Engineering*, Vol. 129, No. 3, pp. 158-164, August 2007.